Ligand Receptor Interactions on Soft Scaffolds: the Influence of Young's Modulus, Ligand Concentration, and Type

Inaugural-Dissertation

to obtain the academic degree

Doctor rerum naturalium (Dr. rer. nat)

submitted to the Department of Biology, Chemistry, and Pharmacy

of Freie Universität Berlin

by

Hanqing Wang

from Xi'an, China

Düsseldorf, March 2017

The work presented in this thesis was accomplished in a period between February 2014 and February 2017 in the Department of Biomolecular System at Max Planck Institute of Colloids and Interfaces, the Institute of Chemistry and Biochemistry at Freie Universität Berlin, and the Institute of Organic Chemistry and Macromolecular Chemistry at Heinrich-Heine-Universität Düsseldorf under the supervision of Prof. Dr. Laura Hartmann and co-supervision of Jun.-Prof. Dr. Stephan Schmidt.

1st Reviewer: Prof. Dr. Laura Hartmann

2nd Reviewer: Prof. Dr. Rainer Haag

Date of defence: 26.06.2017

Table of Contents

Summary

Ligand receptor interactions mediate a great number of biological events such as cell-cell communication, pathogen invasion, or cell growth. Thus it is of great interest to investigate ligand receptor interactions in order to gain a deeper knowledge about their biological function. Such information can then also be applied to derive new and optimized ligands e.g. to block natural ligand receptor interactions in therapeutical applications such as pathogen inhibition. Today, there already exists a great number of theoretical models as well as experimental methods to evaluate the binding of ligands and receptors e.g. in terms of their binding thermodynamics or binding affinities. However, most of these methods are focused on a single ligand receptor pair interaction, or completely dissolved ligand receptor systems. In nature, ligand receptor interactions often take place at soft interfaces such as the cell surface where not a single but assemblies of ligands and receptors interact simultaneously.

Recently, a novel method, soft colloidal probe - reflection interference contrast microscopy (SCP-RICM), was developed to study ligand receptor interactions at soft interfaces. In this technique, poly (ethylene glycol) (PEG) based hydrogel microparticles are functionalized with ligands or receptors as a highly simplified model of the extracellular matrix. As counterpart, glass slides are functionalized with the corresponding receptors or ligands. Upon incubation of the SCPs on the glass slide, ligand receptor binding takes place leading to adhesion of the SCPs on the glass slide. As the SCPs are soft, they can deform to further maximize the contact area and thereby the ligand receptor interactions. Through analysis and read-out of the contact area with RICM and by applying a modified Hertzian elastic contact model, the Johnson, Kendall, and Roberts (JKR) model, the specific adhesion energy between ligands and receptors at the interface can be quantified.

The aim of this work was to further develop the SCP-RICM method and apply the system to investigate ligand receptor interactions at soft, biomimetic interfaces (Figure 1). Specifically, there are three main aspects that were investigated in this work: I) the influence of mechanical properties or flexibility of the anchoring surface (Young's modulus of SCP material), II) the influence of ligand concentration at the interface (degree of functionalization of SCPs), III) the influence of ligand type (weak vs. strong ligand receptor pairs) attached to the soft interface.

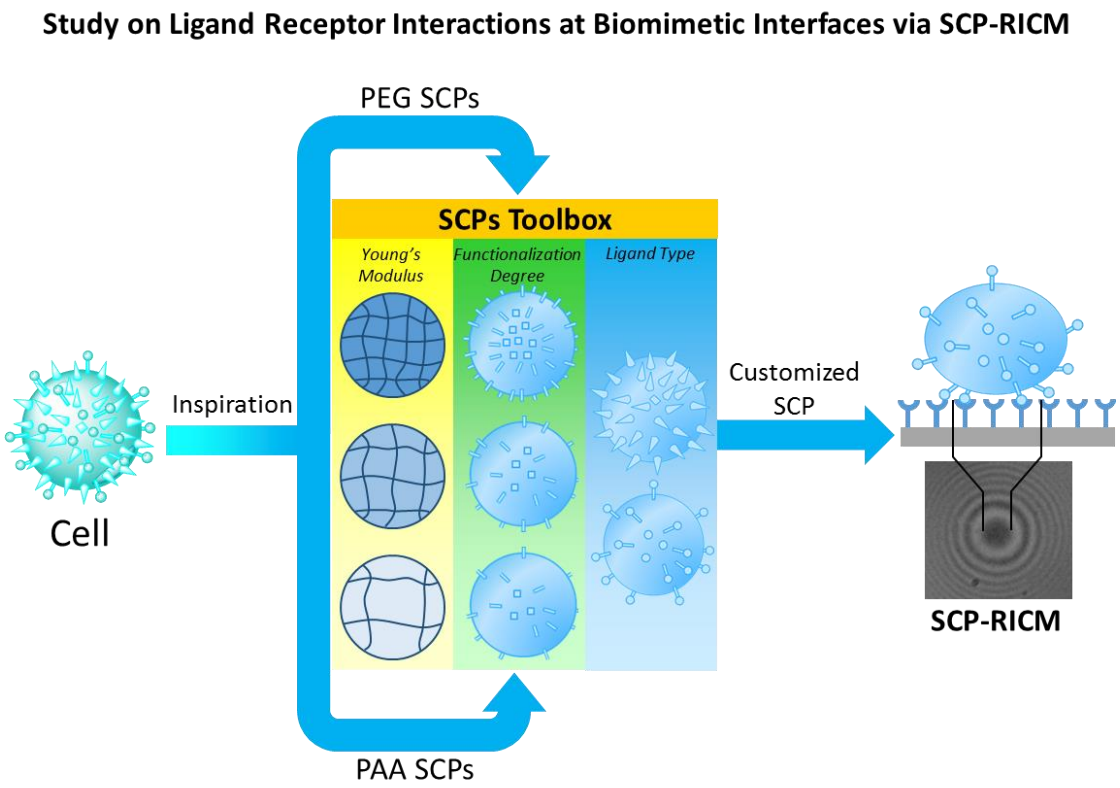

Figure 1: Schematic overview of this work: Inspired by cells, PEG SCPs and poly (acrylic acid) (PAA) SCPs with different Young's modulus, different degrees of functionalization, and different ligands were synthesized to give a SCP toolbox. With these customized SCPs, the influence of mechanical properties or flexibility of the anchoring surface, ligand concentration, and ligand type on ligand receptor interactions at biomimetic interfaces were investigated via SCP-RICM technique.

In the first part, the synthesis of SCPs with different Young's modulus was established. There are two approaches: I) By using a mixture of PEG-based macromonomers and crotonic acid during polymerization, the degree of cross-linking can be tuned and thus SPCs with different Young's modulus in a range of 16 kPa to 319 kPa were obtained. II) As an alternative to PEG SCPs, PAA SCPs were synthesized through inverse suspension polymerization and the degree of cross-linking was controlled by the cross-linker/monomer ratio. The Young's modulus of PAA SCPs were varied in a range of 7 kPa to 53 kPa.

In the second part, the functionalization of SCPs with different ligands and controlling the degree of functionalization was investigated. PEG SCPs with various Young's moduli were functionalized with crotonic acid via benzophenone photochemistry, and then further reacted with aminoethyl linked biotin and mannose via amide coupling. PEG SCPs with various Young's

moduli but similar degree of functionalization of mannose and biotin were obtained. This gave access to study the influence of mechanical properties and flexibility of the anchoring surface, as well as the influence of ligand type on ligand receptor interactions at biomimetic interfaces. PAA SCPs were functionalized with aminoethyl linked mannose via amide coupling and the degree of functionalization of mannose was varied by coupling mixtures of mannose ligand and non-ligand compound monoethanolamine (MEA) in a range of 0 mmol/g to 12.99 mmol/g. This gave access to study the influence of degree of functionalization of ligand on ligand receptor interactions at soft biomimetic interfaces.

In the third part, influence of Young's modulus, ligand concentration, and type were investigated through SCP-RICM experiments using the previously synthesized SCPs. Applying PAA-Man SCPs, it was found that higher ligand concentration leads to a higher overall adhesion energy. However, adhesion seems to reach a plateau when one of the binding partners (ligand or receptor) is saturated due to excess of the opposite binding partner. Investigating the adhesion of PEG-Man SCPs, it was found that higher Young's moduli of SCPs lead to increased adhesion most likely due to entropic effects. However, for PEG-biotin SCPs no dependency on the Young's modulus was observed. Potentially, here a cooperative binding of biotin on softer SCPs overcompensates for the loss of entropy in comparison to the harder SCPs. Cooperative binding in case of PEG-biotin was more likely compared to PEG Man SCPs due to the very large half-life of the biotin - avidin complex. In order to investigate these effects further, negatively charged PEG-CA SCPs were incubated on cationic polyelectrolyte surfaces. For such electrostatic interactions, it was found that higher Young's moduli of SCPs lead to stronger adhesion for PEG-CA SCPs in presence of salt while this effect is reversed in water. In absence of salt, charged groups undergo long range interactions and only the softer SCPs allow for more charged groups to interact with the surface. For the same system in the presence of salt, charges are now screened and similar to the results for the mannose system, entropy favours the adhesion of less flexible SCPs.

Overall, this thesis showed the Young's modulus and ligand functionalization degree can be controlled for PEG and PAA SCPs. The influences of Young's modulus, ligand concentration, and type on ligand receptor interaction were investigated. These new insights into ligand receptor interactions at soft interfaces will also promote the understanding of ligand receptor interactions in biological systems and to potentially design novel therapeutic strategies e.g. in antibacterial or anticancer therapy in the future.

Zusammenfassung

Ligand-Rezeptor-Wechselwirkungen bilden die Grundlage für eine Vielzahl biologischer Prozesse wie zum Beispiel der Zell-Kommunikation, der Invasion durch Krankheitserreger oder dem Zellwachstum. Daher ist es von großem Interesse diese Wechselwirkungen zu untersuchen und das Wissen über ihre biologische Funktion zu vertiefen. Diese Erkenntnisse können bei der Entwicklung und Optimierung von neuartigen Liganden eingesetzt werden, um natürliche Ligand-Rezeptor-Wechselwirkungen wie zum Beispiel den Befall durch Krankheitserreger zu inhibieren. Es existieren sowohl eine Vielzahl von theoretischen Modellen, aber auch experimentelle Methoden, um die Wechselwirkung zwischen Liganden und Rezeptoren, zum Beispiel bezüglich der Thermodynamik oder Bindungsaffinitäten, zu untersuchen. Jedoch lassen diese Methoden häufig nur Aussagen über die Interaktion zwischen einzelnen Ligand-Rezeptor-Paaren oder vollständig in Lösung befindlichen Ligand-Rezeptor-Systemen zu In der Natur finden diese Wechselwirkungen jedoch sehr häufig an weichen Oberflächen wie beispielsweise an Zelloberflächen statt, wo nicht nur eine, sondern eine Vielzahl von Liganden und Rezeptoren gleichzeitig interagieren.

Eine neuartige Methode, die sogenannte *soft colloidal probe - reflection interference contrast microscopy* (SCP-RICM), ermöglicht es, die Wechselwirkungen zwischen Liganden und Rezeptoren auf weichen, biomimemtischen Oberflächen zu untersuchen. Bei dieser Methode werden Mikrogele auf Basis von Polyethylenglycol (PEG) mit Liganden oder Rezeptoren funktionalisiert und dienen als stark vereinfachtes Modell der extrazelluären Matrix. Die korrespondierenden Liganden beziehungsweise Rezeptoren werden auf Glasoberflächen immobilisiert und bilden den Bindungspartner zur SCP. Nach Zugabe der SCPs auf die Glassoberfläche findet eine Bindung zwischen Liganden und Rezeptoren statt, welche zur Adhäsion der SCPs auf der Glasoberfläche führt. Da die SCPs weich sind, wird die Kontaktfläche durch die Deformation erhöht, in der die Liganden und Rezeptoren Wechselwirkungen eingehen. Durch die Analyse der Kontaktfläche mit dem von Johnson, Kendall und Roberts (JKR) modifizierten Modells der Kontaktmechanik, kann die spezifische Adhäsionsenergie zwischen Liganden und Rezeptoren an der Grenzfläche quantifiziert werden.

Das Ziel dieser Arbeit bestand darin, die SCP-RICM Methode weiterzuentwickeln und sie zur Untersuchung der folgenden Parameter von Ligand-Rezeptor-Wechselwirkungen an weichen, biomimetischen Oberflächen anzuwenden:

1. Der Einfluss der mechanischen Eigenschaften der verankernden Oberfläche (Elastizitätsmodul nach Young der SCPs) auf die Adhäsion.

2. Der Einfluss der Ligandenkonzentration an der Grenzfläche (Funktionalisierungsgrad der SCPs) auf die Adhäsion.

3. Der Einfluss der Art des Liganden (schwache bzw. starke Ligand-Rezeptor Paare), welche an den SCPs gebunden sind, auf die Adhäsion.

Im ersten Teil der Arbeit wurde hierzu die Synthese von SCPs mit verschiedenen Elastizitätsmodulen (E-Modul) etabliert. Dabei wurden zwei Ansätze verfolgt: I) Durch den Einsatz von Makromonomeren auf PEG-Basis und Zusatz von Crotonsäure während der Polymerisation, konnte der Vernetzungsgrad variiert werden, wodurch SCPs mit E-Modulen zwischen 16 kPa und 319 kPa synthetisiert wurden. II) Als Alternative zu PEG-SCPs wurden SCPs auf Basis von Polyacrylsäure (PAA) durch inverse Suspensionspolymerisation hergestellt. Der Vernetzungsgrad wurde durch das Verhältnis von Vernetzer zu Monomer kontrolliert. Das E-Modul der PAA-SCPs konnte in einem Bereich von 7 kPa bis 53 kPa variiert werden.

Im zweiten Teil der Arbeit wurde die Funktionalisierung der SCPs mit verschiedenen Liganden, sowie deren Funktionalisierungsgrad untersucht. PEG-SCPs mit verschiedenen E-Modulen wurden mittels Benzophenon-basierter Photochemie mit Crotonsäure funktionalisiert. Anschließend wurden Mannose und Biotin, nach vorheriger Modifizierung mit einer Aminoethyl-Gruppe, durch eine Amidkupplung kovalent an die SCPs gebunden. Dadurch wurden PEG-SCPs mit verschiedenen E-Modulen, aber dem gleichen Funktionalisierungsgrad erhalten. Auf dieser Grundlage konnte der Einfluss der mechanischen Eigenschaften oder der Flexibilität der verankernden Oberfläche, sowie der Einfluss der Art des Liganden auf die Ligand-Rezeptor-Wechselwirkungen an weichen Oberflächen untersucht werden. PAA-SCPs wurden mit Aminoethyl-Mannose durch eine Amidkupplung funktionalisiert, wobei der Funktionalisierungsgrad der Mannose durch die Zugabe von verschiedenen Mengen (0 mmol/g bis 12,99 mmol/g) Monoethanolamine (MEA) zur Reaktionslösung variiert wurde. Mit Hilfe der so erhaltenen PAA-SCPs konnte der Einfluss des Funktionalisierungsgrades auf die Ligand-Rezeptor-Wechselwirkungen an weichen, biomimetischen Oberflächen untersucht werden.

Im dritten Teil der Arbeit wurden der Einfluss des E-Moduls, der Ligandenkonzentration und Art des Liganden mittels SCP-RICM untersucht. Am Beispiel der PAA-SCPs konnte gezeigt werden, dass eine höhere Ligandenkonzentration eine größere Adhäsionsenergie zur Folge hat. Allerdings scheint die Adhäsion ein Plateau zu erreichen, sobald die Sättigung eines Bindungspartners (Ligand oder Rezeptor) durch einen Überschuss des gegenteiligen Bindungspartners erreicht ist. Bei der Untersuchung der Adhäsion der PEG-Man-SCPs konnte beobachtet werden, dass ein größeres E-Modul der SCPs zu einer höheren Adhäsion führt, was mutmaßlich auf entropische Effekte zurückzuführen ist. Für die PEG-Biotin SCPs konnte kein Einfluss des E-Moduls beobachtet werden. Es ist möglich, dass eine kooperative Bindung von Biotin auf weicheren SCPs die entropischen Effekte auf härteren SCPs überkompensiert. Im Fall der Biotin-SCPs sind kooperative Bindungen wahrscheinlich, da der Biotin / Avidin-Komplex eine sehr hohe Halbwertszeit aufweist. Um diesen Effekt tiefergehend zu untersuchen, wurden anionisch geladene PEG-CA SCPs auf einer kationischen Oberfläche inkubiert. Bezüglich der elektrostatischen Wechselwirkungen konnte festgestellt werden, dass ein größeres E-Modul zu einer stärkeren Adhäsion für PEG-CA SCPs in Anwesenheit von Salz führt, während der umgekehrte Effekt ohne Salz beobachtet wurde. Ohne Zusatz von Salz gehen die geladenen Gruppen weitreichende Wechselwirkungen ein und lediglich weichere SCPs ermöglichen es, dass mehrere Gruppen an der Oberfläche interagieren.

Zusammenfassend wurde im Rahmen dieser Arbeit gezeigt, dass das E-Modul und der Funktionalisierungsgrad der Liganden bei PEG und PAA SCPs kontrolliert werden kann. Mit Hilfe der so erhaltenen Modellsysteme wurde dann der Einfluss des E-Moduls, der Ligandenkonzentration und der Art des Liganden bei Ligand-Rezeptor-Wechselwirkungen an weichen Oberflächen untersucht. Es konnte gezeigt werden, dass alle drei Parameter Ligand-Rezeptor vermittelte Adhäsion beeinflussen und insbesondere die Art des Liganden und der Einfluss des E-Moduls eng miteinander verknüpft sind. Diese neuen Erkenntnisse bezüglich Ligand-Rezeptor-Wechselwirkungen an weichen Oberflächen ermöglichen somit potenziell neuer Erkenntnis auch in biologischen Systemen und könnten bei der Entwicklung neuartiger Therapiemethoden z.B. antibakterieller Therapien helfen.

1. General Introduction

1.1 Ligand Receptor Interaction

Ligands are molecules which can form complexes with other molecules through non-covalent interactions, such as hydrogen bonds, [1] ionic bonds, [2] van der Waals forces, [3] or hydrophobic interactions. [4] [5] In biochemistry, especially for molecular recognition, this complex usually contains one protein receptor and a species specifically recognized by this receptor - the ligand. Well-known examples for such ligand receptor systems are antibodies binding to antigens, [6] enzymes binding to a substrate, [7] or proteins to a DNA double helix. [8] Often, a protein receptor has one or more binding sites on its surface that can accommodate the according ligand. [9] The way the ligand binds to the receptor is often described as a key fitting into a lock, [10] so a rather exact fit of two rigid objects. Also other fitting types were introduced such as induced fit, where a protein receptor will alter its confirmation to fit its corresponding ligand; [11] and flexible fit, where a protein receptor has several altered confirmations for its corresponding ligand to fit in. [12] Nowadays, it is generally accepted that the ligand receptor interaction is like 'handshake', where protein receptor and ligand change their confirmation and adapt to each other, in a mutual fit (Figure 2), [13] [14] and the binding between ligand and receptor is not permanent but reversible. [15]

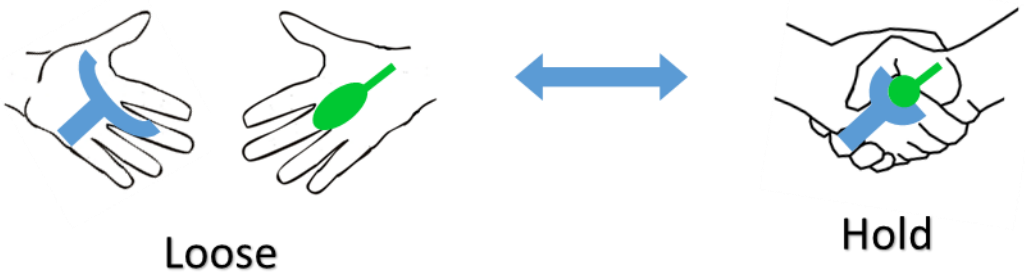

Figure 2: The reversible binding process of ligand receptor interaction, where blue symbol stands for a receptor, green symbol stands for a ligand. When receptor and ligand meet each other, both will change their conformation to fit to each other.

The ligand receptor interaction process can be described with the following equation:

$$L + R \rightleftharpoons LR \qquad \textbf{Equation 1}$$

, where L is ligand, R is receptor, LR is the complex of ligand and receptor.

At equilibrium state, the binding and unbinding should be balanced, which is described as:

$$k_{on}[L][R] = k_{off}[LR] \qquad \textbf{Equation 2}$$

, where k_{on} is the binding rate constant, k_{off} is the unbinding rate constant, $[L]$ is the ligand concentration, $[R]$ is the receptor concentration, $[LR]$ is the concentration of ligand receptor complex. The rate constant k describes how fast the ligand and receptor binds (k_{on}) and unbinds (k_{off}).

In order to further evaluate the affinity of ligand and receptor, two other constants are introduced:

$$K_a = \frac{1}{K_d} = \frac{k_{on}}{k_{off}} = \frac{[LR]}{[L][R]} \qquad \textbf{Equation 3}$$

, where K_a is association constant, K_d is the dissociation constant. K_a describes the propensity of the ligand and receptor to bind, K_d describes the propensity of the ligand receptor to unbind. These two constants play as an index of the ligand receptor affinity, which means association constant K_a is a quantitative associate of the qualitative term 'affinity'. [9]

The affinity of a ligand depends on a range of intermolecular forces when binding to the receptor as mentioned before, e.g. hydrogen bonding but also the release of the hydration shell from ligands and receptors upon binding. [16] At a single bond level, these forces are usually weak. (See Table 1) Even strong ligand receptor interactions like biotin and avidin amount to only 35 k_BT, [17] far lower as compared to covalent interactions, where a common covalent bond amounts in a range of 100 - 300 k_BT. [18] On the other end of the scale, carbohydrate ligands are often viewed as very weak ligands with only a few k_BT, [19] [20] e.g. the mannose Con A amount to ca. 5 k_BT. [21] Nevertheless, carbohydrate ligands play an enormously important role in biology, e.g. in processes like cell adhesion or [22] signalling in inflammation [23] are controlled by interactions between carbohydrate ligands and protein receptors. Here, an additional factor comes into play, the so-called multivalency. [24] In order to achieve binding of very weak ligands, several ligands can interact simultaneously with several receptors or binding sites of a receptor. [25] The overall affinity can then be increased by orders of magnitude e.g. through, several ligands covalently linked together as a cluster and allowing for multivalent binding. [26] A famous example is the interaction of Shiga-like toxins and tailor made multivalent carbohydrate ligands leading to an

increase in binding affinity of a factor of 1 - 10E6 for the multivalent ligand in comparison to the monovalent ligand. [27]

Table 1: Interaction energy of various secondary forces. [28]

Interaction Parameter	Interaction Energy [kJ/mol]
Covalent or chemical bonding forces	200-800
Charge-charge	600-1000
Interactions between polar molecules	<40
Dispersion forces	~1
Hydrogen bonding	10-40
Hydrophobic interactions / Hydrophilic interactions	<20

Remark: 1 k_BT = 2.476 kJ/mol at 298 K.

The multivalent interaction of several ligands thus is of great biological importance but also still gives rise to many questions in terms of the underlying mechanism. In principle, multivalent ligand receptor binding can be classified into three types: positively cooperative binding (synergistic binding), where the binding of first ligand will make it easier for the binding of the next ligand; non cooperative binding (additive binding), where the binding of first ligand has no influence on the binding of the next ligand; and negatively cooperative binding (interfering binding), where the binding of first ligand will make it more difficult for the binding of the next ligand. [9] This theory can also be described with the following equation:

$$\Delta G_{ave}^{multi} = a\Delta G^{mono} \qquad \textbf{Equation 4}$$

, where ΔG_{ave}^{multi} is the average free energy of binding between a single ligand and receptor in a multivalent binding event, a is the degree of cooperativity, ΔG^{mono} is the free energy of binding between a single ligand and a single receptor in an analogous monovalent binding event. When $a>1$, it is positively cooperative binding. When $a=1$ or $a<1$, it is non cooperative binding or negatively cooperative binding correspondingly.

The free energy is defined with the following equation:

$$\Delta G = \Delta H - T\Delta S \qquad \textbf{Equation 5}$$

, where ΔG is the change of free energy, ΔH is the change of enthalpy, T is temperature, ΔS is the change of entropy. [29] Thus, both enthalpic and entropic contributions play a role for the binding event.

First, looking at a rigid cluster of ligands, multivalent binding is usually unfavored by the enthalpy, which means the binding of the first ligand is more favourable than the following one. This can be the case when the bonds connecting the ligands have to be strained to allow for binding of both (or more) ligands. Only when the geometry of the cluster of ligands and receptors matches precisely, the multivalent binding can be achieved without any strain force. (See Figure 3) [9]

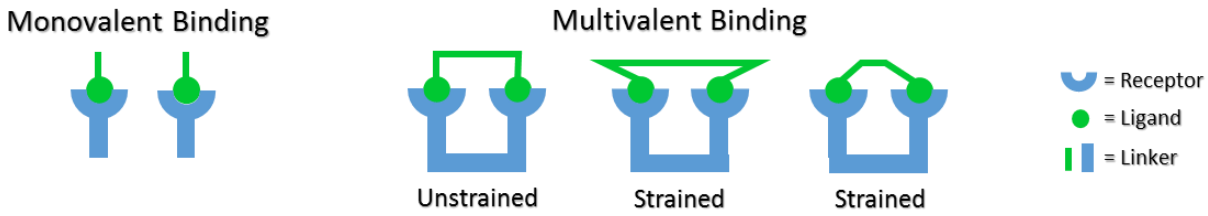

Figure 3: Multivalent binding events affected by the aspect of enthalpy. Divalent binding is used as a highly simplified 2D example for multivalent binding. In the unstrained case, the distance between two ligands on scaffold is the same as the distance between two receptors on scaffold. In the strained case, the distance between ligands is either longer, or shorter than the distance between two receptors.

In the case of entropy, the total entropy of a multivalent binding can be described with the following equation:

$$\Delta S_N^{multi} = \Delta S_{trans,N}^{multi} + \Delta S_{rot,N}^{multi} + \Delta S_{conf,N}^{multi} + \Delta S_{water,N}^{multi} \qquad \textbf{Equation 6}$$

, where ΔS_N^{multi} is the total entropy change during a multivalent binding event, $\Delta S_{trans,N}^{multi}$ is the entropy change of translational freedom of ligands and receptors moving from one to another point through space, $\Delta S_{rot,N}^{multi}$ is the entropy change of rotational freedom of ligands and receptors rotating around all three of its principle axes, $\Delta S_{conf,N}^{multi}$ is the entropy change of conformation changing freedom of ligands and receptors, $\Delta S_{water,N}^{multi}$ is the entropy change of releasing water molecules from the water shell of ligands and receptors when they bind. [9]

When ligands and receptors are connected on a rigid cluster, if the geometry of ligand cluster and receptor cluster can precisely match, only the binding of the first ligand will have an entropy cost. For the binding of the next ligand no or only very little additional entropy has to be paid.

While it is still relevant for many systems to look at a rigid cluster of ligands and receptors, it is now more and more evident, that most clusters of ligands or receptors are somewhat flexible in nature, e.g. ligand receptor binding on lipid bilayers. (See Figure 4) [30]

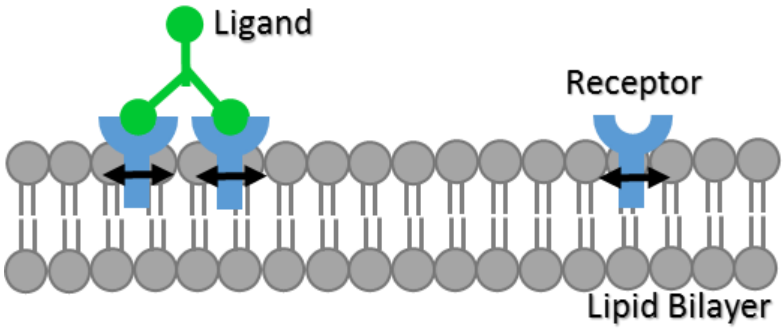

Figure 4: Multivalent ligand receptor interaction at lipid bilayer, where the cluster of receptors on lipid bilayer is flexible as they can flow with the lipid molecules.

When now looking at the free binding energy of more flexible ligand or receptor cluster, different enthalpy and entropy contributions come into play. In principle, conformational entropy is always lost when one ligand of a ligand cluster binds whether it is the first or a following binding. After the first ligand from a ligand cluster binds to a receptor cluster, the conformational entropic cost of binding another ligand from a second ligand cluster can exceed the translational and rotational entropic cost of binding another ligand from the first ligand cluster. So, the second ligand binding of a ligand cluster on the same receptor cluster is usually diminished. (See Figure 5) [9]

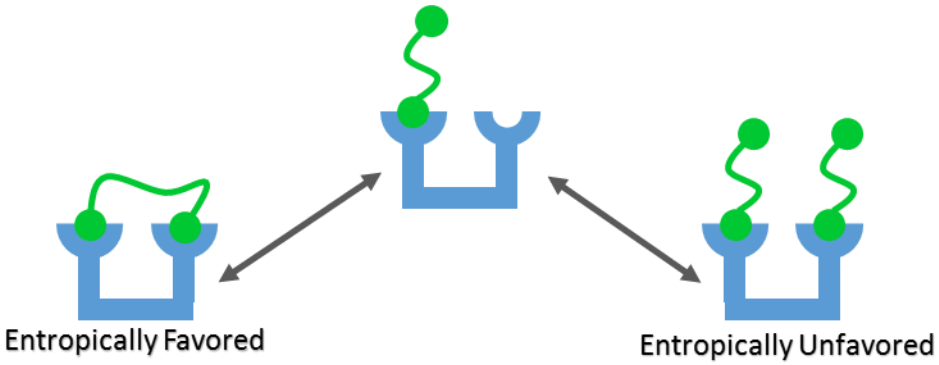

Figure 5: Multivalent binding events affected by the aspect of entropy. Divalent binding is used as a highly simplified 2D example for multivalent binding. After the binding of the first ligand cluster on a receptor cluster, the binding of the second ligand from the first ligand cluster is more entropically favoured than the binding of the second ligand from the second ligand cluster.

Looking at the enthalpy, a more flexible cluster of ligands or receptors usually means a gain in enthalpy with every ligand receptor interaction. Thus, the loss in entropy when binding with a more flexible cluster might be compensated by a gain in enthalpy from the potentially higher number of ligand receptor interactions. For both cases, rigid or more flexible clusters, positively cooperative binding, non-cooperative binding, or negatively cooperative binding is possible and depends on the interplay of the different entropic and enthalpic contributions in this multivalent binding event.

1.2 Methods to Investigate Ligand Receptor Interaction

For the investigation of ligand receptor interactions e.g. in terms of their kinetics and thermodynamics, different well-established techniques are available e.g. surface plasmon resonance spectroscopy, [31] isothermal titration calorimetry, [32] atomic force microscopy, [33] and so on. The following chapter will highlight a few methods used for ligand receptor binding studies with a special focus on ligand receptor binding at surfaces.

1.2.1 Surface Plasmon Resonance Spectroscopy (SPR)

Surface plasmon resonance spectroscopy is a method that applies the resonant oscillation of evanescent wave and plasma wave in a metal surface to detect the absorption of material onto this planar metal surface. [34]

Most of the commercially available SPR set-ups use the Kretschmann configuration [35] as detection scheme. Briefly, a laser passing through a prism is shot on the metal surface back side of a chip sensor, and then is reflected to a laser detector. At a certain incident angel, the light is absorbed by the electrons on the metal surfaces and causes the surface plasmon resonance. Thus, a dark band appears on the laser detector. As surface plasmon is sensitive to its surrounding environment, any changes on the front side of the chip sensor can cause a different surface plasmon resonance angel, and the corresponding dark band will also be shifted. Through detecting the

change of the dark band position, the change of chip sensor surface can be detected. There are several assay formats for SPR measurement. (See Figure 6)

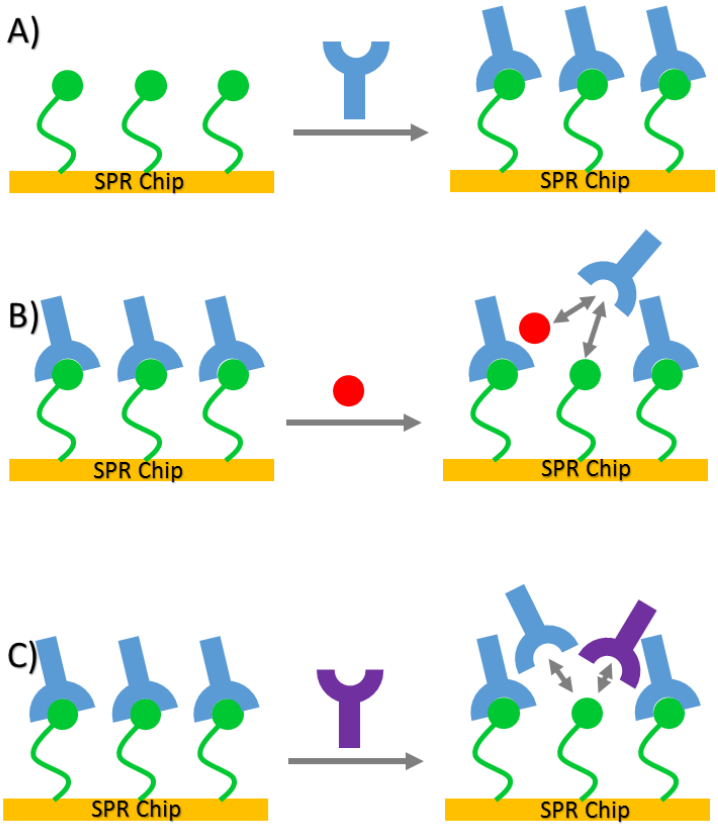

Figure 6: Schematic illustration of SPR assay formats. A) Direct binding assay: the ligands are attached to the SPR chip and the receptors (usually molecular weight ≥ 5000 Dalton) are injected. B) Inhibition assay (solution competition assay): Ligands are attached to the SPR chip while the receptors binds to the ligands. Then a constant amount of competing ligands is injected. C) Surface competition assay: Ligands are attached to the SPR chip while the receptors bind to the ligands. Then a constant amount of competing receptors is injected. Two types of receptors are competing for binding with the ligands on SPR chip surface.

Due to its real-time, [36] label-free, [37] and non-invasive nature, [38] SPR plays an important role in biochemistry, biology and pharmaceutical science. The method allows determination of ligand receptor affinity, by various modes, can also measure the ligand receptor association constant and half maximal inhibitory concentration (IC_{50}), [39] for example, screening for antibody affinity, [40] and multivalent interactions between selectins and polyglycerol surfaces. [41]

1.2.2 Atomic Force Microscopy (AFM)

Atomic force microscopy is a type of nanoscale high resolution scanning probe microscope, which was introduced by Binnig, Quate, and Gerber in 1980s. [42] AFM has been applied in imaging and surface topological study due to its atomic level resolution and compatibility to both conductor and insulator. Since the early 1990s, AFM is also routinely used to collect the force information between the AFM tip and substrate surfaces. [43] Because the measurement environment for AFM tip can be either air or aqueous solutions, AFM were also widely used in biochemistry and biological studies, e.g. single molecular force spectroscopy of polysaccharides. [44]

In Scheme 1, a typical AFM apparatus is shown. In typical bio AFM setups, a cantilever with a tip is held by quartz glass which is connected to a piezo. The piezo will control the movement of the tip. A laser is shot onto the backside of cantilever and then reflected to the detector. When the tip senses a force from the measurement substrate, the cantilever will be bended by this force. As a result, the reflected laser will move its position from one point to another on the detector. [45]

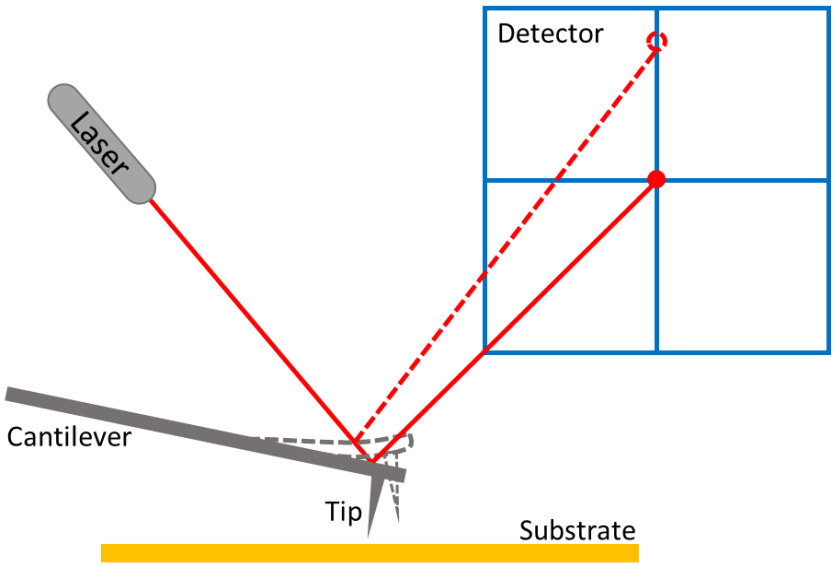

Scheme 1: Schematic setup of atomic force spectroscopy. When the AFM tip senses a force from substrate, the cantilever will be bended, thus the laser reflection route will be changed and the laser will shoot on a different point on the laser detector.

When using AFM to measure the ligand receptor interactions, the surface substrate can be functionalized with receptors, and the AFM tip will be functionalized with the corresponding ligands. Then, the cantilever will approach the surface and ligands and receptors are binding. When retracing the cantilever, the cantilever will be bended, due to the binding forces between the ligands and receptors. Since the binding force is not as strong as the restoring force of the cantilever, the ligands and receptors will be separated, and the cantilever will recover to its original shape. The force required to separate ligands and receptors gives the characteristic rupture force of the complex. The raw data is recorded in the form of the position change of the piezo ΔZ_p versus the volt change measured by the detector ΔV. Upon determining the information of cantilever sensitivity and the spring constant of cantilever. The data can be transformed into distance versus force.

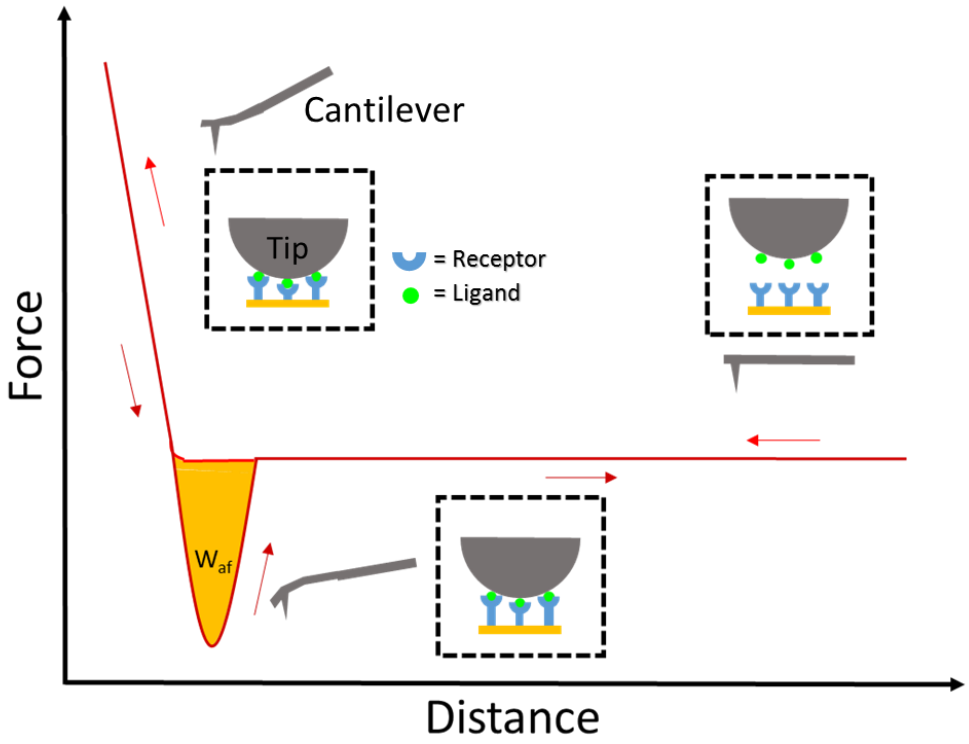

Figure 7: Atomic force spectroscopy force measurement to investigate ligand receptor interactions at bio-interfaces, where W_{af} is the overall binding affinity energy between ligands and receptors. [46]

With AFM method, the binding strength of ligand and receptors can be characterized. For example, molecular interaction between bacteriophages and lipopolysaccharide bilayers, [47] and adhesion forces between individual biotin avidin ligand receptor pairs. [3] Comparing to SPR,

AFM makes it possible to investigate single ligand receptor binding event, and the ligand receptor binding event at solid interface.

1.3 Soft Colloidal Probe - Reflection Interference Contrast Microscope

In the previous chapter, different methods to analyse ligand receptor binding were introduced. However, most methods detect only the ligand receptor interactions in solution, e.g. fluorescence, [48] various colorimetric immune assays; at liquid/solid interfaces, e.g. SPR [49]; or in the circumstances of single ligand receptor interactions, e.g. AFM. [50] In order to detect the ligand receptor interactions at soft solid interfaces, SCP-RICM technique was developed in previous work by Daniel Pussak. [51]

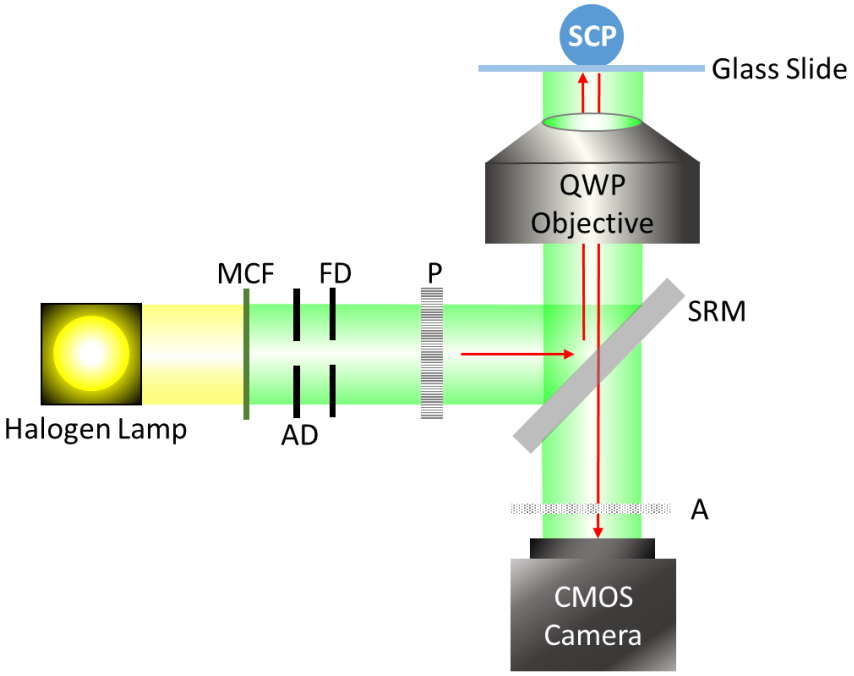

Scheme 2: Schematic setup for and optical path for reflection interference contrast microscope (RICM), where MCF is monochrome filter, AD is aperture diaphragm, FD is field diaphragm, P is liner polarizer filter, SRM is semi-reflecting mirror, A is analyser, QWP objective is quarter wave plate equipped objective.

Scheme 2 shows a typical setup of RICM with its optical path. A halogen lamp is typically used as the working light source. The light beam is firstly filtered by a monochrome filter. Then, the monochrome light beam passes through two adjustable diaphragms, which are called aperture diaphragm and field diaphragm. These two diaphragms will realize an extremely even Köhler illumination. [52] The followed linear polarizer makes the light into a polarized light. Then, the light beam reaches a semi-reflecting mirror, which can reflect the light beam, as well as let the light beam pass through. The original incident light will be reflected to the quarter wave plate (QWP) equipped objective. This objective can convert the linear polarized light beam into circular polarized light beam, which will subsequently be reflected and transmitted by the glass slides and the SCP. The reflected light will pass through the QWP objective again and be converted back to linear polarized light, but the direction will be turned 90° comparing to the incident light. Finally, the light will pass through an analyser and reach the CMOS camera. The interference pattern will be recorded on the camera for further analysis. [53]

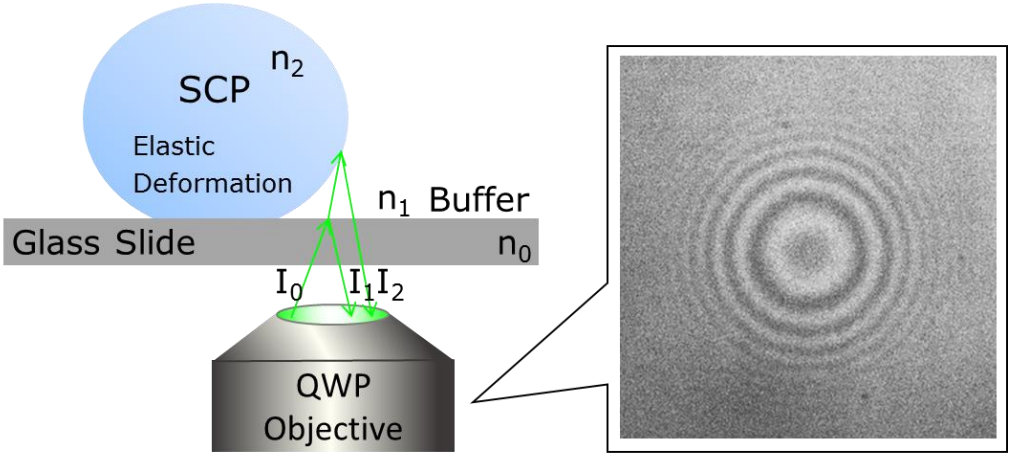

Scheme 3: Schematic representation of reflection interference contrast microscope principle and the interference pattern of a soft colloidal probe on a glass slide.

The principle of interference is shown in Scheme 3. Part of polarized light (I_0) is reflected by the glass slide / buffer interface as I_1, part of the polarized light (I_0) is reflected by the SCP / buffer interface as I_2. The light intensity at a certain position on the image is calculated from the following equations:

$$I(x) = I_1 + I_2 + 2\sqrt{I_1 I_2}\cos(2kh(x) + \pi) \qquad \textbf{Equation 7}$$

$$k = 2\pi n/\lambda \qquad \textbf{Equation 8}$$

, where n is the refraction index of water, λ is the wavelength of the polarized monochromatic light.

Due to the different light intensity at different positions, Newton rings are formed as the interference pattern. [54] The first minimum light intensity ring is generated, when the SCP touches the surface of glass slides. Thus, the radius of the first minimum light intensity ring shows the contact radius.

In order to calculate the adhesion energy between the SCP and the substrate surface, Johnson, Kendall, and Roberts (JKR) model, which was developed in 1971, can be applied in RICM experiments. Comparing to the classic Hertzian theory of non-adhesive elastic contact, JKR model describes an elastic contact with considering the adhesion inside the contact area. [55] For contact between two spheres, the Hertz equation according to JKR model is written below:

$$a^3 = \frac{3R}{4E}\left(F + 3W\pi R + \sqrt{6W\pi RF + (3W\pi R)^2}\right) \qquad \textbf{Equation 9}$$

, where a is the contact radius, R is the effective radius, E is the effective Young's modulus, F is the loading force to push one sphere to the other, W is the adhesion energy at the contact area between two surfaces.

The effective radius R and effective Young's modulus E is calculated as below:

$$\frac{1}{R} = \frac{1}{R_1} + \frac{1}{R_2} \qquad \textbf{Equation 10}$$

$$\frac{1}{E} = \frac{1-\vartheta_1^2}{E_1} + \frac{1-\vartheta_2^2}{E_2} \qquad \textbf{Equation 11}$$

, where R_1, R_2 is the radius of the two spheres, E_1, E_2 is the Young's modulus of the two spheres.

As in the SCP-RICM experiment, the contact is between a hydrogel microparticle (SCP) and a glass slide. Comparing to the SCP, the radius of the glass slide and the Young's modulus of the glass slide can be considered to be infinitely large. [56] Thus, $\frac{1}{R_{glass}}$ and $\frac{1-\vartheta_{glass}^2}{E_{glass}}$ are zero and the above equations can be written as:

$$R = R_{SCP} \qquad \textbf{Equation 12}$$

$$E = \frac{1}{1-\vartheta_{SCP}^2} E_{SCP} \qquad \textbf{Equation 13}$$

, where R_{SCP} is the radius of SCP, ϑ is the Poisson ratio of SCP, E_{SCP} is the Young's modulus of the SCP.

In the SCP-RICM experiment, the SCPs sediment on the glass surface without any extra loading force, which means the loading force F equals zero. The Hertz equation according to JKR model can be transformed to:

$$a^3 = \frac{3R}{4E}\left(0 + 3W\pi R + \sqrt{0 + (3W\pi R)^2}\right) = \frac{3R}{4E} \times 6W\pi R \qquad \textbf{Equation 14}$$

When substituting the R with RSCP, and E with ESCP, the JKR model can be further transformed as:

$$a^3 = 6\pi \frac{W}{\frac{4}{3}E_{SCP}/(1-\vartheta^2)} R_{SCP}^2 \qquad \textbf{Equation 15}$$

The adhesion energy between SCP and the substrate surface is calculated as:

$$W = \frac{\frac{4}{3}a^3 E_{SCP}/(1-\vartheta^2)}{6\pi R_{SCP}^2} \qquad \textbf{Equation 16}$$

In this work, the hydrogel SCPs are assumed to be incompressible material, so the Poisson ratio will be 0.5. [57] The Young's modulus of SCPs needs to be determined as part of the measurement e.g. in an additional experiment by AFM.

1.4 Synthesis of Hydrogel Microparticles as Soft Colloidal Probes

1.4.1 Methods to Synthesize Polymer Particles

There are several methods to make polymer particles. Depending on the reaction scheme, they are classified as following:

Suspension Polymerization

Suspension polymerization is a free radical polymerization process where water insoluble monomers and initiators are suspended in water under vigorous agitation. Polymerization occurs in each monomer droplet. Within these droplets, the polymerization can be considered as bulk polymerization. [58] When water soluble monomers are used as suspended phase and oil is used as continuous phase, the reaction is called an inverse suspension polymerization. [59] The acquired particle size is normally in a range of 10 - 1000 µm, [60] which is negatively correlated to the stirring speed during polymerization. [61]

Precipitation and Dispersion Polymerization

Precipitation polymerization refers to the reaction where monomer and initiator are completely soluble in the continuous phase, while the polymeric product is insoluble and thus precipitates. After precipitation, the polymerization proceeds on the surface of precipitated polymer particles, which contain an active free radical chain end can further catch monomers and precipitated oligomers from the solution. [62] [63] In dispersion polymerization, a dispersant, e.g. a polymer or inorganic dispersant, is used to stabilize polymer particles in solution. When the insoluble polymer product is formed, it can form particles dispersed in the continuous phase and further react. These particles are the main locus of polymerization. Due to the addition of dispersant, the resulting particles from dispersion polymerization are more regular than the particles from precipitation polymerization. [64] The resulting particle size from precipitation polymerization usually is in a range of 0.1 - 10 µm, and the particles size from dispersion polymerization stays in a range of 0.5 - 10 µm. [60]

Emulsion Polymerization

Emulsion polymerization is a traditional free radical polymerization method developed a century ago to give straightforward access to a large variety of polymer particles. [65] However, the mechanism of emulsion polymerization remained unknown, until Harkins, [66] Smith, and Ewart [67] developed the first successful theory to explain the process. There are three intervals in the emulsion polymerization process. In the first interval, oil soluble monomer is added to the continuous water phase and forms large droplets with the help of emulsifier under agitation. At the meantime, excess emulsifier will form small micelles, which is the aggregate of emulsifier molecules in water phase. Small number of monomers will diffuse to micelles from monomer droplets. Water soluble initiators are also added to the system. In the second interval, the free radical polymerization is initiated in the micelles. Along with the depletion of monomers in micelles, more monomers also diffuse into the micelles to keep the polymerization going on. As a result, the size and amount of monomer droplets is decreasing at this moment. In the third interval,

all the monomers have diffused into micelles and monomer droplets disappear. The polymerization in micelles is terminated due to the lack of polymerizable monomer.

The particles size from emulsion polymerization normally stays in a range of 50 - 130 nm. When emulsifier free emulsion polymerization is applied, the particle size stays in a range of 0.1 - 1 μm. [60]

1.4.2 Synthesis and Functionalization of PEG based SCPs

1.4.2.1 Synthesis of PEG SCPs via Precipitation Polymerization

PEG is a highly water-soluble polymer. The solubility of PEG with a molecular weight of 8000 Da as was used in this work reaches almost 630 mg/mL, [68] which is 63 wt. % in water, at 20 °C. Nevertheless, PEG can be made water insoluble forming droplets in water that allow for chemical crosslinking of such droplets and straightforward synthesis of PEG microgels. [69]

In order to change water from a good solvent for PEG to a poor solvent for PEG, it is possible to elevate the temperature of PEG aqueous solution above its lower critical solution temperature (LCST). Above the LCST, water becomes a poor solvent for the polymer, where water expands much rapidly than PEG. The combination of water molecules to PEG results a loss of entropy, which is entropically unflavoured. Thus, without combining with water, PEG cannot be dissolved in water, and water becomes a poor solvent for PEG. [70] For example, the PEG 8000 Da aqueous solution can be separated into a PEG rich phase and PEG poor phase above 121 °C, [71] [72]. The other strategy is to use kosmotropic salts to lower the LCST of PEG to room temperature. The potential salts can be selected through the Hofmeister series. Hofmeister series is a classification of ions according to their influence on the dissolution behaviour of macromolecules and proteins. [73]

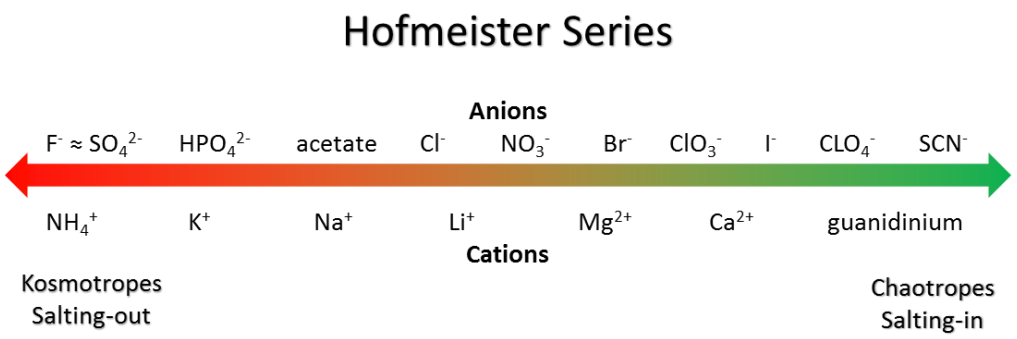

Figure 8: Hofmeister Series show the classification of anions and cations according to their influence on the phase behaviour of macromolecules and proteins.

In the above figure, the ions on the left side are called kosmotropes. They can increase solvent surface tension and strengthen the hydrophobic interaction. In other words, they can stabilize the construction of water-water interactions and intramolecular interactions of macromolecules and proteins, which will lead to the salting out or precipitation of macromolecules. The ions on the right side are called chaotropes. They can weaken the hydrophobic effect and disrupting water-water structure. Thus, chaotropes will lead to the salting in of macromolecules and denaturation of proteins. [74] [75]

By using sodium sulfate as kosmotropic salt, the LCST of PEG can be decreased below room temperature. This effect was then used to synthesize PEG hydrogel microparticles for later use as SCPs. Pussak *et. al.* used PEG-diacrylamide (PEG-dAAm) as reactive macromonomers for radical crosslinking and formation of hydrogel microparticles. [51] In short, PEG-dAAm was precipitated in sodium sulfate solution and the solution was separated into a PEG rich phase and a PEG poor phase. Upon vigorous shaking of both phases, the PEG rich phase was dispersed into micro meter sized droplets by shear force. Next, in order to initiate the free radical polymerization of the acrylamide groups cross-linking the PEG chains in the micro meter level droplets, a commercially available water soluble free radical photo initiator Irgacure 2959 was added to the PEG-dAAm solution. The micro meter level droplets were then photopolymerized by applying short time UV irradiation.

1.4.2.2 Procedures to Control the Functionalization Degree of PEG SCPs via Carboxylic Acid Functionalization

The functionalization of PEG SCPs with carboxylic group was achieved by benzophenone grafting method. Briefly, under UV irradiation, benzophenone is excited to its triplet state and has the ability to abstract a hydrogen atom from the backbone of the PEG chain. Thus, a free radical is formed on the PEG chain. When adding carboxylic acids with an unsaturated carbon-carbon bond, e.g. acrylic acid, free radical polymerization can be initiated by this radical and the carboxylic acid monomer will be grafted onto the PEG chain. Hence, the carboxylic groups can be introduced to the PEG hydrogel network.

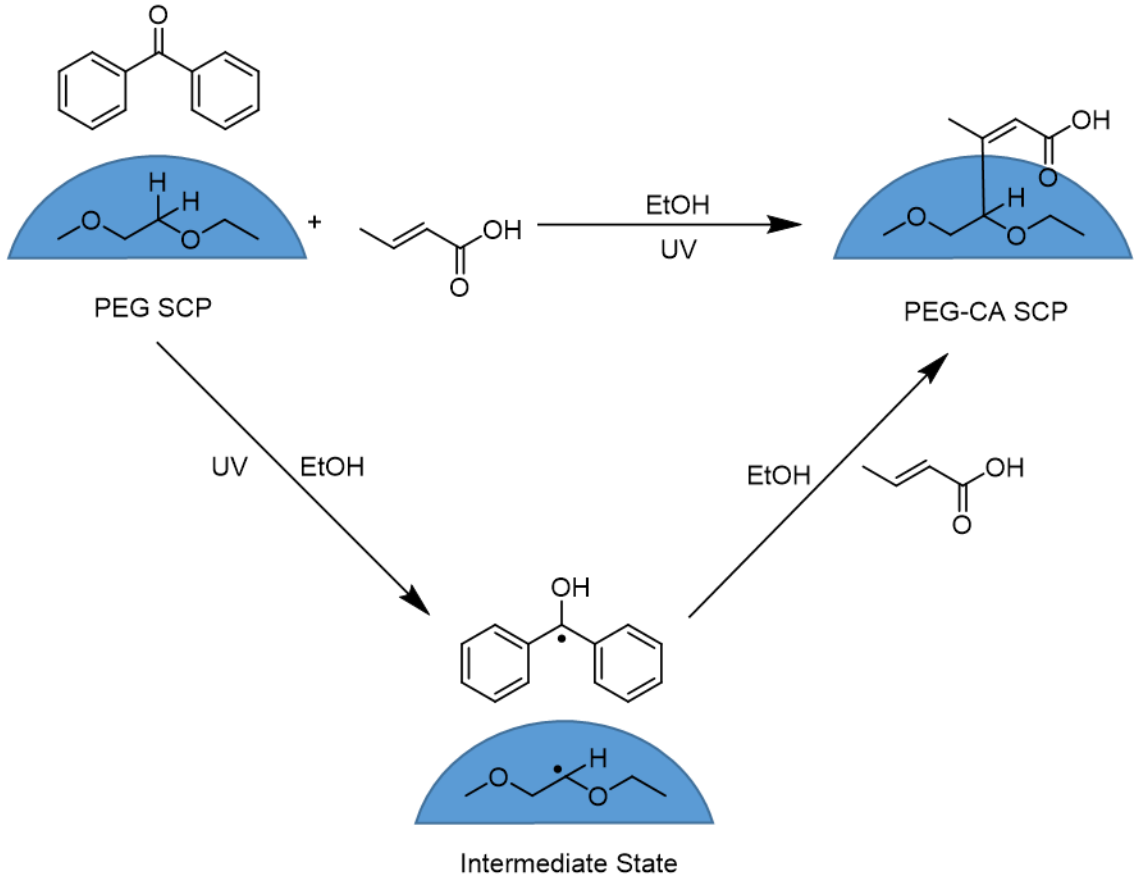

Scheme 4: Reaction scheme of crotonic acid functionalization of PEG hydrogel based SCPs through benzophenone radical surface chemistry. [51]

In order to control the carboxylic group functionalization degree, two procedures based on this method were developed previously together with Stephan Schmidt and Daniel Pussak [76] [77]

and were applied in this work to tune the degree of functionalization of PEG-c-CA SCPs with different Young's modulus.

Grafting of Single or Polymeric Carboxylic Groups

The approach to graft acrylic acid and its derivatives via the benzophenone method does not only allow to tune the concentration of carboxylic groups on the SCPs but also to realize different presentations of the carboxylic groups, e.g. single groups or oligomeric chains. Therefore, acrylic acid, and its derivatives methacrylic acid, crotonic acid were used to functionalize the PEG hydrogel based SCPs. Due to their different reactivity in free radical polymerization, following the previously established method, [76] crotonic acid functionalized PEG SCPs (PEG-CA) with a degree of functionalization of ~ 50 µmol/g were obtained. When changing the carboxylic acid from crotonic acid to acrylic acid (AA) while keeping the reaction conditions constant, the degree of functionalization of PEG-AA reached ~100 µmol/g. When using methacrylic acid (MA), which has the highest reactivity in free radical polymerization among these three carboxylic acids, an even higher degree of functionalization of ~ 250 µmol/g was obtained. Here the difference in degree of functionalization stems from the difference in grafting type. As has been reported in literature, [76] it can be expected that acrylic acid undergoes grafting onto mechanism, while methacrylic acid undergoes grafting from mechanism. Crotonic acid cannot be homopolymerized and thus should mainly lead to single carboxylic groups. [78] [77]

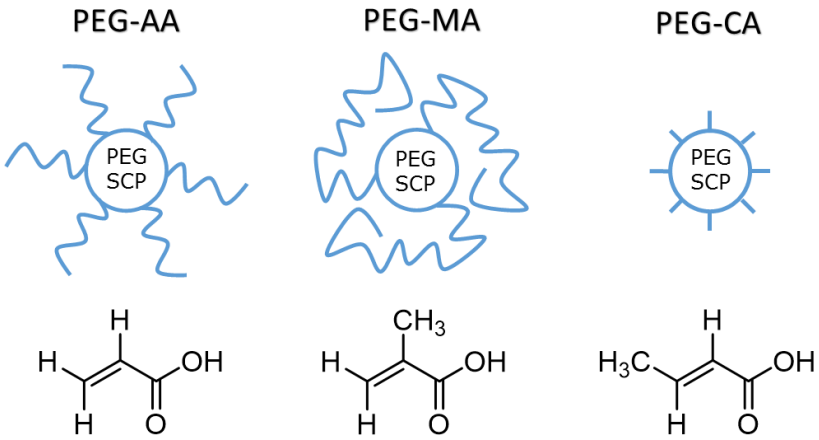

Figure 9: Different grafting types of PEG-AA SCPs, PEG-MA SCPs, and PEG-CA SCPs

Multiple Grafting with Crotonic Acid

When only using crotonic acid in order to achieve mainly single carboxylic acid groups on the SCPs, increasing the degree of functionalization cannot be achieved by using higher concentrations or longer irradiation times. This is most likely due to a hindered diffusion of the reactants in the hydrogel as well as a short lifetime of the radicals required for the grafting process. In order to overcome these limitations, the reaction solution was exchanged with fresh reaction solution after several irradiations to replenish with fresh reactants and increase the overall reactant concentration. Through this multiple solution exchange, more grafting points were created on the backbone of PEG chain. Through controlling the total irradiation time and the number of the used fresh solution, the carboxylic group functionalization degree can be tuned. [76] [77]

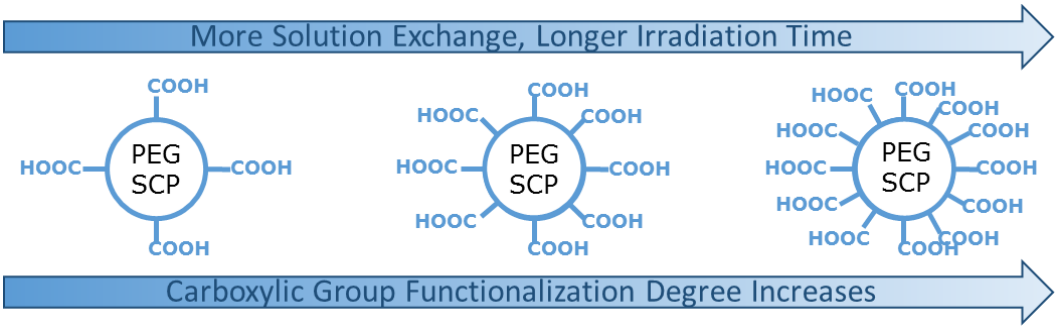

Figure 10: Controlling the carboxylic group functionalization degree with crotonic acid through controlling the number of reaction solutions and irradiation time.

2. Aims and Outline

Many biological processes are mediated by ligand receptor interactions, such as cell communication, virus infections, and cell identification. Therefore, a better understanding of the underlying mechanisms of ligand receptor interactions will help to evaluate their role in biology and medicine and help to also derive novel ligands e.g. in therapeutic applications. Accordingly, many theoretical models and experimental methods have been introduced to study the structures, thermodynamics and binding mechanisms of ligand receptor interactions. Most of these studies are focused on a single ligand receptor pair interaction, or dissolved ligand receptor interactions. In nature, however, many of these interactions take place at a soft interface, e.g. cell surfaces.

Recently, a novel method, the so-called SCP-RICM, to study the ligand receptor interactions at soft biomimetic interfaces was introduced by Pussak, *et. al.* In this technique, PEG based hydrogel microparticles were functionalized with ligands or receptors to give a simplified model of a soft biointerface. Glass slides were functionalized with the corresponding receptors or ligands and the SCPs were incubated on the glass slide. Through ligand receptor interaction, the SCPs bind to the glass surface and form a distinct contact area. Through a modified Hertzian elastic contact model, the JKR model, the adhesion energy of the SCP can be quantified via RICM.

The aim of this work is to further study ligand receptor interactions at soft biomimetic interfaces through SCP-RICM techniques. Specifically, this thesis aims at investigating three aspects: I) the influence of mechanical properties or flexibility of the anchoring surface (Young's modulus of SCP material), II) the influence of ligand concentration (degree of functionalization of SCPs), III) the influence of ligand type (weak vs. strong ligand receptor pairs) at soft interfaces.

Therefore, PEG hydrogel microparticles as well as PAA hydrogel microparticles with various Young's modulus should be synthesized. These SCPs will then be functionalized with biotin (strong ligand), and mannose (weak ligand) realizing different degrees of functionalization (concentration of bound ligands). As counterpart, glass slides will be functionalized with corresponding receptors avidin and Con A. The adhesion energy of the different sets of SCPs will then be analysed via RICM. Furthermore, inhibition experiments will be performed giving further information of the ligand receptor interactions at soft interfaces in presence of a competing ligand.

Overall, this thesis thus aims at promoting a better understanding of ligand receptor interactions at soft interfaces with a special focus on the influence of interface flexibility, ligand

concentration, and ligand type. Potentially this information will help to modulate ligand receptor interactions in biological systems more effectively and to design novel therapeutic strategies e.g. in antibacterial or anticancer therapy.

3. Results and Discussion

3.1 Synthesis and Characterization of SCPs

The objective of this work is to investigate ligand receptor interactions at soft biomimetic interfaces and to study how different factors affect these interactions. In this work, three factors were studied: Young's modulus of SCPs, ligand concentration, and ligand type.

In order to measure the ligand receptor interactions at soft biomimetic interfaces, the recently developed SCP-RICM method was applied. [51] Briefly, in the first part of this thesis PEG and PAA based hydrogel microparticles were synthesized as SCPs. Here, major focus was on the controlled variation of the Young's modulus of the SCPs. These SCPs were then functionalized with acrylic acid, or crotonic acid to introduce carboxylic groups within the hydrogel network for the further functionalization with ligands, receptors, or other functional groups. Here, special focus was devoted to the control of the degree of ligand functionalization. As a second sensor interface, a glass surface was functionalized with the corresponding receptor, ligand, or other corresponding functional groups. Due to the interactions between the ligands and receptors, adhesion occurred between the SCPs and according glass slides. Using RICM, the adhesion areas and the radii of SCPs were detected. With the help of the JKR model, [55] adhesion energies could be derived.

Traditional Procedures to Control the Young's Modulus of SCPs.

A major aim of this work is to understand the role of Young's modulus of specifically interacting materials. In previous work by Pussak *et. al.*, this was done as follows: PEG-diacrylamide (PEG-dAAm) macromonomers were dissolved in an aqueous solution. Kosmotropic sodium sulfate salt was added to the solution to decrease the solubility of PEG-dAAm in water and thus to form micro meter level droplets of PEG-dAAm rich phase. With an addition of photo initiator, the PEG-dAAm chains in these droplets were polymerized and cross-linked under UV irradiation. Three different molecular weights of PEG-dAAm (M_n = 4000 Da, 8000 Da, and

20000 Da) were used previously to obtain SCPs with different Young's Modulus (80 ± 5 kPa, 32 ± 5 kPa, and 15 ± 3 kPa). As an alternative approach, variation of photo initiator concentrations for PEG_{20k} (0.01 wt. %, 0.03 wt. %, 0.005 wt. %, and 0.0025 wt. %) were also used to obtain SCPs with different Young's Modulus (15 ± 3 kPa, 22 ± 6 kPa, 4 ± 1 kPa, and 0.3 ± 0.1 kPa). [79] [53]

However, there are some drawbacks of these approaches. The Young's Modulus range of obtained SCPs is only from 0.3 kPa to 80 kPa, which limits the investigation of the interface flexibility on ligand receptor interactions to a rather narrow range of approximate 80 kPa. One limitation is the limited number of commercially available PEG with different molecular weights. Moreover, PEG with different molecular weights requires different reaction conditions during microgel synthesis. The higher the PEG molecular weight, the lower is the kosmotropic salt concentration required for droplet formation. The lower the PEG molecular weight, the higher is the kosmotropic salt concentration or temperature required. Since the solubility of kosmotropic salts in water is limited, it is difficult to adapt the procedure for lower molecular weight PEGs and thus SCPs with higher Young's modulus.

A Novel Approach to Control the Young's Modulus of SCPs

For solving these problems, two new approaches for SCP synthesis with different Young's Modulus were developed in this work.

PEG-c-CA Approach:

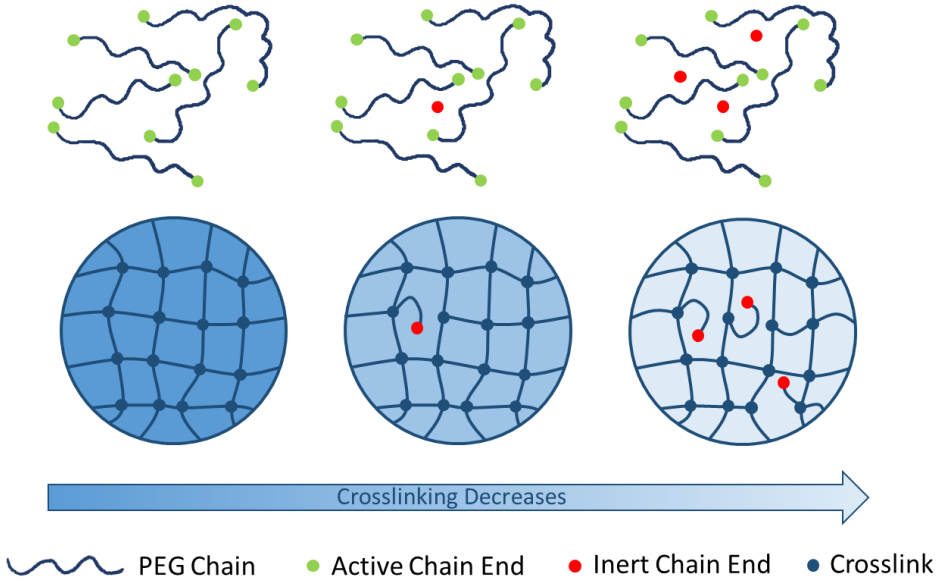

Figure 11: Variation of SCPs Young's modulus through PEG-c-CA approach, where blue curve is PEG chain, green dot is acrylamide group of PEG chain end (active chain end), red dot is crotonic acid (inert chain end), and blue dot is crosslink on SCP hydrogel network.

The Young's modulus of a microgel can be tuned by the degree of crosslinking. Thus, when reducing the degree of crosslinking, SCPs with a lower Young's modulus should be obtained. Here, PEG-dAAm (M_n = 8000 Da) was used in this work. If not noted otherwise, PEG-dAAm will always have a M_n of 8000 Da in the following content. The acrylamide group at the chain end of PEG-dAAm contains a polymerizable C=C bond. Thus, every end group of the polymer chains can react during the radical polymerization and can be considered 'active'. To reduce the number of ''active'' chain ends and thus the degree of crosslinking, crotonic acid was added to the reaction system for its low reactivity in free radical polymerization. [78] During the reaction, crotonic acid will react with acrylamide group and transfer the chain end from ''active'' state to ''inert'' state as no further addition of crotonic acid or reaction with other acrylamide end groups should take place. Thus, the cross-linking degree as well as the Young's modulus can be controlled by varying the amount of crotonic acid in the reaction mixture. (See Figure 11)

PAA Approach:

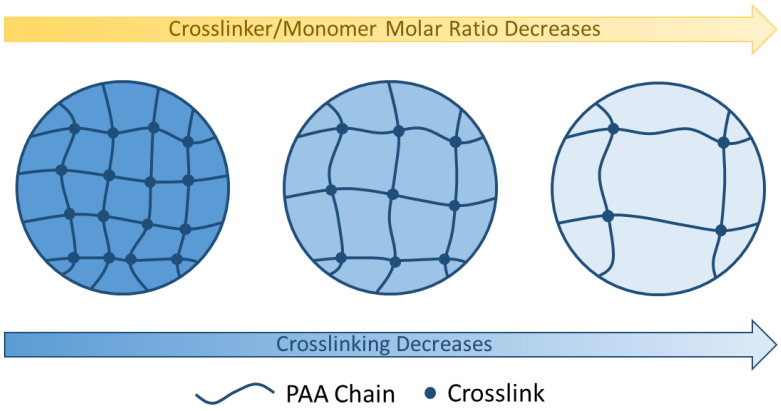

Figure 12: Variation of SCPs Young's modulus through PAA approach. When decreasing the crosslinker / monomer ratio, the crosslinking decreases, and further leads to a decrease in Young's modulus. Thus, the Young's modulus of PAA SCPs can be tuned.

PEG SCPs synthesized according to the previously established protocols do not offer functional groups for attaching ligands or receptors and need to be functionalized first e.g. with carboxylic acid groups. Alternatively, a hydrogel comprising functional groups for further attachment of ligands and receptors could be used. Therefore, acrylic acid was used in this work to synthesize PAA based SCPs as an alternative to PEG SCPs. While the PEG-dAAm macromonomers act as monomer and cross-linker at the same time, acrylic acid is only a monomer. Therefore N, N'-Methylenebisacrylamide (MBAm) was added to the reaction system as cross-linker. Through variation of the cross-linker / monomer ratio, the cross-linking degree and thus the Young's modulus can be tuned. (See Figure 12)

3.1.1 Synthesis and Characterization of PEG and PEG-c-CA SCPs

To be used as SCPs, the hydrogel microparticles need to fulfil several requirements. Firstly, the size of hydrogel microparticles should be in the range of 10 - 100 µm. From the smallest human cell (sperm cell [80]) to the largest human cell (oocyte cell [81]), the size range of human cells is between 4 - 180 µm. Because of the microscope resolution and field of view limitation, hydrogel

microparticles in the size range of 10 - 100 µm can be used for SCP-RICM. With the SCPs in this size range, it is easy to operate the SCP-RICM experiment and analyse the acquired data, meanwhile this range also covers most human cell species. Secondly, the SCPs should be clean, clear, and optically transparent. Opaque hydrogel microparticles and impurities in the hydrogel microparticles will disturb the interference pattern during SCP-RICM measurement and would lead to experiment failure. Thirdly, the Young's Modulus of hydrogel microparticles should not be too low. Very soft particles in the range of 1 kPa will be almost invisible and hard to detect with optical microscopy and increase the operational difficulty of the SCP-RICM experiment.

As described in at the beginning of chapter 3.1 (see Figure 11), in order to create PEG SCPs with varying degree of crosslinking, crotonic acid can be added to the PEG-dAAm precipitation polymerization system. It was found that only about 0.3 mg crotonic acid could be dissolved in 1 mL 1 M Na_2SO_4 solution. This value is significantly lower than the 94 mg/mL crotonic acid solubility in water. [82] The reason for this solubility difference is the low pH condition upon addition of crotonic acid in contrast to non-buffered Na_2SO_4 solution. So as to increase the solubility of crotonic acid in 1 M Na_2SO_4 solution and wider the range of crotonic acid concentration in the reaction solution, 1 M Na_2SO_4 was buffered with PBS (10 mM phosphate buffer pH 7.4 with 2.7 mM potassium chloride, and 137 mM sodium chloride). The solubility of deprotonated crotonic acid in this solution increased to 12.4 mg/mL. Here, PEG-dAAm and crotonic acid was mixed in Na_2SO_4/PBS solution. PEG-dAAm was precipitated and the solution was separated into a PEG rich phase and a PEG poor phase. Upon vigorous shaking of both phases, the PEG rich phase was dispersed into micro meter sized droplets by shear force.

2-Hydroxy-4´-(2-hydroxyethoxy)-2-methylpropiophenone (Irgacure 2959) was used as the photo initiator. Under UV irradiation, the free radical polymerization was initiated and PEG-dAAm and crotonic acid were copolymerized. (See Scheme 5 and Figure 13) The PEG-dAAm chains of resulting micro particles were covalently bonded and could not be dissolved in water and any other organic solvent.

The acquired SCPs was washed with water three times via centrifugation to remove the salts and other impurities from the SCPs.

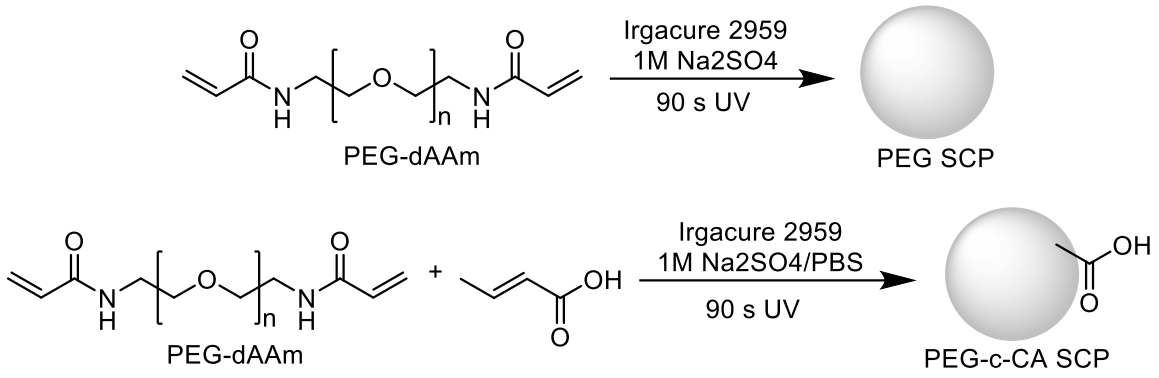

Scheme 5: PEG SCPs and PEG-c-CA SCPs synthesis scheme via precipitation free radical photopolymerization

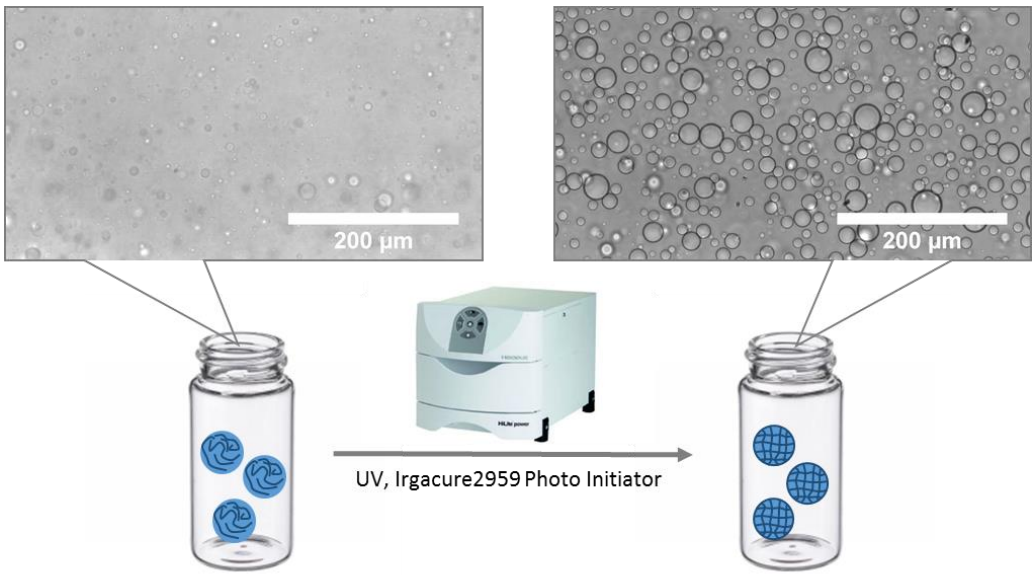

Figure 13: Microscope image of the PEG-dAAm rich phase droplets before crosslinking and the PEG-dAAm based SCPs after crosslinking.

In this work, seven batches of PEG-c-CA microparticles were synthesized (see Table 2). Due to the low reactivity of crotonic acid in free radical polymerization, a large proportion of crotonic acid should be added to reaction system in order to be co-polymerized with acrylamide group of PEG-dAAm, [83] and thus reduce the reactivity of PEG chain end in free radical polymerization. When the CA/AAm molar ratio increases from 0 to 120, the Young's modulus of the micro particles is expected to decrease significantly.

It was found that even when the CA/AAm molar ratio reaches 120, there is still sufficient reactive PEG chain end to be polymerized and form SCPs. However, the resulting SCPs were almost not visible under optical microscope, most likely because the cross-linking degree was too low and the microparticles were too soft. This led to microparticles with a high content of water almost the same refraction index as water. Thus, only the other six batches with lower concentrations of crotonic acid were further characterized and will be discussed in the following discussion.

Table 2: Synthesis of PEG SCPs and PEG-c-CA SCPs with various CA/AAm ratio.

Sample Name	PEG-dAAm [µmol]	AAm [µmol]	CA [µmol]	CA/AAm Molar Ratio
PEG-c-CA(0)	6.3	12.6	0	0
PEG-c-CA(10)	6.3	12.6	126	10
PEG-c-CA(20)	6.3	12.6	252	20
PEG-c-CA(30)	6.3	12.6	379	30
PEG-c-CA(40)	6.3	12.6	504	40
PEG-c-CA(60)	6.3	12.6	756	60
PEG-c-CA(120)	6.3	12.6	1512	120

As a first mean of characterization, the particles directly after UV crosslinking were checked by an inverted optical microscope measuring the size distribution of the SPCs. The perimeters of the maximum cross-section from around 100 SCPs were measured with image processing software ImageJ through manually identifying the outer edges of SCPs. The diameters of these SCPs were then calculated from the acquired perimeters. For each group of SCPs, average diameter and its standard deviation was counted as an indicator of the SCPs size dispersity.

Figure 14 shows the optical microscope images of PEG-c-CA SCPs with various crotonic acid CA/AAm ratio. As mentioned before, SCPs synthesized with 120 CA/AAm molar ratio were not visible and are not considered for further experiments, all the other SCP batches are optically visible. Here, it shows that the visible SCPs are also clean, clear, and transparent. In all groups, the size distribution of SCPs is broad. The smallest SCP is 9 µm, the biggest SCP is 68 µm. This is expected, as without stabilizer, the precipitation method gives a mixture of smaller and bigger

PEG droplets, which is expected to lead to a mixture of sizes for PEG-c-CA microparticles. The average sizes of the PEG-c-CA SCPs synthesized with various CA/AAm molar ratio stays constant, which confirms that the presence of crotonic acid does not influence the precipitation process of PEG. (See Table 3)

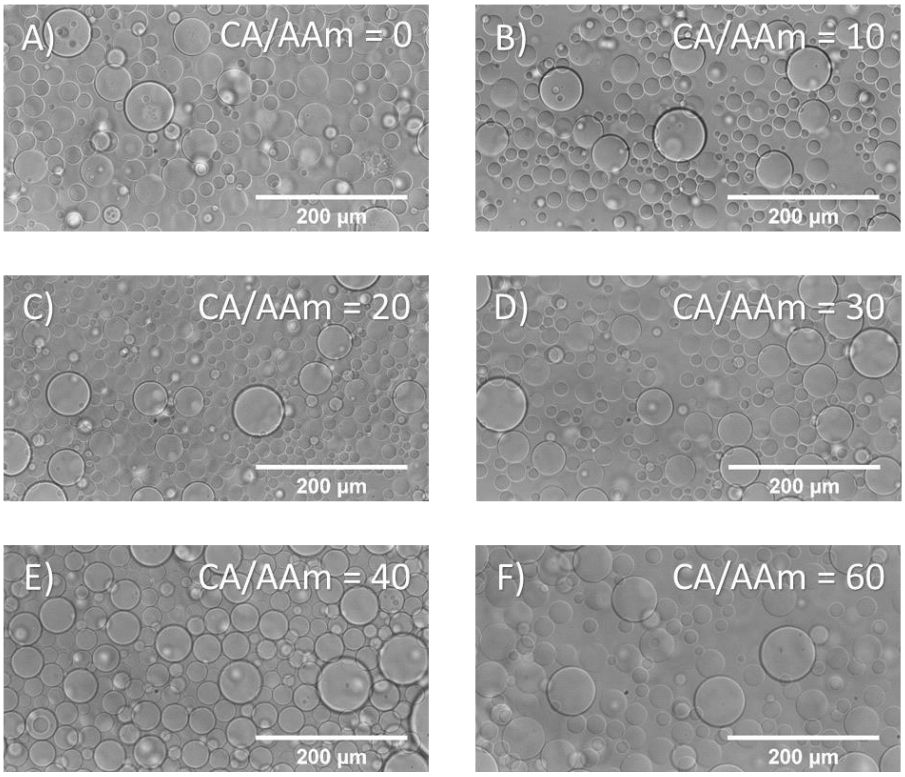

Figure 14: Optical microscope images of PEG-c-CA SCPs synthesized with different CA/AAm molar ratio. A) PEG-c-CA(0), CA/AAm molar ratio = 0; B) PEG-c-CA(10), CA/AAm molar ratio = 10; C) PEG-c-CA(20), CA/AAm molar ratio = 20; D) PEG-c-CA(30), CA/AAm molar ratio = 30; E) PEG-c-CA(40), CA/AAm molar ratio = 40; F) PEG-c-CA(60), CA/AAm molar ratio = 60. (The contrast and brightness of these images are modified with Microsoft Power Point for a better view in printed and electronic versions.)

Table 3: Particle size of PEG SCPs and PEG-c-CA SCPs synthesized with various CA/AAm molar ratio.

Sample Name	CA/AAm Molar Ratio	Average Diameter [µm]
PEG-c-CA(0)	0	24 ± 9
PEG-c-CA(10)	10	24 ± 10
PEG-c-CA(20)	20	22 ± 8
PEG-c-CA(30)	30	22 ± 8
PEG-c-CA(40)	40	26 ± 8
PEG-c-CA(60)	60	27 ± 12

One aim of this work is to investigate how the elastic properties of SCPs will affect the ligand-receptor binding process. In order to achieve this goal, hydrogel microparticles with various Young's modulus need to be synthesized as the base material of SCPs.

The Young's modulus of hydrogel microparticles was measured through the colloidal probe AFM indentation measurements. Briefly, hydrogel microparticles were swollen in the future SCP-RICM measurement solution, for example, lectin binding buffer (LBB), until equilibrium. As colloidal AFM indentation probe, a glass bead with a diameter of 4 - 5 µm was glued to a tipless AFM cantilever. During the measurement, the AFM colloidal probe was approached to the apex of the hydrogel micro particle. When the colloidal probe touched the hydrogel microparticle, the particle is mechanically deformed due to the force applied by the AFM cantilever.

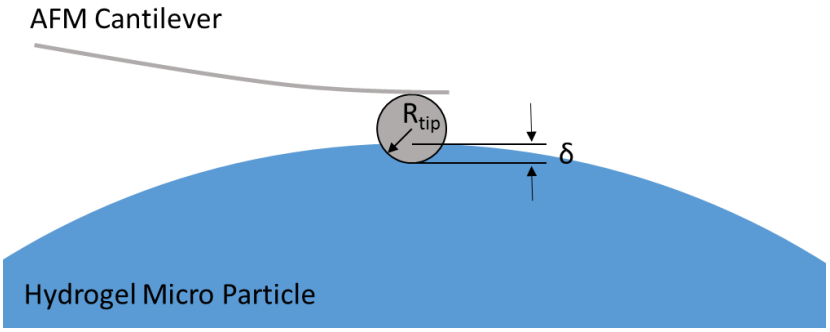

Figure 15: Scheme of hydrogel microparticle Young's modulus investigation through AFM indentation measurements with the Hertz Model. [53]

With the information of AFM tip spring constant and sensitivity, AFM records the sample deformation and the force applied to induce this deformation. Through the Hertzian model, the

Young's modulus of hydrogel microparticles can be calculated. [84] [85] The Hertz equation is shown below:

$$F = \frac{4E}{3(1-\nu^2)}\sqrt{R}\delta^{\frac{3}{2}} \qquad \textbf{Equation 17}$$

, where F is the applied force on the hydrogel micro particles, E is the Young's modulus, ϑ is the Poisson ratio, which is 0.5 in this case, [86] R is the effective radius calculated from the radius of colloidal probe and the radius of the hydrogel micro particle, δ is the indentation of the hydrogel microparticle.

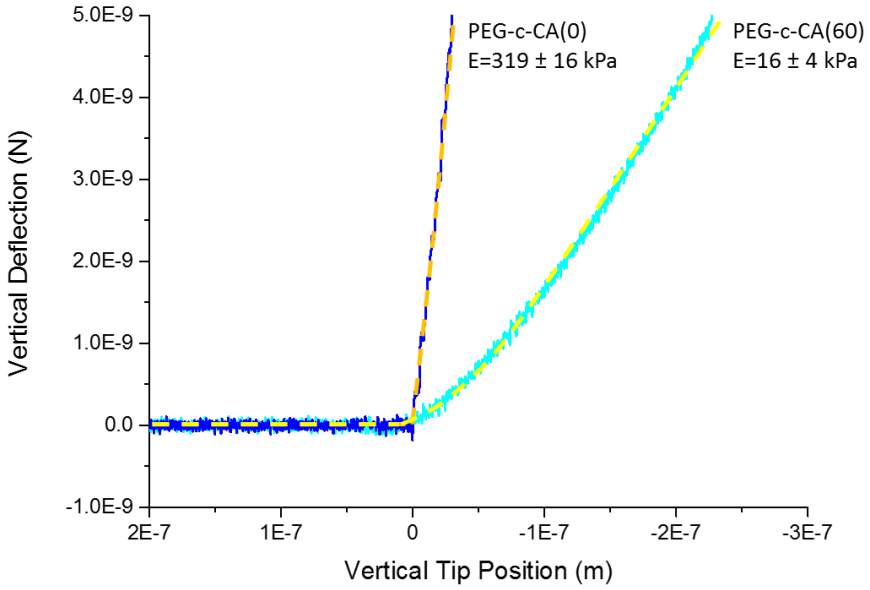

Figure 16: Typical Young's modulus measurement curve and the corresponding Hertz fit curve of the hardest PEG-c-CA(0) SCPs and the softest PEG-c-CA(60) SCPs

All PEG-c-CA SCPs were analysed for their Young's modulus using the AFM indentation method. From Figure 17 and Table 4, it can be observed that when there is no crotonic acid presenting, the Young's modulus of acquired SCPs is 319 ± 16 kPa. With 10 CA/AAm molar ratio, the Young's modulus of SCPs was tuned to 252 ± 21 kPa. As expected, with introduction of CA and decrease of the crosslinking within the PEG network, the Young's modulus decreased significantly. When 60 CA/AAm molar ratio was applied to the reaction system, the Young's

modulus decreased further to 16 ± 4 kPa. This result indicates that the PEG-c-CA approach is a successful way to tune the Young's Modulus of SCPs.

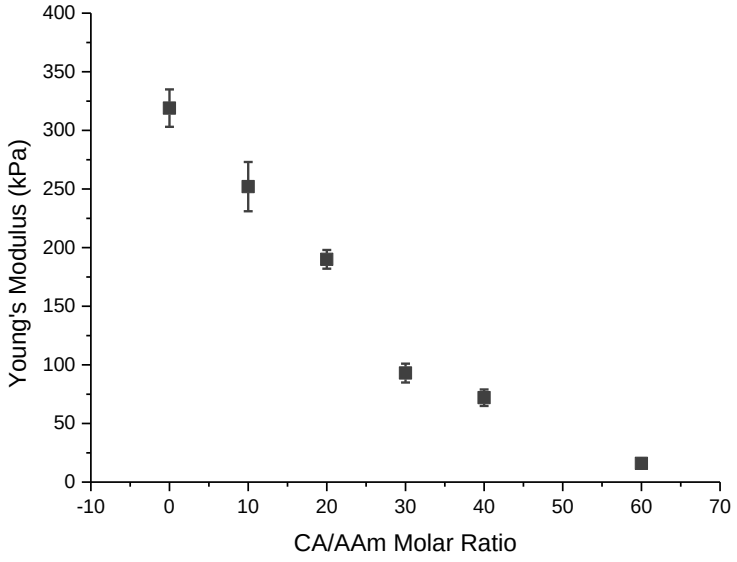

Figure 17: Tuning the Young's modulus of PEG-c-CA SCPs through CA/AAm ratio.

Table 4: Young's modulus of PEG SCPs and PEG-c-CA SCPs measured via colloidal probe AFM indentation measurement

Sample Name	CA/AAm Molar Ratio	Young's Modulus [kPa]
PEG-c-CA(0)	0	319 ± 16
PEG-c-CA(10)	10	252 ± 21
PEG-c-CA(20)	20	190 ± 8
PEG-c-CA(30)	30	93 ± 8
PEG-c-CA(40)	40	72 ± 7
PEG-c-CA(60)	60	16 ± 4

3.1.2 Synthesis and Characterization of PAA SCPs

As described before, one option to drastically increase the number of functional groups in SCPs is to directly use PAA as the hydrogel material. The requirements of SCPs synthesized from both approaches are the same: the size of SCPs should be in the range of 10 - 100 µm; the SCPs should be clean, clear, and transparent; the SCPs should be optically visible and thus the Young's Modulus should not be too low. To fulfil the above requirements, inverse suspension polymerization of acrylic acid was used in this work.

The monomer acrylic acid, crosslinker MBAm, and initiator APS were mixed with water. Commercial dispersants ABIL EM 90 and polyglycerol polyricinoleate (PGPR) were mixed with high viscosity paraffin oil. Water phase was dispersed to micro droplets in oil phase due to the strong sheer force from agitation with a mechanical stirrer. Upon heating, the thermal initiator APS decomposed and initiated free radical polymerization in the micro droplets. These micro droplets act as many micro reactors for solution polymerization of acrylic acid. With the crosslinker MBAm, the compositions within the droplets were fixed a stable hydrogel network. Thus, the resulting hydrogel particles inherited the size of the precursor droplets and became microparticles. To achieve various cross-linking degree, 4 batches of SCPs with 1.0 mol. %, 3.8 mol. %, 7.4 mol. %, and 14.7 mol. % MBAm/AA ratio were synthesized (See Table 5).

The acquired microparticles were washed three times with a mixture of 50% toluene 50% water to remove non-water soluble and water soluble impurities via centrifugation, three times with isopropanol to remove the left toluene, and then three times with water to remove isopropanol. The cleaned PAA microparticles is stored in water for further use.

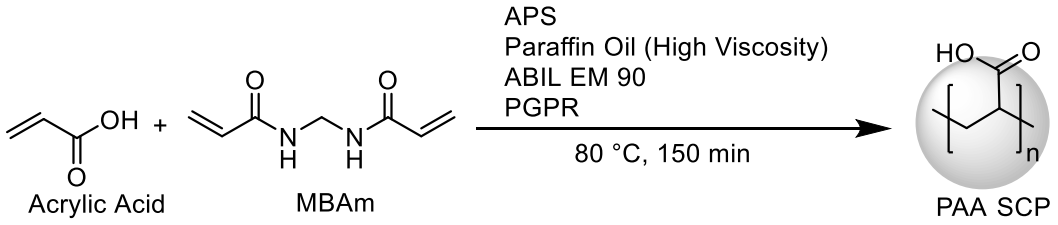

Scheme 6: PAA SCPs synthesis scheme via inverse suspension free radical polymerization

Table 5: Synthesis of PAA SCPs with various MBAm/AA ratio.

Sample Name	AA [mmol]	MBAm [mmol]	MBAm/AA Ratio [mol. %]
PAA(14.7)	31.2	4.6	14.7
PAA(7.4)	31.2	2.3	7.4
PAA(3.8)	31.2	1.2	3.8
PAA(1.0)	31.2	0.3	1.0

PAA based SCPs intrinsically contain one carboxylic group per monomer and are ready to be further functionalized with ligands, receptors, or other functional groups. To carry out further reactions, the functionalization degree of PAA SCPs needs to be determined. As the composition of PAA SCPs is known and only AA contains carboxylic groups, the theoretical degree of functionalization can be easily calculated.

$$PAA\ SCPs\ Carboxylic\ Group\ Func.Deg. = \frac{10^6}{72.06+R\times 154.17}\ \mu mol/g \quad \textbf{Equation 18}$$

, where *R* is MBAm / AA mol. Ratio with a unit of mol. %, 72.06 is the molar mass of acrylic acid with a unit of g/mol, 154.14 is the molar mass of MBAm with a unit of g/mol.

Table 6: Carboxylic group functionalization degree of PAA SCPs

Sample Name	MBAm/AA Ratio [mol. %]	Carboxylic Group Functionalization Degree [mmol/g]
PAA(14.7)	14.7	10.5
PAA(7.4)	7.4	12.0
PAA(3.8)	3.8	12.8
PAA(1.0)	1.0	13.6

It was found that the carboxylic group functionalization degree of PAA SCPs is in the range of 10.5 to 13.6 mmol/g. Because the crosslinker MBAm does not contain any carboxylic groups, the functionalization degree decreases when the MBAm / AA ratio increases. At 1.0 mol. %, the carboxylic group functionalization degree is 13.6 mmol/g. By increasing the ratio to 3.8 mol. %, the functionalization degree decreased to 12.8 mmol/g. Further increase of the ratio to 7.4 mol. % and 14.7 mol. % led to the decrease of the functionalization degree to 12.0 mmol/g and 10.5

mmol/g. Overall, the degree of functionalization is rather similar for the different batches of PAA SCPs with the differences in the degree of functionalization being less than 10 %.

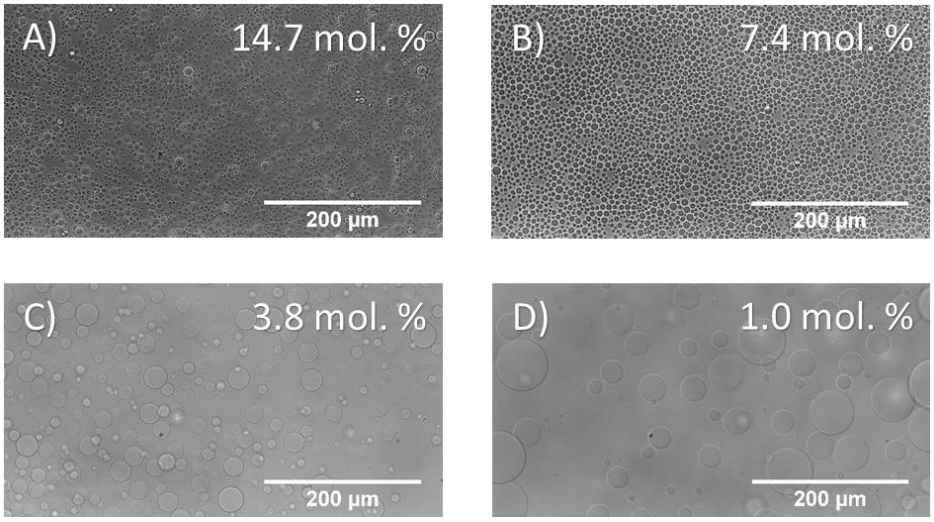

Figure 18: Optical microscope images of PAA SCPs synthesized with different MBAm/AA ratio. A) PAA(14.7), 14.7 mol. % MBAm/AA; B) PAA(7.4), 7.4 mol. % MBAm/AA; C) PAA(3.8), 3.8 mol. % MBAm/AA; D) PAA(1.0), 1.0 mol. % MBAm/AA. (The contrast and brightness of these images are modified with Microsoft Power Point for a better view in printed and electronic version.)

The size of the PAA SCPs was determined in the same way as for the PEG-c-SCPs by using optical microscopy. Figure 18 shows the optical microscope images of PAA SCPs with various MBAm/AA ratio. The hydrogel microparticles synthesized with the highest 14.7 mol. % MBAm/AA ratio in A) is opaque. This is due to the high cross-linking degree. Dispersants used in the synthesis procedure were ‘‘locked’’ in the highly dense hydrogel network, and thus led to the different refractive index there. The other three groups of hydrogel microparticles synthesized with MBAm/AA ratios lower than 7.4 mol. % are all clean.

Figure 18 also shows the influence of MBAm/AA ratio on the size of PAA hydrogel micro particles. At a MBAm/AA ratio of 14.7 mol. %, the average size of the micro particles is 4 ± 2 µm. The smallest particle is 2 µm, the largest particle is 12 µm. When decreasing the MBAm/AA ratio to 7.4 mol. %, the size of microparticles is slightly increased to 5 ± 1 µm, but still less than 10 µm. The sizes larger than 10 µm were obtained after decreasing the MBAm/AA ratio to 3.8 mol. %. In Figure 18 C), the microparticles synthesized with 3.8 mol. % MBAm/AA ratio have a size of 17 ± 6 µm. The smallest particle is 7 µm, the largest particle is 29 µm. Then, with the lowest MBAm/AA ratio in this work, 1.0 mol. %, the size of the microparticles increased to 26 ± 13 µm. The smallest

particle is 8 µm, which did not change much comparing to the previous group. Meanwhile, the size of the largest micro particles significantly increased to 79 µm.

As described before, the PAA microparticles were synthesized through inverse suspension polymerization. The water phase was dispersed into micro droplets under vigorous agitation. On one hand, the size of the micro droplets determines the size of the resulting microparticle. On the other hand, after the microparticles were purified and swollen in water, the size of these microparticles is determined by their degree of crosslinking, which is correlated to MBAm/AA ratio.

Table 7: Particle size of PAA SCPs synthesized with various MBAm/AA ratio.

Sample Name	MBAm/AA Ratio [mol. %]	Average Diameter [µm]
PAA(14.7)	14.7	4 ± 2
PAA(7.4)	7.4	5 ± 1
PAA(3.8)	3.8	17 ± 6
PAA(1.0)	1.0	26 ± 13

As the cross-linking degree is the main factor that influences the elastic properties of SCPs, the Young's modulus of PAA SCPs should be tuned by tuning the MBAm/AA ratio. The more MBAm as crosslinker was added to the reaction system, the higher the achieved crosslinking degree should be and thus a higher Young's modulus was expected.

However, in the case of PAA approach, when the MBAm/AA ratio increased to 7.4 mol. %, the microparticles turned opaque and the average size of these microparticles was smaller than 10 µm. These drawbacks prevented the PAA microparticles to be used as SCPs in SCP-RICM experiment. As described before, only the group with 3.8 mol. % and 1.0 mol. % MBAm/AA ratio, respectively fulfilled the requirements of SCPs, thus only the Young's moduli of these two groups were measured. In Table 8, it can be found that by adding 1.0 mol. % MBAm, the Young's modulus was 7 ± 1 kPa. When increasing the MBAm concentration to 3.8 mol. %, the Young's modulus increased to 53 ± 5 kPa. This results confirms the expectations: a higher MBAm/AA ratio led to higher cross-linking degree; higher cross-linking degree led to larger Young's modulus. Through tuning the MBAm/AA ratio, the Young's modulus of SCPs was successfully varied. However, there is only a small window within the tuning of the Young's modulus of PAA hydrogel based

SCPs is possible, as for higher crosslinker contents, obtained microparticles are not suitable for SCP-RICM.

Table 8: Young's modulus of PAA SCPs measured via colloidal probe AFM indentation measurement

Sample Name	MBAm/AA Ratio [mol. %]	Young's Modulus [kPa]
PAA(3.8)	3.74	53 ± 5
PAA(1.0)	0.93	7 ± 1

3.2 Functionalization of SCPs

The objective of this work is to investigate the influence of different parameters on the interaction of ligand and receptors at soft biomimetic interfaces by using SCP-RICM. In chapter 3.1, SCPs with various Young's modulus were prepared through PEG-c-CA SCPs approach and PAA SCPs approach. In this chapter, synthesis of SCPs with different degrees of functionalization and attachment of two different ligands will be presented.

In order to functionalize SCPs with ligands or receptors or other functional groups, in a first step carboxylic groups were introduced to the SCPs as the starting point for the further functionalization. In the case of PEG-c-CA SCPs, one possibility is to directly use the co-polymerized crotonic acid side chains as functional groups. However, due to the low free radical polymerization reactivity of crotonic acid, the concentration of carboxylic groups on PEG-c-CA SCPs is very low. The other possibility is to introduce more carboxylic groups on PEG-c-CA SCPs through benzophenone radical surface chemistry. [51] [87] This method was therefore also applied for the PEG-c-CA SCPs to further increase the concentration of carboxylic groups of the SCPs. In the case of PAA SCPs, as the hydrogel network was synthesized from acrylic acid, amine presenting ligands or receptors can be easily attached to the carboxylic groups through amide coupling reactions e.g. with carbodiimide chemistry [88] or by using PyBOP and HOBt [89] . As will be discussed in the following section, both approaches were applied in this work.

In order to quantify the degree of functionalization of both, PEG and PAA SCPs, a colorimetric test was used – the so-called toluidine blue O (TBO) titration. [90] Briefly, dried SCPs with known weight are swollen in a TBO titration solution with known concentration at pH 10-11. TBO is a dye which can bind to carboxylic groups at pH 10-11. After overnight reaction, each individual carboxylic group on the SCPs binds with a TBO cation. The concentration of TBO in titration solution is reduced. The Beer-Lambert law is usually written as:

$$A = \varepsilon bc \qquad \textbf{Equation 19}$$

, where A is the absorbance of light, ε is the wavelength-dependent molar absorption coefficient, b is the path length of light in the sample, c is the coloured compound concentration.

Through Beer-Lambert law, the absorption at 633 nm of a TBO solution is directly correlated to the concentration of free TBO in solution. Through measuring the change of absorption of the TBO solution before and after titration of the SCPs, the amount of TBO bound on the SCPs, which equals to the amount of carboxylic group on SCPs, can be calculated. Thus, the functionalization degree of carboxylic groups can be calculated with the following equation:

$$D_{carboxylic\ group} = \frac{M_{carboxylic\ group}}{m_{SCP}} \qquad \textbf{Equation 20}$$

, where $D_{carboxylic\ group}$ is the carboxylic group functionalization degree of SCPs, $M_{carboxylic}$ group is the mole amount of carboxylic group on measured SCPs, m_{SCP} is the mass of SCPs.

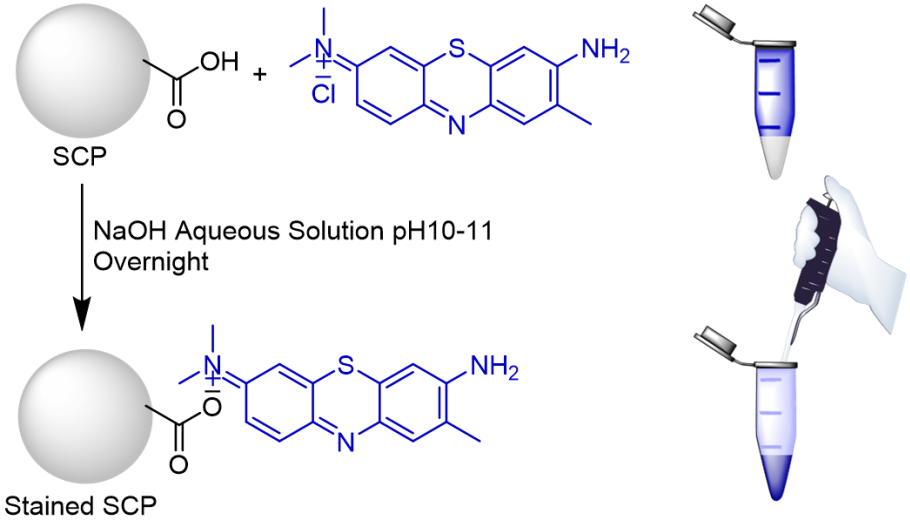

Figure 19: Schematic presentation for the TBO titration of SCPs measuring the degree of functionalization of carboxylic groups

However, the TBO titration usually needs a large amount of SCPs. For precious ligand functionalized SCPs, this titration method is not practical and economical. In order to test the ligand functionalization degree, microscope TBO was developed in this work.

Briefly, a small amount of SCPs before and after ligand functionalization were dyed by TBO with the same procedure as TBO titration. Then, the excess TBO in the SCPs was washed away with sodium hydroxide solution at pH10-11. These dyed SCPs were analysed with optical microscopy and the image was recorded monochromatically with a CMOS camera. Because TBO does not bind to the ligand, the SCPs will be brighter after ligand functionalization. Through measuring the grey value of the dyed SCPs, the ligand functionalization degree can be calculated taking into account known carboxylic group functionalization degree of SCPs before ligand functionalization.

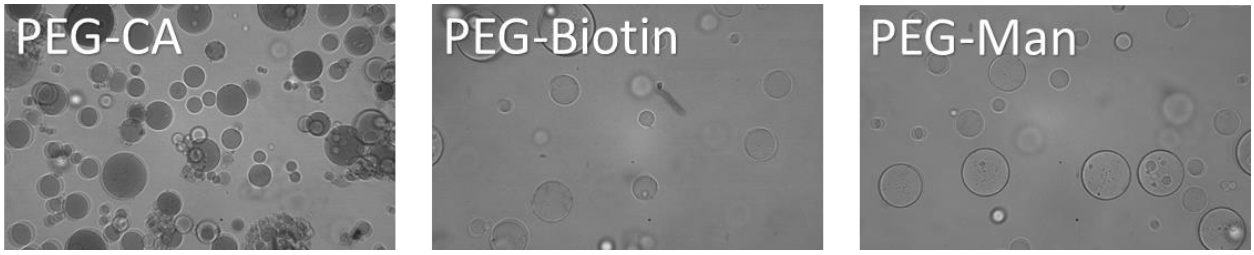

Figure 20: Microscope image of TBO dyed carboxylic functionalized PEG-CA SCPs, and its corresponding biotin ligand functionalized PEG-Biotin SCPs, mannose ligand functionalized PEG-Man SCPs.

When using PEG SCPs, the degree of functionalization can be tuned by using different grafting methods as was shown in previous work [77] and further extended in this work. However, the highest degree of functionalization achieved was about 250 µmol/g [76] and it would be interesting for later SCP-RICM experiments to further increase this value. Therefore, PAA SCPs were developed in this work.

As PAA SCPs are based on poly(acrylic acid) polymers, every repeating unit of the hydrogel network carries a carboxylic group side chain. A degree of functionalization of ~13600 µmol/g was achieved for PAA SCPs, which is around 50 times higher than the carboxylic group functionalization achieved for PEG-MA SCPs. [76] The challenge of this PAA SCPs approach is mainly on the controlling of final ligand functionalization degree.

To tune the ligand functionalization degree for PAA SCPs, the concentration of carboxylic groups needs to be reduced. This is done in the second step of SCP functionalization - the

attachment of the ligands. In this work, two different approaches were realized for tuning the degree of functionalization of PAA SCPs:

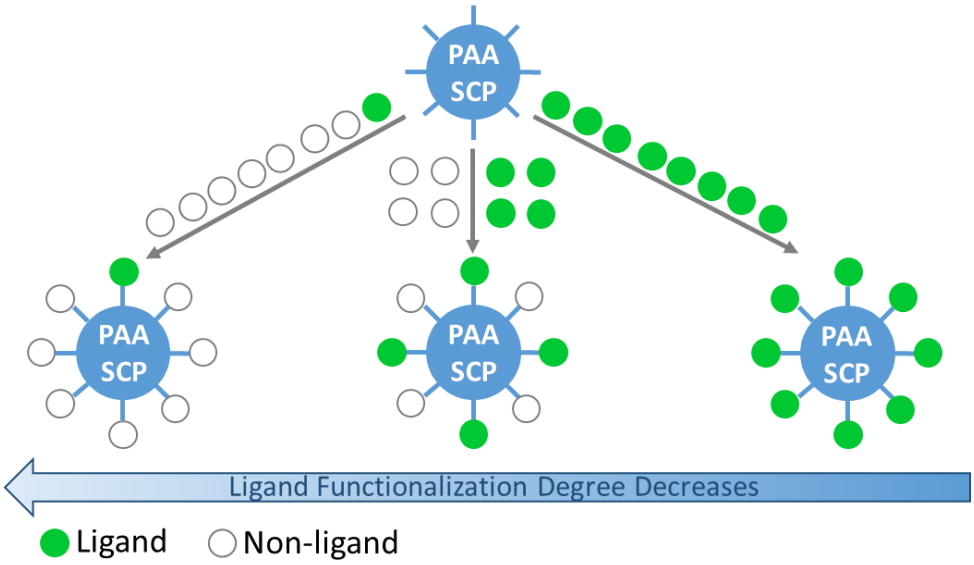

Scheme 7: Tuning ligand functionalization degree of PAA SCPs through co-coupling of ligand and non-ligand molecules, where the green dot represents ligands, the white dots represents non-ligands.

I) Co-coupling of ligand and non-ligand molecules: During the coupling reaction of ligand and carboxylic group on SCPs, a certain percent of the ligand was replaced by a non-ligand with the same functional group. Since the reactivity of both molecules is assumed to be similar, statistical functionalization should take place. This should then lead to different degrees of ligand functionalization depending on the ligand/non-ligand ratio during reaction. (See Scheme 7)

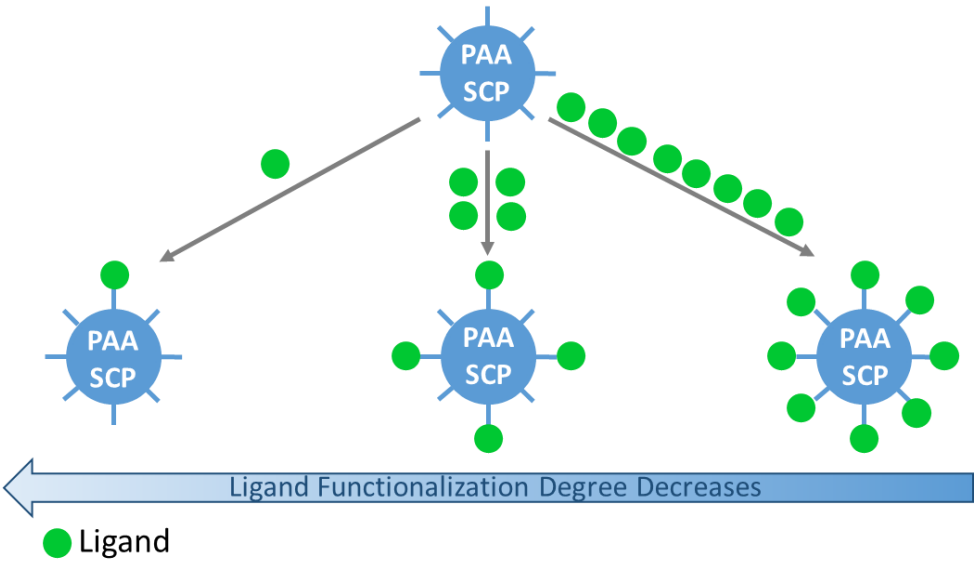

Scheme 8: Tuning ligand functionalization degree of PAA SCPs via tuning the reactants equivalent during coupling reaction, where the green dot represents ligands.

II) Tuning the reactant equivalent: During the ligand functionalization of carboxylic SCPs, typically excess amounts of reactants, e.g. ligand and coupling catalyst, are added to achieve the highest reaction yield and highest ligand functionalization. For functionalization of PAA SCPs, a reduced amount of reactants should lead to a reduced reaction yield and thus a reduced ligand functionalization. (See Scheme 8)

3.2.1 Carboxylic Acid Functionalization of PEG and PEG-c-CA SCPs

In this work, the PEG-c-CA SCPs were synthesized as explained in chapter 3.1.1. The morphology and Young's modulus were characterized directly after synthesis. Due to the very low carboxylic group concentration from the co-polymerization, the SCPs must be functionalized with additional carboxylic acid groups through grafting processes.

Here, six batches of PEG-c-CA SCPs with various Young's modulus from 319 ± 16 kPa (PEG-c-CA(0)) to 16 ± 4 kPa (PEG-c-CA(60)) were functionalized with crotonic acid via the previously developed grafting method. [76] Additionally, another group of PEG-c-CA(0) were functionalized with acrylic acid to obtain SCPs with oligomeric carboxylic acid chains on the PEG network.

Table 9: Carboxylic group functionalization degree measured via TBO titration of PEG-c-CA SCPs with various Young's modulus

Sample Name	CA/AAm Molar Ratio	Young's Modulus [kPa]	Carboxylic Group Functionalization Degree [µmol/g]
PEG-CA(0)	0	319 ± 16	117 ± 6
PEG-CA(10)	10	252 ± 21	113 ± 5
PEG-CA(20)	20	190 ± 8	102 ± 6
PEG-CA(30)	30	93 ± 8	79 ± 7
PEG-CA(40)	40	72 ± 7	104 ± 5
PEG-CA(60)	60	16 ± 4	81 ± 2

Table 9 shows carboxylic group functionalization degree of PEG-CA SCPs with various Young's modulus. The degree of functionalization is in the range of 100 ± 20 µmol/g for all PEG-CA systems. PEG-CA(30)-CA has the lowest degree of carboxylic group functionalization of 79 ± 7 µmol/g. PEG-CA(0)-CA has the highest degree of carboxylic group functionalization of 117 ± 6 µmol/g. This result suggests that Young's modulus of the PEG-CA SCPs does not affect the functionalization process and resulting degree of functionalization.

3.2.2 Ligand Functionalization of PEG-CA and PEG-c-CA-CA SCPs

In the next step, carboxylic functionalized SCPs were ready for further functionalization with ligands, receptors, or other functional groups.

In this work, mannose - Con A and biotin - avidin were selected as ligand receptor pairs to study the ligand receptor interactions at soft biomimetic interfaces. Biotin-avidin is one of the strongest non-covalent binding in nature, [20] [91] while mannose-Con A is a comparably weak ligand receptor pair. [20] In order to further functionalize the carboxylic group functionalized SCPs with ligands, the ligands were firstly modified and functionalized with amine groups. Then, the

aminoethyl-linked ligands were connected to the carboxylic group on the SCPs through amide coupling reaction with PyBOP and HOBt. [79] The reaction mechanism is shown in Scheme 9.

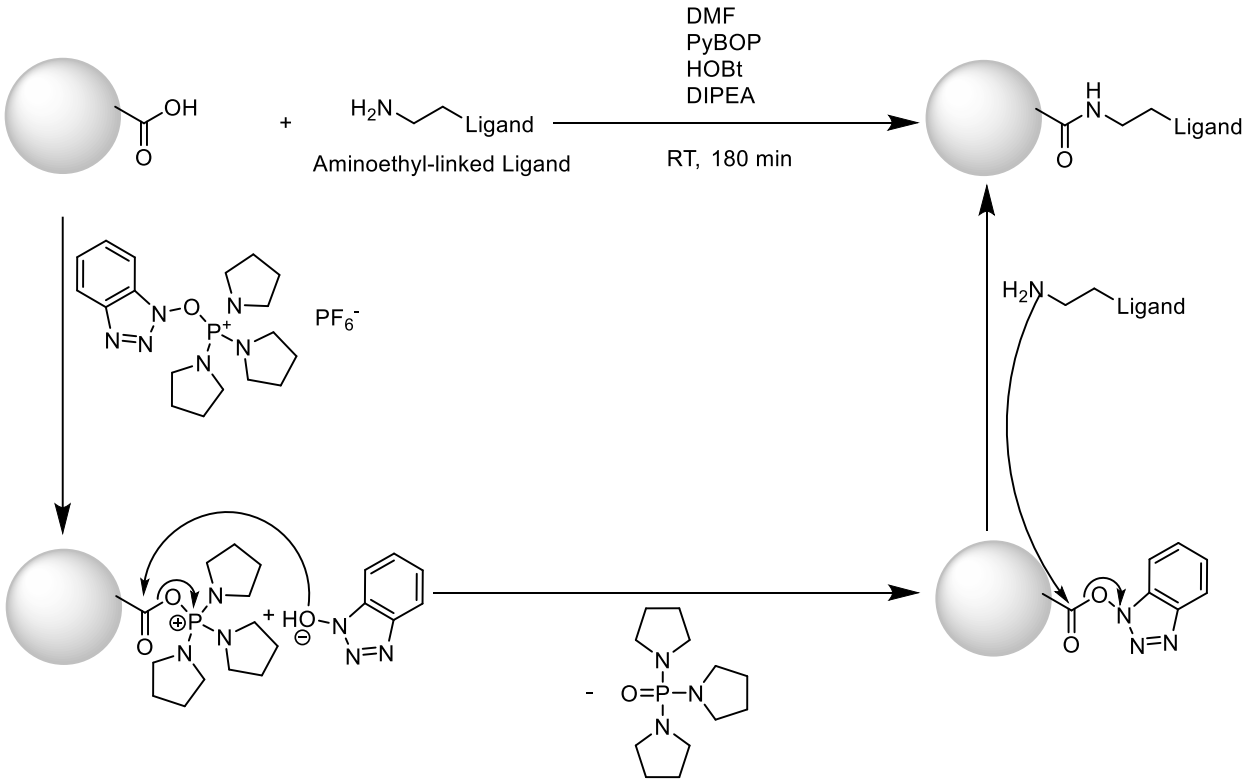

Scheme 9: Reaction mechanism of the coupling reaction of aminoethyl-linked ligand to carboxylic group of SCPs through PyBOP and HOBt. [53]

3.2.2.1 Functionalization of PEG-CA SPCs with Mannose

In order to couple mannose to the carboxylic group functionalized SCPs, a free amine group had to be installed onto the mannose. Therefore, commercially available mannose was protected with acetyl groups and modified with an aminoethyl linker on the anomeric position by Fawad Jacobi according to literature protocols by Ponader *et. al* [92] adapted from Geng *et. al.* [93] In a standard protocol (see Experimental Section), SCPs were washed with DMF to remove the ethanol from previous steps and then 10 eq. PyBOP, 5 eq. HOBt, 10 eq. DIPEA, and 10 eq. aminoethyl-linked mannose were added to the reaction mixture and shaken 180 min at room temperature. After the reaction, the SCPs were washed with DMF to remove the unreacted mannose and other residues, and then washed with methanol. Sodium methoxide in methanol was added to the SCPs dispersion

and shaken for 30 min at room temperature to deprotect the mannose. Finally, the resulting PEG-Man SCPs were washed with methanol and then water to be ready for the SCP-RICM experiments.

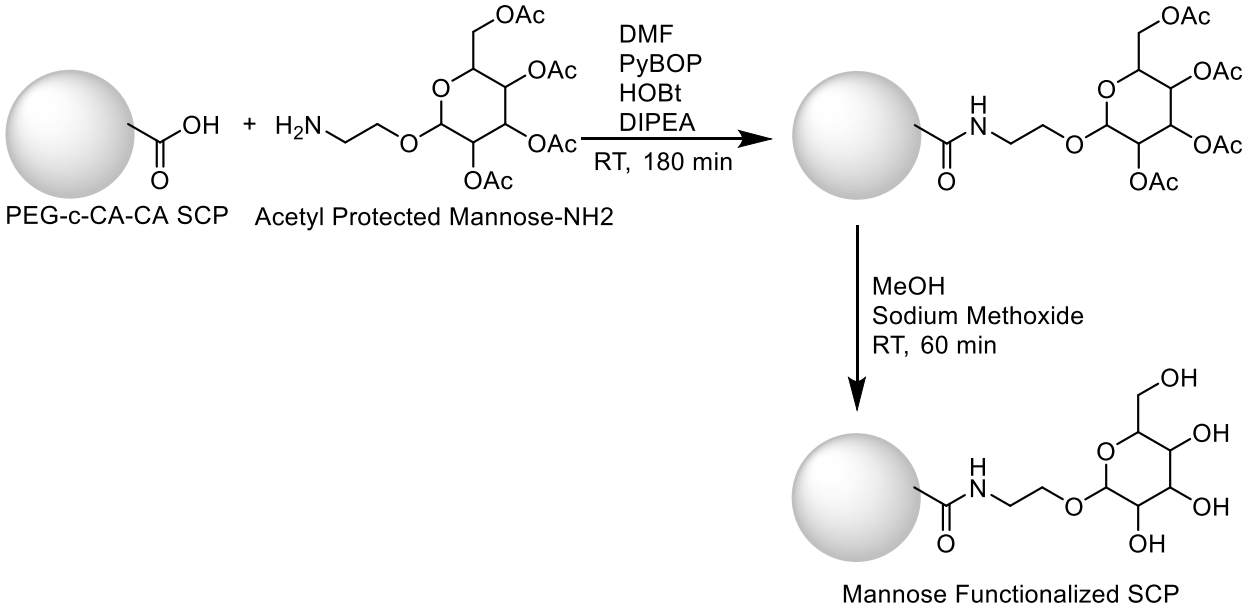

Scheme 10: Coupling reaction of aminoethyl-linked mannose to carboxylic group of PEG-c-CA-CA SCPs via standard PyBOP and HOBt peptide coupling chemistry.

The degree of functionalization of PEG-Man SCPs was determined via microscope TBO assay. Briefly, the carboxylic group functionalization degree was measured before and after the coupling reaction with aminoethyl linked mannose. The difference in degree of carboxylic group functionalization before and after the coupling reaction then equals degree of mannose functionalization as no side reactions decreasing the number of free carboxylic groups is expected. Figure 21 shows the results for the degree of mannose functionalization of the series of PEG-SCPs with different Young's modulus. It can be found that the degree of mannose functionalization for all SCPs is in the range of 90 ± 20 µmol/g. Furthermore, most of the carboxylic groups on PEG-CA SCPs were coupled with aminoethyl linked mannose. Only around 5 ± 5 µmol/g carboxylic groups were left after ligand functionalization. The detailed results are summarized in Table 10. It shows the reaction yield on average is 93 ± 6 % for the different SCPs, which again confirms that the elastic property does not influence the coupling reaction of SCPs carboxylic group with aminoethyl linked mannose.

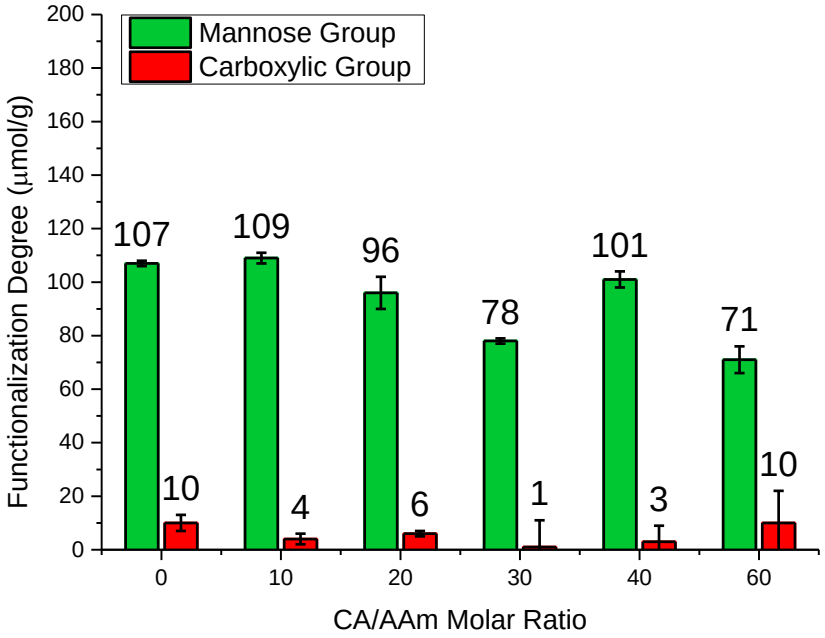

Figure 21: Mannose group functionalization degree and carboxylic group functionalization degree of PEG-Man SCPs.

Table 10: Results of functionalization of the carboxylic group functionalized SCPs with aminoethyl linked mannose.

Sample	Carboxylic Group Functionalization Degree of PEG-c-CA-CA SCPs [µmol/g]	Unreacted Carboxylic Group Functionalization Degree of PEG-Man SCPs [µmol/g]	Mannose Group Functionalization Degree of PEG-Man SCPs [µmol/g]	Yield [%]
PEG(0)-Man	117 ± 6	10 ± 3	107 ± 1	91
PEG(10)-Man	113 ± 5	4 ± 2	109 ± 2	96
PEG(20)-Man	102 ± 6	6 ± 1	96 ± 6	94
PEG(30)-Man	79 ± 7	1 ± 10	78 ± 1	99
PEG(40)-Man	104 ± 5	3 ± 6	101 ± 3	97
PEG(60)-Man	81 ± 2	10 ± 12	71 ± 5	88

After mannose functionalization, the Young's modulus of PEG-Man SCPs was again determined through AFM indentation measurements applying the Hertzian model. As expected, the trend of the Young's modulus stays the same. The more crotonic acid was added to the reaction during PEG-c-CA SCPs synthesis, the smaller Young's modulus the PEG-Man SCPs have. However, it can also be found that the Young's modulus of PEG-Man does not follow the exact same trend as the Young's modulus of PEG-c-CA SCPs. For all SCPs, the Young's modulus gets smaller after mannose functionalization. This can be due to two reasons. One reason is that remaining unreacted and thus free PEG chains entangled in the hydrogel network were washed out during the functionalization steps. During the mannose functionalization process, there were more than eighteen additional washing steps. Theses vigorous washing steps could potentially wash all unreacted free PEG chains out from the hydrogel network leading to a smaller Young's modulus. The other reason can be due to the aging of the SCPs. On the one hand, the PEG-c-CA SCPs were irradiated with UV light for a comparably long time during the carboxylic group functionalization process. On the other hand, the whole carboxylic group functionalization process and mannose functionalization process takes several weeks in practice. Both of them may cause breaking and partial loss of covalent bonds of the network causing a reduced Young's modulus through the so-called aging of the SCPs.

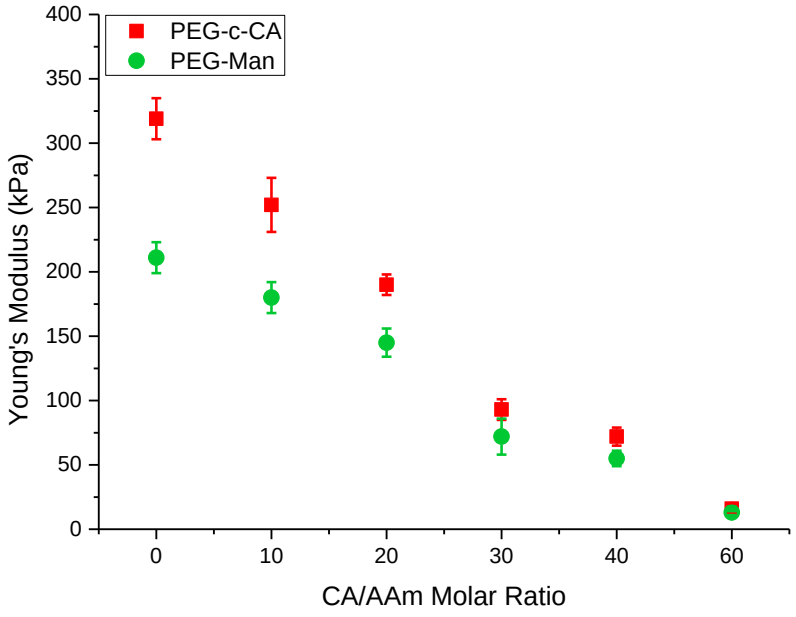

Figure 22: Young's modulus of PEG-c-CA SCPs and PEG-Man SCPs.

3.2.2.2 Functionalization of PEG-CA SPCs with Biotin-NH_2

Biotin avidin is one of the ligand receptor pair investigated in this work. In order to functionalize the PEG-CA SCPs with biotin, amine groups must be brought onto the structure of biotin first. Here, biotin was modified with ethylenediamine through a protocol adapted from Tao *et. al*. [94] To produce aminoethyl linked biotin, biotin methyl ester was firstly synthesized. Commercially available biotin was mixed with methanol and strong acidic cation exchange resin for 65 h under room temperature. The methyl group was detected by NMR, which was based on the presence of a singlet at 3.67 ppm. Then, a high excess amount of ethylene diamine was mixed with biotin methyl ester and methanol for 48 h at 60 °C under condensation reflux. The final product, aminoethyl linked biotin, was identified by NMR, based on the presence of a specific multiplet at 2.62 ppm (see Experimental Section and Spectral Appendix).

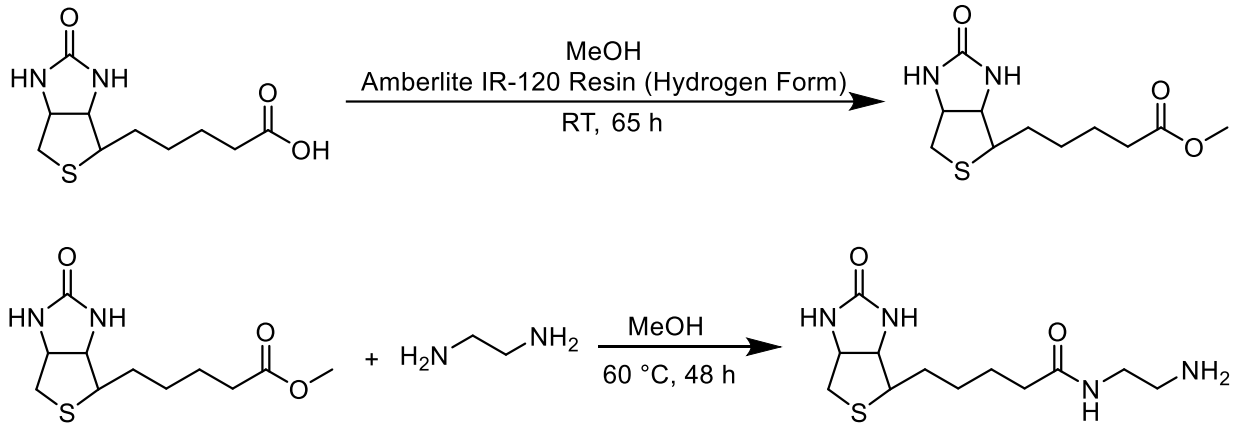

Scheme 11: Reaction scheme of biotin modification with aminoethyl group. [94]

In a standard protocol (see Experimental Section), PEG-CA SCPs was washed with DMF to remove the ethanol from previous steps and 10 eq. PyBOP, 5 eq. HOBt, 10 eq. DIPEA, and 10 eq. aminoethyl-linked biotin were added to the reaction mixture and shaken 180 min under room temperature. After the reaction, the SCPs were washed with DMF to remove the unreacted biotin and other residues. At the end, the PEG-Biotin SCPs were washed with Type I water in preparation for the SCP-RICM experiment.

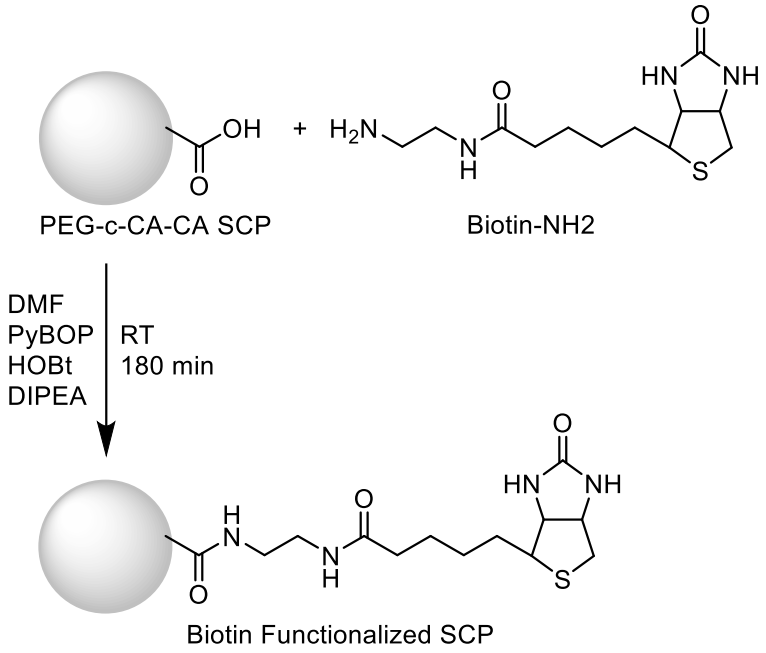

Scheme 12: Coupling reaction of aminoethyl-linked biotin to carboxylic group of PEG-c-CA-CA SCPs via standard PyBOP and HOBt peptide coupling chemistry.

The functionalization degree of PEG-Biotin SCPs was also determined through microscope TBO assay as previously discussed for the PEG-Man SCPs. From Figure 23 it can be found the biotin functionalization degree is in a range of 90 ± 25 µmol/g. Most of the carboxylic groups on PEG-CA SCPs were coupled with aminoethyl linked biotin. Only around 9 ± 6 µmol/g carboxylic group remained free. The detailed results are summarized in Table 10. It shows the reaction yield stays in the range of 91 ± 8 % for different groups of SCPs, which indicates the elastic property does not influence the coupling reaction of SCPs carboxylic group with aminoethyl linked biotin.

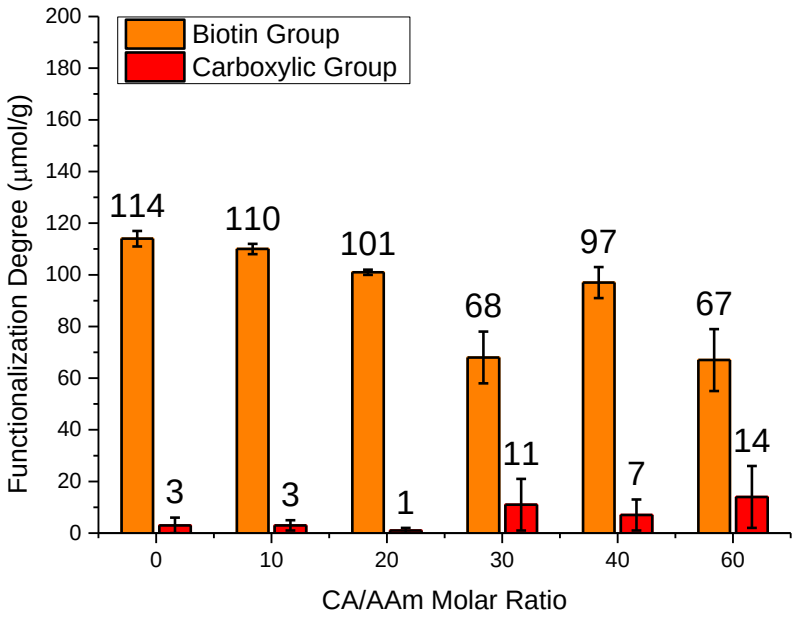

Figure 23: Biotin group functionalization degree and carboxylic group functionalization degree of PEG-Biotin SCPs.

Table 11: Results of functionalization of the carboxylic group functionalized SCPs with aminoethyl linked biotin.

Sample	Carboxylic Group Functionalization Degree of PEG-c-CA-CA SCPs [µmol/g]	Unreacted Carboxylic Group Functionalization Degree of PEG-Biotin SCPs [µmol/g]	Biotin Group Functionalization Degree of PEG-Biotin SCPs [µmol/g]	Yield [%]
PEG(0)-Biotin	117 ± 6	3 ± 3	114 ± 3	97
PEG(10)-Biotin	113 ± 5	3 ± 2	110 ± 2	89
PEG(20)-Biotin	102 ± 6	1 ± 1	101 ± 1	99
PEG(30)-Biotin	79 ± 7	11 ± 10	68 ± 10	86
PEG(40)-Biotin	104 ± 5	7 ± 6	97 ± 6	93
PEG(60)-Biotin	81 ± 2	14 ± 12	67 ± 5	83

After biotin functionalization, the Young's modulus of PEG-Biotin SCPs was determined through AFM indentation measurement applying the Hertzian model. Similar to the PEG-Man SCPs, the trend of the Young's modulus stayed the same as for the original PEG-c-CA SCPs. The more crotonic acid was added to the reaction during PEG-c-CA SCPs synthesis, the smaller is the Young's modulus of the PEG-Man SCPs. It was also found that the Young's modulus of PEG-Man did not fully inherit the Young's modulus of PEG-c-CA SCPs. For all the groups, the Young's modulus gets smaller after mannose functionalization. This phenomenon also occurred in the case of PEG-Biotin SCPs potentially caused by washing out of unreacted PEG and/or aging of the SCPs as discussed previously.

In addition, one could also observe that the Young's modulus of PEG-Biotin SCPs for all groups is slightly higher than for the PEG-Man SCPs. This is most likely due to the hydrophobicity of the biotin ligand. When the hydrogel network is functionalized with a large amount of biotin, the network will become more hydrophobic, which will reduce the swelling of the hydrogel network in aqueous solution, e.g. during the AFM indentation measurement in PBS. When the hydrogel shrinks, the hydrogel network will become denser, thus the Young's modulus is higher.

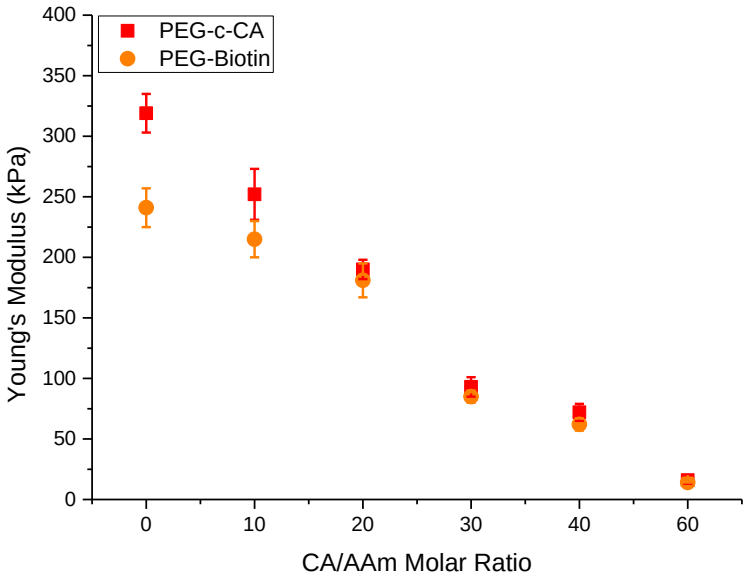

Figure 24: Young's modulus of PEG-c-CA SCPs and PEG-Biotin SCPs.

3.2.3 Ligand Functionalization of PAA SCPs

For PEG hydrogel based SCPs, the ligand concentration was mainly controlled through controlling the degree of carboxylic group functionalization via grafting reaction. One method is to use the different free radical polymerization reactivity of acrylic acid, methacrylic acid, and crotonic acid to control the grafting of poly(carboxylic acid) chain length to control the degree of carboxylic group functionalization of SCPs. The other method is to increase the degree of carboxylic group functionalization by multiple cycles of irradiation and exchanged fresh reaction solution. With these two methods, the carboxylic group functionalization degree was previously varied in the range of 50 - 250 µmol/g. [77] [76] [53]

In order to tune the ligand functionalization degree of SCPs in a wider range, in this work PAA hydrogel based SCPs were introduced. The Young's modulus of PAA SCPs was successfully controlled through by tuning the crosslinking degree via the crosslinker/monomer ratio in Chapter 3.1.2. However, a new method that allows tuning the ligand concentration had to be developed. As presented at the beginning of this chapter, one approach is to combine ligands and non-ligands during the coupling step. By changing the ratio of ligand and non-ligand compounds, the final ligand concentration can be controlled. The other approach is to control the ligand concentration through tuning the coupling reaction equivalent. By decreasing the concentration of ligand in the reaction mixture, lower degrees of functionalization can be achieved.

3.2.3.1 Co-coupling of Mannose and Monoethanolamine on PAA SCPs

In order to tune the ligand concentration of PAA hydrogel based SCPs, the co-coupling approach was developed here. For a normal coupling reaction, 10 mL of PAA SCPs were washed with DMF to remove water from SCPs. 10 eq. ligand, 10 eq. PyBOP, 5 eq. HOBt, and 10 eq. DIPEA were added to SCPs. In the case of co-coupling, a certain percentage of mannose ligand was replaced by monoethanolamine (MEA) as a non-ligand. (See Table 12) MEA is a small compound, which has an amine group that can be readily used for coupling to the carboxylic acid functionalized SCPs, while the hydroxyl group has no specific interaction with proteins and should give no undesired interactions during the SCP-RICM experiments. For example, when 90 mol. % of mannose were replaced by MEA, it was expected that the resulting coupled functional groups

contains 10 mol. % mannose and 90 mol. % MEA. After the reaction, the SCPs were washed with DMF to remove the unreacted mannose and other residues, and then washed with methanol. Sodium methoxide in methanol was added to the reaction mixture and shaken for 30 min at room temperature to deprotect the mannose. At the end, the PAA-Man SCPs were washed with methanol and then Type I water for the SCP-RICM experiment.

Table 12: Synthesis of PAA-Man SCPs with different mannose functionalization degree via replacing ligand mannose with non-ligand MEA.

Sample Name	Mannose-NH_2 [µmol]	MEA [µmol]
PAA(1.0)-0%Man	0	1075
PAA(1.0)-1%Man	12	1058
PAA(1.0)-10%Man	108	959
PAA(1.0)-100%Man	1080	0

The total functionalization degree of mannose and monoethanolamine were determined with TBO titration. According to the molar ratio of mannose and monoethanolamine, the degree of functionalization was calculated from the total degree of functionalization degree. From Figure 25 it can be found the functionalization degree were successfully tuned through the co-coupling approach. Four groups of PAA-Man SCPs with 0 ± 22 µmol/g, 135 ± 8 µmol/g, 1350 ± 6 µmol/g, 12990 ± 19 µmol/g mannose functionalizaiton degree were achieved. Table 13 summarized the results of mannose functionalized PAA SCPs. One should notice that although mannose functionalization degree can be controlled through this approach, the amount of MEA group is also quite high for all three samples. This may potentially change the properties of SCPs, such as Young's modulus or influence later adhesion experiments.

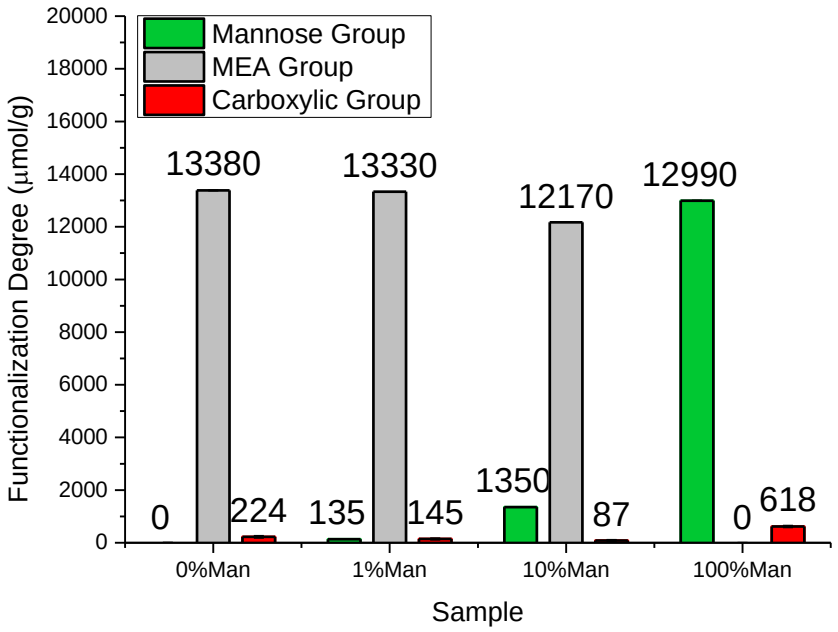

Figure 25: Mannose group functionalization degree, MEA group functionalization degree, and carboxylic group functionalization degree of PAA-Man SCPs, where 0%Man, 1%Man, 10%Man, and 100%Man stands for the sample PAA(1.0)-0%Man, PAA(1.0)-1%Man, PAA(1.0)-10%Man, PAA(1.0)-100%Man.

Table 13: Results of functionalization of PAA SCPs through co-coupling reaction with aminoethyl linked biotin and monoethanolamine.

Sample Name	Functionalization Degree [µmol/g]		
	Unreacted Carboxylic Group	Mannose	MEA
PAA(1.0)-0%Man	224 ± 22	0 ± 22	13380 ± 22
PAA(1.0)-1%Man	145 ± 8	135 ± 8	13330 ± 8
PAA(1.0)-10%Man	87 ± 6	1350 ± 6	12170 ± 6
PAA(1.0)-100%Man	618 ± 19	12990 ± 19	0 ± 19

The Young's modulus of PAA-Man SCPs was determined in lectin binding buffer (LBB) at pH7.4 via AFM indentation measurements applying the Hertzian model. Figure 26 shows the Young's modulus of PAA SCPs. It can be found that for bare PAA SCPs without further functionalization, the Young's modulus of PAA SCPs measured in PBS at pH7.4 is only 7 ± 1 kPa,

but when measuring in LBB at pH 7.4, the Young's modulus of PAA SCPs increased to 53 ± 5 kPa. This is due to the presence of divalent cations Ca^{2+} and Mn^{2+} in LBB, which act as crosslinker between deprotonated carboxylic groups from PAA chains through electrostatic interactions. These crosslinking points will increase the crosslinking degree of PAA SCPs, and thus also the Young's modulus of PAA SCPs. For functionalization with only MEA (PAA-0%Man100%), the Young's modulus does not change and stays at 55 kPa. This indicates that the functionalization of PAA SCPs with MEA does not influence the Young's modulus of SCPs. However, when mannose was bound to the SCPs, the Young's modulus decreased to 10 - 15 kPa. Even for the lowest degree of functionalization of 135 + 8 µmol/g of mannose, the Young's modulus is still strongly affected. This could be due to the hydrophilicity of the mannose ligand and the resulting stronger swelling of the hydrogel leading to a decrease in Young's modulus.

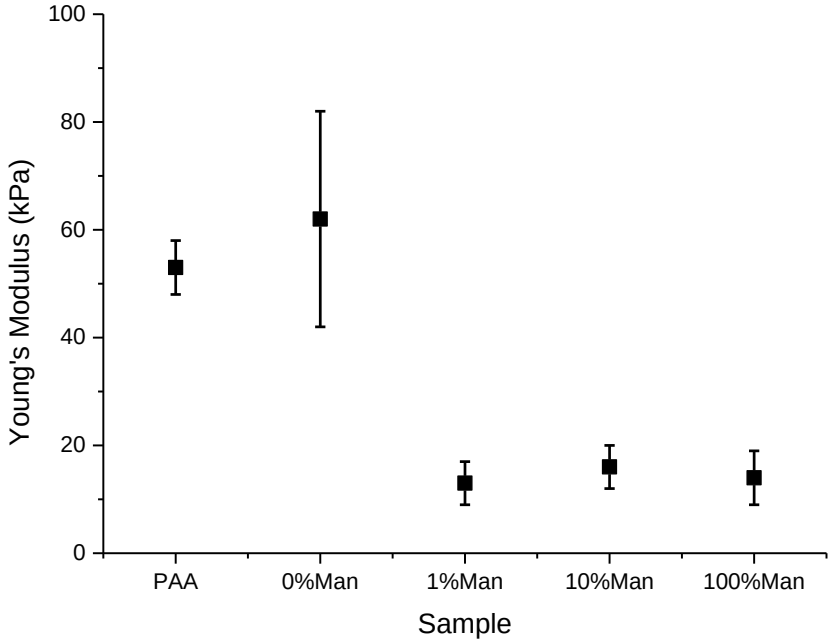

Figure 26: Young's modulus of PAA SCPs and PAA-Man SCPs measured in LBB7.4, where 0%Man, 1%Man, 10%Man, and 100%Man stands for the sample PAA(1.0)-0%Man, PAA(1.0)-1%Man, PAA(1.0)-10%Man, PAA(1.0)-100%Man.

3.2.3.2 Tuning the reactant equivalent during ligand coupling on PAA SCPs

Another approach to tune the ligand concentration on PAA hydrogel based SCPs is tuning the coupling reaction equivalent. In the previous experiments, high excess of reactants was used in order to achieve maximum functionalization of the SCPs. Results have shown that the coupling reaction yield achieved is in the range of 90 ± 10 %, which indicates most of the carboxylic groups on the PAA SCPs were reacted. Thus, reducing the excess of reagents could potentially lower the coupling reaction yield. Through this method, the concentration of ligand, receptor, or other functional groups on PAA SCPs could be controlled.

Here, monoethanolamine (MEA) was used as a model functional group as the first test to analyse if control of functionalization degree by varying the chemical equivalent is viable.

In this work, six groups of PAA-MEA SCPs were synthesized with different equivalents of MEA from 10 eq.to 0.01 eq. MEA. The other reactants were kept constant in molar ratios according to the standard protocol (see Experimental Section). For example, in the group of 10 eq. MEA, 10 eq. PyBOP, 5 eq. HOBt, and 10 eq. DIPEA were added to the reaction. The mole ratio of theses reactants was MEA:PyBOP:HOBt:DIPEA=2:2:1:2. When the MEA equivalent was reduced to 1 eq. the equivalent of PyBOP, HOBt, and DIPEA were also correspondingly reduced to 1 eq., 0.5 eq., and 1 eq., respectively. The molar ratio of these reactants thus was constant at MEA:PyBOP:HOBt:DIPEA=2:2:1:2.

For the functionalization step, PAA SCPs were washed with DMF to remove water. MEA, PyBOP, HOBt, and DIPEA were added to PAA SCPs. The reaction mixture was shaken for 180 min at room temperature. After the reaction, the PAA SCPs were washed with DMF to remove unreacted compounds and other residues, and then washed by water to remove DMF for characterization via microscope TBO assay.

The degree of functionalization of PAA-MEA SCPs was determined via microscope TBO assay as described previously. From Figure 27 it can be found that the MEA functionalization degree decreased when the reaction equivalent decreases. However, there is no linear correlation between the MEA functionalization degree and reaction equivalent in the range of 10 eq. to 0.01 eq. From 10 eq. to 1 eq., the functionalization degree only decreased from 10580 ± 320 µmol/g to 7580 ± 400 µmol/g. 10 % MEA still leads to 72 % of the MEA functionalization degree of the standard protocol. In the range below 0.1 equivalent, it can also be found that the yield stays in the range of

0.1 % to 2.0 %. Meanwhile, when reducing the reaction equivalent from 1 eq. to 0.1 eq., the MEA functionalization degree significantly decreased from 7580 ± 400 µmol/g to 270 ± 200 µmol/g. This indicates that the range of 1 - 0.1 eq. is most efficient tuning range of the MEA functionalization degree of PAA hydrogel based SCPs. In conclusion, the results show that the MEA functionalization degree can be tuned through controlling the reaction equivalent. However, the relation of reactants equivalent and MEA functionalization degree is not linear. The most efficient tuning range is 1 eq. to 0.1 eq. Overall, this approach to tune the degree of functionalization proved to be less controlled as compared to varying the ratio between ligands/non-ligands (see Chapter 3.2.3.1).

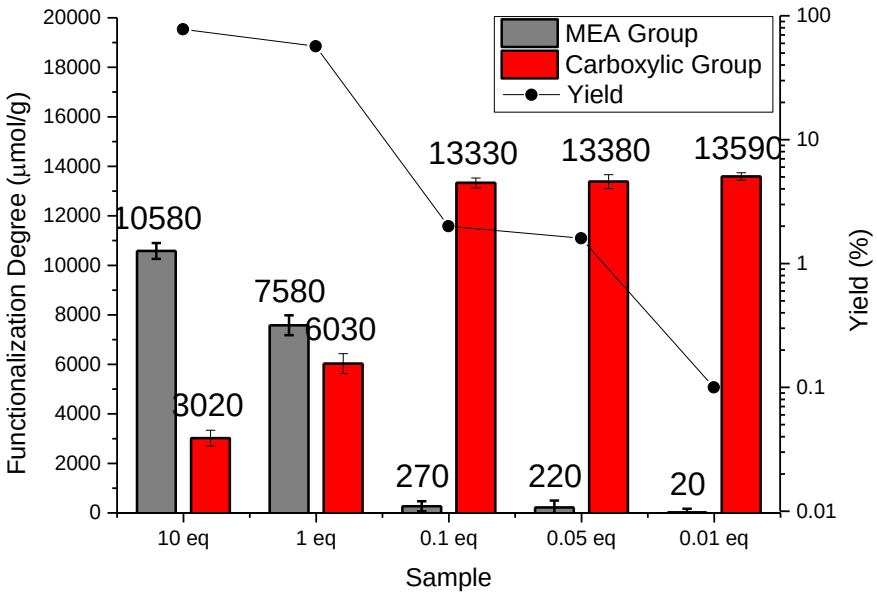

Figure 27: MEA functionalization degree and the unreacted carboxylic group functionalization degree of PAA-MEA SCPs synthesized with various reactants equivalent, where 10 eq, 1, eq, 0.1 eq, 0.05 eq. and 0.01 eq stands for PAA(1.0)-10eqMEA, PAA(1.0)-0eqMEA, PAA(1.0)-0.1eqMEA, PAA(1.0)-0.05eqMEA, PAA(1.0)-0.01eqMEA synthesized with corresponding MEA equivalent.

Table 14: Results of functionalization of PAA-MEA SCPs through reactants equivalent tuning with MEA.

Sample	Functionalization Degree [µmol/g]		Yield [%]
	MEA	Unreacted Carboxylic Group	
PAA(1.0)-10MEA	10580 ± 320	3020 ± 320	77.8
PAA(1.0)-1MEA	7580 ± 400	6030 ± 400	56.7
PAA(1.0)-0.1MEA	270 ± 200	13330 ± 200	2.0
PAA(1.0)-0.05MEA	220 ± 280	13380 ± 280	1.6
PAA(1.0)-0.01MEA	20 ± 150	13590 ± 150	0.1

Summary: Synthesis and Functionalization of SCPs

Firstly, SCPs with different Young's modulus were synthesized to tune the flexibility of ligand presenting soft biomimetic interfaces in the SCP-RICM set-up. One possibility to tune the Young's modulus was to tune the cross-linking degree of the hydrogel, thus two approaches were applied here. In PEG-c-CA approach, PEG-dAAm was used a macromonomer and a cross-linker at the same time, meanwhile, crotonic acid was used as a co-monomer. Due to the low reactivity of crotonic acid in polymerization, the active chain ends of PEG-dAAm were blocked and the cross-linking degree was reduced. As a result, the Young's modulus could be controlled in a range of 16 ± 4 kPa to 319 ± 16 kPa. In the PAA approach, acrylic acid and MBAm as crosslinker were used to synthesize SCPs. The cross-linking degree was directly tuned by cross-linker/monomer ratio during polymerization. However, due to the small SCPs size and opaque SCPs for highly cross-linked SCPs, the Young's modulus can only be controlled in a range of 7 ± 1 to 53 ± 5 kPa.

Secondly, the both SCP systems were functionalized further with different ligands via amide coupling. Here, special focus was devoted to tuning the degree of functionalization for PAA SCPs, the ligand concentration was tuned through two approaches. Through one approach, amino ethyl linked ligand and the monoethanolamine were mixed with certain ratio and co-coupled to the carboxylic group at the same time. The ligand concentration can be controlled through controlling the ligand/monoethanolamine ratio. Through the other approach, the reaction equivalent was tuned to control the ligand concentration on PAA SCPs. For a normal SCPs ligand functionalization, a high excess 10 eq. ligands were used in the coupling reaction for a 100 % yield. Here, the

equivalent was decreased to reduce the coupling reaction yield, thus reduce the ligand concentration on PAA SCPs.

3.3 Specific Interaction Measurements with Ligand Functionalized SCPs via RICM

The objective of this work was to investigate the influence of mechanical properties of SCP material, ligand concentration, and ligand type on ligand receptor interactions at soft biomimetic interfaces by using the SCP-RICM method. In order to achieve the above goals, SCPs with controlled variations in these parameters were synthesized and functionalized (see Chapter 3.1 and Chapter 3.2).

In this chapter, the ligand functionalized SCPs were ready to be used in the SCP-RICM experiment to investigate the ligand receptor interaction process. In this first subchapter, proof of principle measurements of the PAA SCPs system are presented. This is important because PAA as hydrogel material for SCPs and biotin avidin as ligand receptor pair is studied here for the first time. The influence of ligand concentration on ligand receptor specific adhesion between ligand receptor surfaces will be discussed. Previous work showed the overall adhesion energy increases with the increasing of the concentration of ligand on SCPs. [76] However, due to the limitation of the highest ligand concentration on PEG hydrogel based SCPs, the results have only shown the relation of ligand concentration and adhesion energy below 193 ± 29 µmol/g. [76] When further increasing the ligand concentration on SCPs, the behaviour is still unknown. In the second subchapter, proof of principle measurements of biotin avidin ligand receptor pair are presented. The influence of Young's modulus of soft interfaces on ligand receptor specific adhesion will be discussed. PEG-c-CA hydrogel based SCPs with various Young's moduli functionalized with aminoethyl linked mannose and aminoethyl linked biotin will be discussed. The different trend of biotin avidin ligand receptor pair and mannose Con A ligand receptor pair versus SCP Young's modulus will be analysed as well.

3.3.1 Investigation on Ligand Receptor Interaction via PAA SCP-RICM

3.3.1.1 Mannose Con A Interaction and Inhibition on PAA SCPs System

In order to use PAA hydrogel based SCPs in the SCP-RICM experiment, their compatibility with the set-up had to be tested. Firstly, the surfaces used in SCP-RICM experiment were prepared. According to the ligand receptor pairs investigated in this thesis, slides were coated with Con A as binding partner to the mannose functionalized SCPs and with bovine serum albumin (BSA) as non-binding receptor for a negative control. Secondly, surfaces were covered with LBB at pH7.4, which contains Ca^{2+} and Mn^{2+} to help mannose binding to Con A. [95] Thirdly, PAA SCPs were added onto the Con A functionalized surface in LBB7.4. PAA-Man SCPs were added on three surfaces under different experiment condition: Con A functionalized surface in LBB7.4, Con A functionalized surface in LBB7.4 with 25 mM methyl mannose (MeMan), BSA functionalized surface in LBB7.4. Finally, the slides were studied by RICM, taking images of contact areas of the SCPs. The images were record with a CMOS camera and analysed with software ImageJ, Hydrogel, and Igor Pro for the corresponding adhesion energy.

Figure 28 shows the typical RICM images of PAA and PAA-Man SCPs on Con A or BSA surfaces under different experiment conditions. As introduced in the Chapter 1.3, the larger contact area reflects the higher adhesion energy given identical SCP size and Young's modulus. It was found that PAA SCPs has small unspecific adhesion with Con A surface, which is most likely caused by the secondary interactions between carboxylic group on PAA SCPs and the positively charged groups, e.g. amine group on Con A. PAA-Man SCPs have the highest adhesion energy on Con A as expected. When inhibiting the surface with MeMan, the adhesion energy of PAA-Man SCPs reduces significantly. The MeMan ligands are competing with the mannose bound on the SCPs. When all the binding sites on Con A surface are occupied by MeMan, the PAA-Man SCPs detaches from the surface. This indicates that the interaction between the mannose functionalized SCPs and the Con A surface is due to specific interactions. In addition, PAA-Man SCPs have no adhesion energy with BSA surface, again indicating that the adhesion of the PAA-Man SCPs to Con A surface is based on specific ligand receptor interactions.

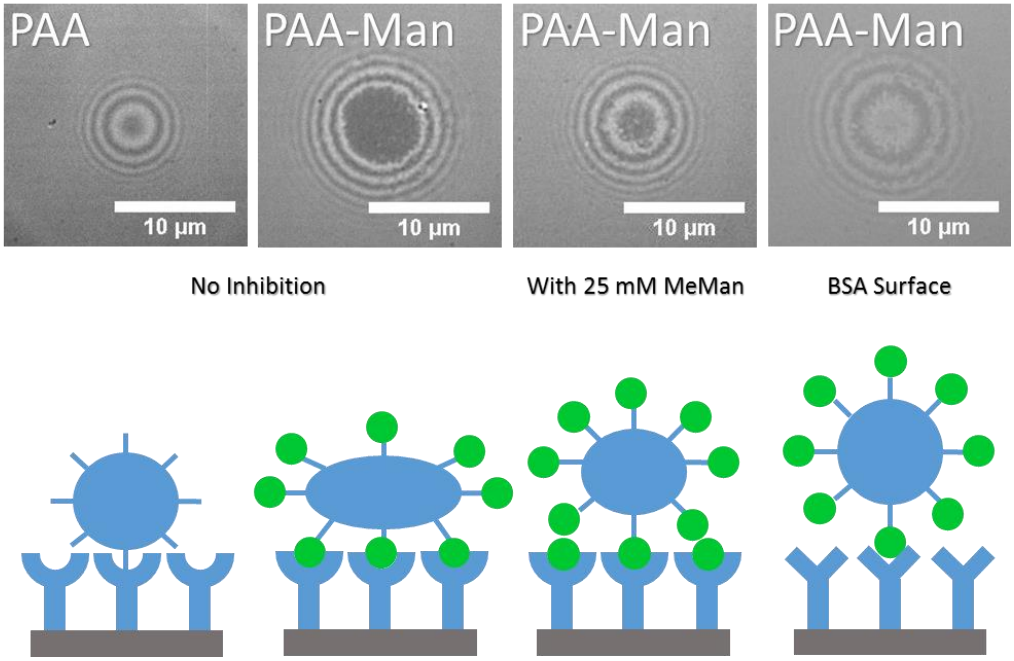

Figure 28: Typical RICM image and binding scheme of PAA SCPs and PAA-Man SCPs under different experiment condition.

In Figure 29, the normalized adhesion energy values for PAA SCPs are depicted. The adhesion energy of PAA-Man SCPs on Con A surface in LBB7.4 was set to 100% (full adhesion). The adhesion energy under other conditions was normalized according to this 100 % adhesion. It can be found that when inhibiting the Con A surfaces with 25 mM MeMan, the adhesion energy significantly decreases to 24 %. This indicates that the majority of the adhesion energy between PAA-Man SCPs and Con A surface is based on specific adhesion. Although the adhesion energy decreases a lot upon inhibition, there is still some remaining adhesion with the Con A slides under the presence of 25mM MeMan. This is due to the high concentration of mannose groups on the PAA SCPs. The mannose group concentration on PAA hydrogel network is ~100 mM. However, as introduced in Chapter 1.1, the binding between ligand and receptor is not permanent, but rather a dynamic process. When competing with the mannose groups from PAA-Man hydrogel network, part of the MeMan blocked binding sites on Con A surfaces were passed to mannose groups of PAA-Man SCPs, and thus led to the adhesion between PAA-Man SCPs and Con A surface. As the water solubility of MeMan is 4.4 M, it is possible in the future to further increase MeMan inhibition concentration in SCP-RICM experiment, and higher inhibition yield is expected to be achieved.

As mannose has no specific binding to BSA, the adhesion energy of PAA-Man SCPs decreases to only 2 % on BSA slides. This again confirms that the adhesion energy between PAA-Man SCPs and Con A surface is mainly from specific ligand receptor binding.

When PAA SCPs without mannose functionalization were used as a reference, it can be found that normalized adhesion energy between PAA SCPs and Con A surfaces is 10 ± 1 %. This indicates that carboxylic groups lead to unspecific adhesion of SCPs with the Con A surface. However, this unspecific adhesion will only slightly contribute to the overall adhesion between PAA-SCPs and Con A surface, as the number of remaining carboxylic groups on PAA-Man SCPs is only 1 – 2 mol. % of the number of carboxylic groups on PAA SCPs.

Thus PAA based SCPs can be applied for SCP-RICM experiment for investigating the interaction between mannose and Con A. However, as carboxylic groups always have unspecific adhesion with protein surfaces, the remaining carboxylic groups of ligand functionalized SCPs should be covered with non-ligands, or normalized in the calculation procedure.

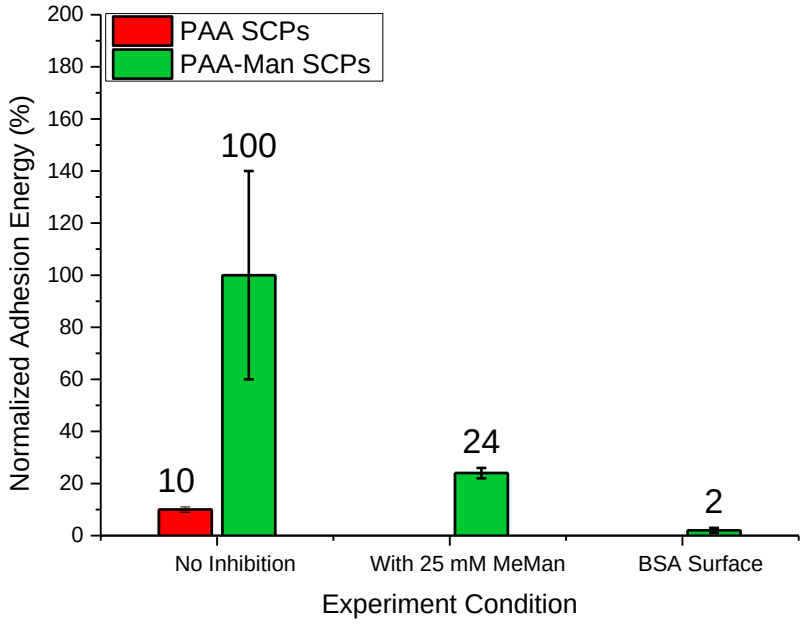

Figure 29: Normalized adhesion energy of PAA SCPs and PAA-Man SCPs under different experiment condition.

3.3.1.2 Effects of Ligand Concentration on SCP Adhesions

The influence of ligand concentration on mannose Con A interactions were investigated with PAA-Man SCPs. In previous preliminary study, it was found that the higher the ligand concentration of the SCPs, the higher the specific adhesion energy that was detected, and the ligand concentration and the specific adhesion energy so far showed a linear correlation. [76] However, due to the limitation of ligand functionalization degree of PEG hydrogel based SCPs, the highest ligand concentration in previous studies only reached 200 µmol/g. When further increasing the ligand concentration on SCPs, it is possible that there might also be a plateau and potentially even decrease in adhesion if the degree of ligand functionalization goes higher and higher. In order to test the relation between ligand concentration and adhesion energy above 200 µmol/g, PAA-Man SCP RICM experiment was performed.

Here, the ligand concentration on SCPs was pushed much higher with the help of PAA based SCPs. Through the ligand (mannose)/non-ligand (monoethanolamine) coupling strategy, the ligand concentration on PAA SCPs was controlled (see chapter 3.2.3.1). To perform the SCP-RICM experiment, glass slides were coated with Con A. The slides were immersed in LBB at pH 7.4 and 10 µL of the different SCPs, PAA(1.0)-100%Man, PAA(1.0)-10%Man, PAA(1.0)-1%Man, and PAA(1.0)-0%Man were added on the slides separately. All slides were studied by RICM and images were record with a CMOS camera and analysed with software ImageJ, Hydrogel, and Igor Pro for measuring the direct binding adhesion energies.

Then, as a mean to test for specific adhesion, a certain amount of MeMan (25 mM) was added into the LBB at pH7.4 to inhibit the specific adhesion between mannose functionalized SCPs and Con A functionalized surfaces. The remaining adhesion energies were considered as non-specific adhesion, and thus subtracted from the direct binding adhesion energies measured without inhibition in previous step. Then, the calculated specific adhesion energy of PAA(1.0)-100%Man SCPs was set as 100 %, and the calculated specific adhesion energy of other batches of SCPs were normalized according to this batch.

Table 15: Influence of mannose ligand concentration on mannose Con A specific adhesion energy investigated via PAA-Man SCP-RICM

Sample Name	Functionalization Degree [µmol/g]			Normalized Specific Adhesion Energy [%]
	Unreacted Carboxylic Group	Mannose	MEA	
PAA(1.0)-0%Man	224 ± 22	0 ± 22	13380 ± 22	0 ± 3
PAA(1.0)-1%Man	145 ± 8	135 ± 8	13330 ± 8	3 ± 6
PAA(1.0)-10%Man	87 ± 6	1350 ± 6	12170 ± 6	53 ± 22
PAA(1.0)-100%Man	618 ± 19	12990 ± 19	0 ± 19	100 ± 8

Table 15 shows the results for the PAA-Man SCPs with different degree of functionalization and their normalized adhesion energy on Con A surfaces. It was found that the mannose Con A adhesion energy increases when increasing the mannose ligand concentration on SCPs in the range of 0 - 2000 µmol/g. However, the increase in adhesion energy is not linear anymore for higher degrees of functionalization but seems to stall and potentially will reach a plateau for concentration of 13 mmol/g and higher. This is expected as the number of binding sites on Con A is limited. The hydrodynamic radius of Con A is 3.3 nm. [96] If it is assumed that Con A is cubic, the volume of a Con A is 3.6E-23 L, thus the binding site concentration of Con A is 185 mM. Considering the Con A proteins in SCP-RICM experiment are all immobilized on glass surface. The maximum accessible binding site concentration will only be half of the binding sites (93 mM). However, as discussed before, the highest mannose concentration of PAA(1.0)-100%Man SCPs is ~100 mM, which is almost the same concentration as the accessible binding sites. This is the potential reason why when using the PAA(1.0)-100%Man SCPs, the adhesion energy seems to reach a plateau. Therefore, when available binding partner (ligand or receptor) is saturated, addition of further binding partners does not lead to further increase in adhesion.

3.3.2 Investigation on Ligand Receptor Interaction via PEG SCP-RICM

3.3.2.1 Biotin-Avidin Interaction and Inhibition on PEG SCPs System

In previous work, the SCP-RICM method has been successfully applied to investigate ligand receptor interactions using PEG SCPs. However, the ligands in this experiment were always weakly interacting sugar ligands. [46] [51] [79]. The compatibility of the SCP-RICM method for non-sugar and potentially stronger binding ligands is still unknown. Here, biotin avidin interactions with SCPs were analysed for the first time. Thus, before using SCP-RICM to investigate the biotin avidin interactions, the compatibility of SCP-RICM method to biotin avidin ligand receptor pair must be tested.

In order to test the biotin avidin ligand receptor pair, glass slides were coated with avidin, or with biotin avidin mixture in a biotin:avidin weight ratio of 3:200. Then, the slides were covered with PBS at pH 7.4. PEG SCPs, PEG-AA SCPs, and PEG-Biotin SCPs were added on these slides separately. Additionally, a second set of avidin slides were covered with PBS 7.4 with 0.2 mM Biotin, HCl-KCl buffer at pH 2.0, or NaOH-KCl buffer at pH 12.0. PEG-Biotin SCPs were added onto these slides. The biotin inhibited avidin coated slide was covered with PBS 7.4, and PEG-Biotin SCPs were added onto this slide. All slides were studied by RICM and images were record with a CMOS camera and analysed with software ImageJ, Hydrogel, and Igor Pro for the corresponding adhesion energy.

As here focus was on a general compatibility test, the Young’s modulus and the functionalization degree of the SCPs were not characterized in detail. The PEG-Biotin SCPs on avidin functionalized surface in PBS at pH 7.4 shows full adhesion of biotin avidin ligand receptor pair. Thus, this adhesion energy value was set as 100 %. The adhesion energy of the other groups was normalized according to this group.

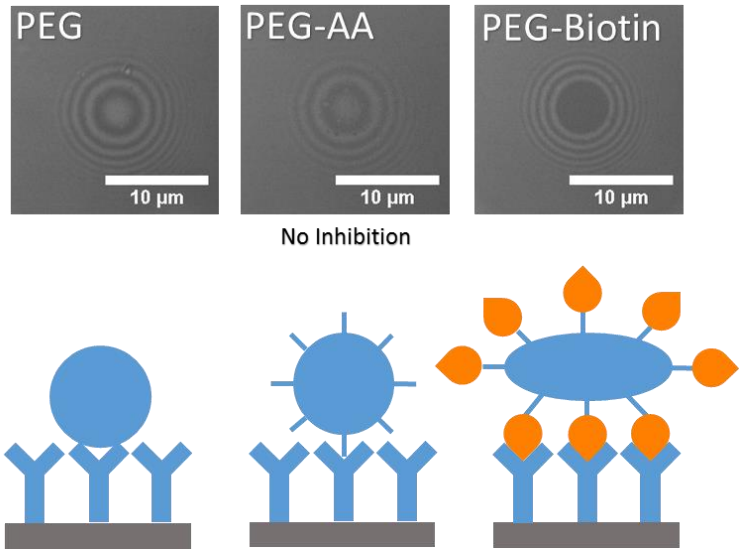

Figure 30: Typical RICM image and schematic presentation of PEG SCPs, PEG-AA SCPs, and PEG-Biotin SCPs on avidin functionalized surface.

Figure 30 shows three typical RICM images and its schematic presentation of PEG SCPs, PEG-AA SCPs, and PEG-Biotin SCPs on avidin functionalized surface. Table 16 shows PEG SCPs and PEG-AA SCPs only have 2 % and 1 % adhesion energy on avidin surface, respectively, which confirms that PEG SCPs have neither specific nor non-specific interactions with avidin.

Table 16: Normalized adhesion energy of PEG SCPs, PEG-AA SCPs, and PEG-Biotin SCPs via RICM experiment

Sample	Normalized Adhesion Energy [%]
PEG	2 ± 1
PEG-AA	1 ± 1
PEG-Biotin	100 ± 1

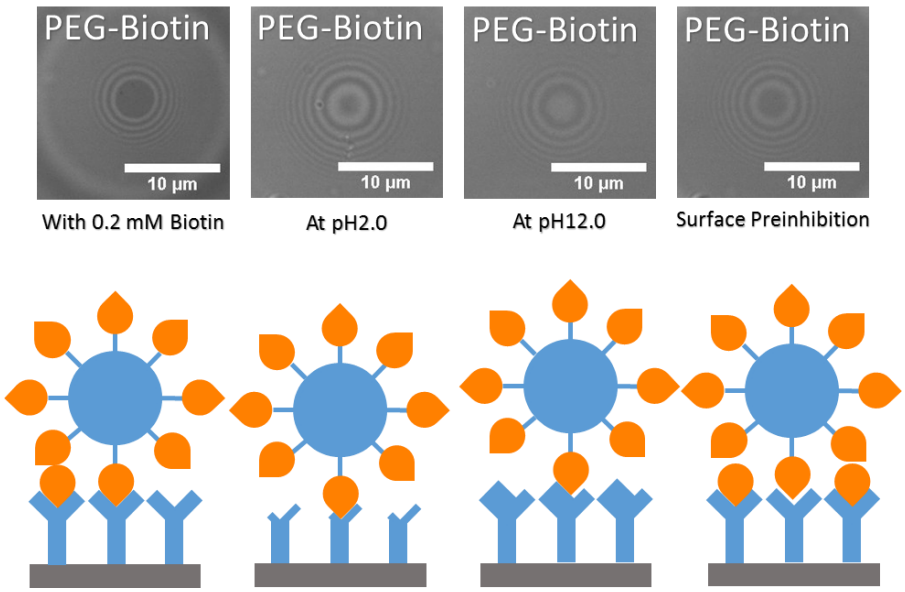

Figure 31: Typical RICM image and schematic presentation of PEG-Biotin SCPs on avidin functionalized surfaces under different experiment condition.

In order to test for the specificity of ligand receptor interaction and get a better understanding for the system, a series of inhibition experiments was carried out using four different approaches: direct inhibition with free biotin in solution, denaturation of the avidin protein under acidic or basic conditions, pre-incubation of the avidin with biotin before the surface coating step. Figure 31 shows four typical RICM images and its schematic presentation of PEG-Biotin SCPs under the different inhibition conditions.

Table 17 summarizes the inhibition experiment results. At maximum 0.2 mM biotin can be dissolved in PBS at pH 7.4. Due to the low solubility of biotin, there is probably not enough free biotin that can be added in the solution to efficiently inhibit the binding of PEG-Biotin SCPs and avidin surfaces. The adhesion energy stays at 83 ± 6 %. To solve this problem, another approach was investigated. Avidin was preinhibited with biotin to form a biotin-avidin complex in solution. This inhibited biotin-avidin complex was used to functionalize the surface in SCP-RICM experiment. The results show that the adhesion energy decreased to 44 ± 5 %. The inhibition is more efficient, but still no full inhibition was possible. As avidin and biotin were mixed and directly used for surface functionalization, there is probably not enough time for biotin to form a

complex with avidin. Longer mixing and binding times before prior to surface functionalization might solve this problem in the future.

In order to test for the inhibition of biotin avidin interactions in strong acidic or basic condition, the denaturation of protein at pH 2.0 and pH 12.0 were carried out. This method worked quite efficiently. Under strong acidic condition, 15 ± 6 % adhesion energy remained. Under strong basic condition, 1 ± 1 % adhesion energy remained. Under these conditions, the protein was denatured and binding pockets are lost. Thus the binding between biotin and avidin was inhibited. The work of Moy *et. al.* in 1999 also shows similar results with agarose beads: at low pH and high pH range, the adhesion energy significantly reduces between biotin and avidin. [97]

Table 17: Normalized adhesion energy of PEG SCPs, PEG-AA SCPs, and PEG-Biotin SCPs via RICM experiment

Sample	Experimental Condition	Normalized Adhesion Energy [%]
PEG-Biotin	PBS at pH 7.4	100 ± 1
PEG-Biotin	With 0.2 mM Biotin	83 ± 6
PEG-Biotin	pH 2.0	15 ± 6
PEG-Biotin	pH 12.0	1 ± 1
PEG-Biotin	Surface Preinhibition	44 ± 5

3.3.2.2 Effects of SCPs Elasticity on Mannose Con A Interaction

The influence of mechanical properties or flexibility of the anchoring surface on ligand receptor interactions was investigated through studying a series of SCPs with different Young's modulus in the SCP-RICM experiment. In this work, three different interactions were investigated: I) mannose Con A interactions, as an example for weak binders; II) biotin avidin interactions, as an example for strong binders; III) negatively charged carboxylic groups and positively charged amine groups, as an example for electrostatic interactions.

The mannose Con A adhesion interactions were investigated through the SCP-RICM experiment. Six groups of mannose functionalized PEG SCPs with various Young's modulus were synthesized and characterized (see chapter 3.2.2.1). Glass slides were functionalized with Con A and immersed in LBB at pH 7.4 to study direct binding of SCPs as previously described.

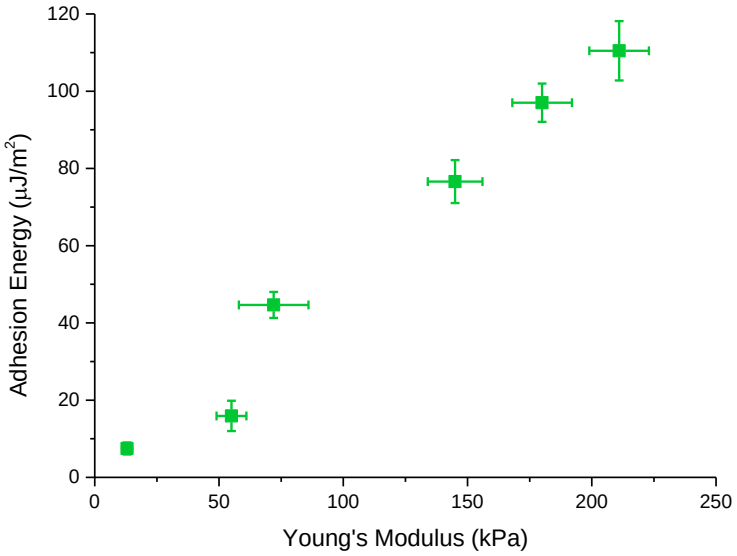

Figure 32: Adhesion energy of PEG-Man SCPs with various Young's modulus on Con A coated surface in LBB at pH 7.4.

Figure 32 shows the results for adhesion energy of PEG-Man SCPs with various Young's modulus on Con A coated surface in LBB at pH 7.4. It was found that the overall adhesion energy between PEG-Man SCPs and Con A surface increases with an increasing Young's modulus of the SCPs. However, this is not only an effect of the flexibility of the SCPs. The increase is at least partially due the increased density of mannose ligands at higher Young's moduli. Although SCPs with various Young's modulus have similar functionalization degree in µmol ligand per gram PEG in the dry state, the actual ligand amount per volume SCP is much lower for SCPs with lower Young's modulus as they are more swollen in water (see Figure 33). This is because the SCPs with lower Young's modulus have fewer crosslinking points and thus can swell more.

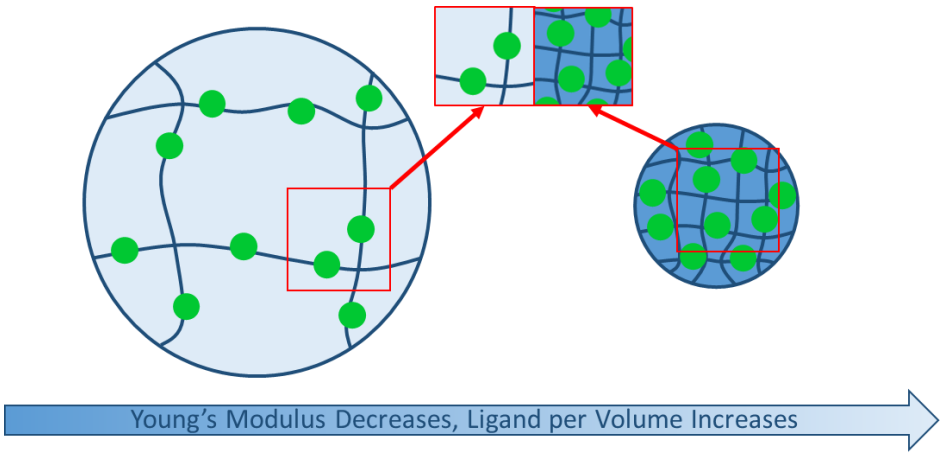

Figure 33: With similar ligand per mass (µmol/g) ligand functionalization degree, the ligand per volume increases (µmol/mL) with the increasing of Young's modulus.

In order to get a volume functionalization degree of SCPs, the swelling degree of SCPs were measured by optical microscopy. Then, the same SCP were tracked and dried with a heat gun under the microscope, and the image of this dry SCP was recorded. However, due to surface tension and gravity, SCPs will not always shrink to a sphere. Thus, the dry SCP were scanned under AFM. With the help of AFM, it can be detected whether SCPs shrink to a sphere, a half-sphere, or a pancake. Through software ImageJ, the volume of the dry SCP can then be calculated.

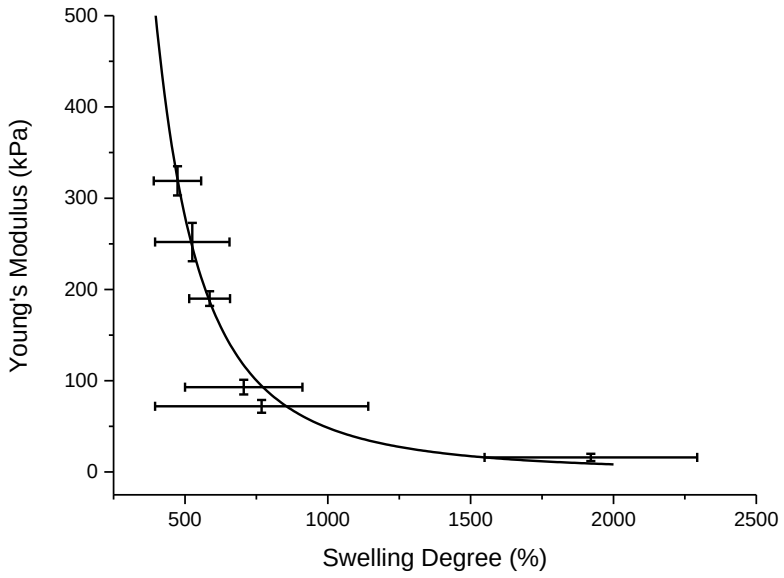

Figure 34: Measure swelling degree of SCPs with various Young's modulus and the theoretical relation between SCP swelling degree and SCP Young's modulus.

Figure 34 shows the relation between the swelling degree of SCPs and the Young's modulus of SCPs. The data points with error bars are the measured swelling degree vs. Young's modulus of PEG hydrogel based SCPs. The continuous curve is the theoretical swelling degree vs. Young's modulus published by Hild *et. al* in 1986. [98] The theoretical curve fits well to the measured data points in this work. Because tracking and measuring each individual SCP is very difficult and brings a lot of error, the swelling degree of each group of SCPs were directly read from the theoretical curve according to its Young's modulus. Thus, the unit of degree of mannose functionalization at swollen state can also be calculated as:

$$D\ [\mu mol/mL] = D\ [\mu mol/mL] \times \rho_{PEG} / Q_{theo} \qquad \textbf{Equation 21}$$

, where D is the degree of functionalization, ρ_{PEG} is the density of PEG equals 1.1977 g/mL, Q_{theo} is the theoretical swelling degree. The results are shown in Table 18.

Table 18: Degree of mannose ligand functionalization in different unit of PEG-Man SCPs with various Young's modulus

Sample	Young's Modulus [kPa]	Swelling Degree [vol. %]	Mannose Functionalization Degree	
			µmol/g	µmol/mL
PEG(0)-Man	211	559	107	23
PEG(10)-Man	180	595	109	22
PEG(20)-Man	145	648	96	18
PEG(30)-Man	72	855	78	11
PEG(40)-Man	55	951	101	13
PEG(60)-Man	13	1680	71	5

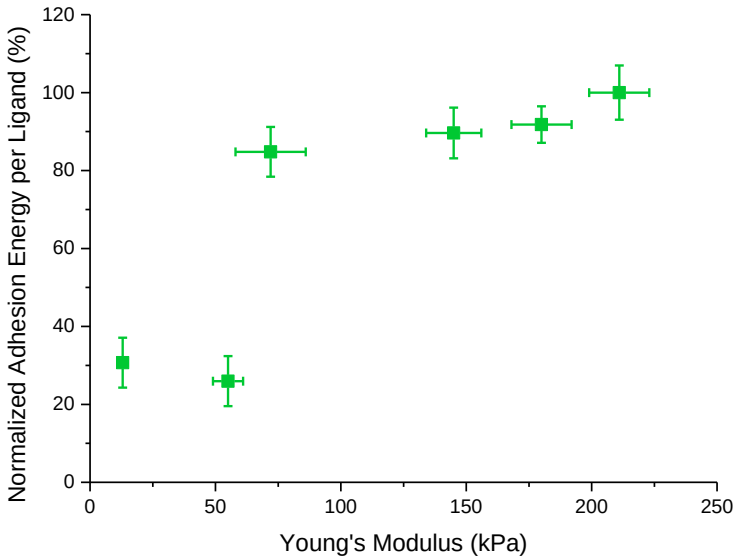

Figure 35: Normalized adhesion energy of PEG-Man SCPs with various Young's modulus on Con A coated surface in LBB7.4.

In order to evaluate how the Young's modulus of the SCP influences the adhesion energy, the adhesion energy was then firstly normalized by the ligand concentration of SCPs (degree of mannose functionalization in a unit of µmol/mL). Then, the highest adhesion energy per ligand was set as 100%, the other adhesion energy values were normalized according to this value. Figure 35 shows the normalized adhesion energy per ligand of SCPs with varying Young's modulus. It can be found that when the Young's modulus is lower than 55 ± 6 kPa, the normalized adhesion energy per ligand is around 30 %. When the Young's modulus is higher than 72 ± 14 kPa, the normalized adhesion energy per ligand significantly increased to around 90 %. This indicates that the mannose on SCPs with higher Young's modulus binds more easily to the Con A surface than the mannose on SCPs with lower Young's modulus.

The data shows that the normalized adhesion energy per ligand increases along with the increasing Young's modulus of SCPs, which indicates that mannose on a more rigid scaffold binds more easily to Con A surfaces than the mannose on a more flexible scaffold (Figure 35). During a binding event, when mannose on a soft scaffold binds to the Con A on the surfaces, the number of conformational states Ω (probable states under certain thermal dynamic conditions, which can be evaluated by entropy) of this soft scaffold is reduced, which will lead to an entropy loss of this

system. It is known that more flexible scaffolds have more conformational states. Thus, when a more rigid scaffold and a more flexible scaffold achieve the same adhesion (the same number of bound states), the more flexible scaffold lost a higher number of conformational states. As such a loss in entropy is usually unfavored, mannose on a more flexible scaffold binding to Con A surfaces should lead to smaller adhesion energies as for a more rigid scaffold, as was observed here.

Previously in this thesis, inhibition of the SCPs bound on the surface was used to prove specific ligand receptor interactions. Additionally, performing such an inhibition/competition experiment adding free soluble ligand to the SCP-RICM experiment can also give information on the accessibility of the ligands bound to the SCP as well as the receptors bound on the glass slide. In previous studies, SCP-RICM has also been used to determine the inhibitory potential of soluble ligands. [99] Therefore, increasing concentrations of the soluble ligand were incubated with the SCPs prior to contact with the glass slide. Depending on the affinity of the soluble ligand, a decreased contact area and thus adhesion energy was detected for the SCPs with increasing ligand concentration. When plotting the normalized adhesion energy against the ligand concentration, a so-called Hill plot is derived giving access to the half-maximum inhibitory potential (IC_{50}). [100]

In order to further investigate the effect of Young's modulus of PEG-Man SCPs when binding to Con A surfaces, inhibition/competition experiments determining the IC_{50} value were performed (Figure 36). The softest PEG-Man SCPs and the hardest PEG-Man SCPs were chosen for comparison.

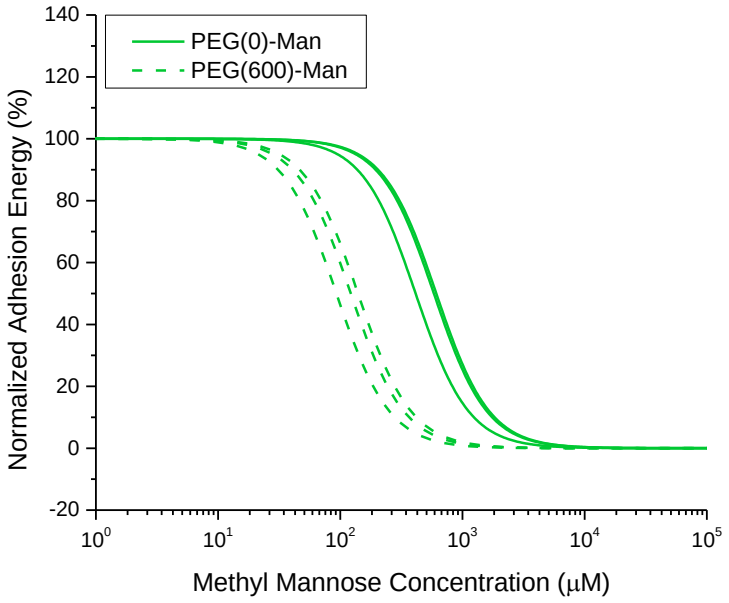

Figure 36: IC_{50} measurement of mannose Con A interaction with soft PEG-Man SCPs and hard PEG-Man SCPs showing three repetitive experiments for each case.

The adhesion energy of softest SCPs and hardest SCPs were normalized according to the highest adhesion energy value of each group and plotted versus methyl mannose concentration. The IC_{50} refers to the required MeMan concentration to inhibit 50 % of the adhesion interaction between mannose functionalized PEG-Man SCPs and Con A functionalized surfaces. Figure 36 shows the results. The IC_{50} for the hardest PEG(0)-Man SCPs was 535 ± 122 µM. The IC_{50} for the softest PEG(60)-Man SCPs was 118 ± 25 µM. Thus, it was found that less MeMan was needed to inhibit the softest PEG-Man adhesion interaction on Con A surface in comparison to the SCPs with higher Young's modulus. As explained before, when a more rigid scaffold and a more flexible scaffold achieve the adhesion, the more flexible scaffold experienced a higher entropic loss. In the reverse process (inhibition of binding events), when a more rigid scaffold and a more flexible scaffold both get released from the same binding events, the more flexible scaffold will now regain a higher number of conformational states. Thus this should be entropically favoured and it should be easier for mannose on a more flexible scaffold to unbind from the Con A surface. Indeed, in this study the softer SCPs showed a lower IC_{50} value, where less competing ligand was required to detach the SCPs from the surface.

3.3.2.3 Effects of SCPs Elasticity on Biotin Avidin Interaction

Similar to the mannose Con A study in the previous chapter, biotin avidin adhesion interactions were investigated via the SCP-RICM experiment. Six batches of biotin functionalized PEG based SCPs with various Young's modulus were synthesized and characterized (see chapter 3.2.2.2) Glass slides were functionalized with avidin and immersed in PBS at pH 7.4 as measurement buffer and the SCP adhesion energies were measured as usual.

Figure 37 shows the results for the direct adhesion experiment. It was found that the overall adhesion energy between PEG-Biotin SCPs and avidin surface increases with the increasing of the Young's modulus of SCPs. It is important to note that the adhesion energy increase from the softest to the hardest SCPs by a factor of four, whereas the increase from the softest to hardest SCPs in case of mannose ligands was more than twelve. This already suggests that the biotin SCPs proved to be significantly less mechanosensitive.

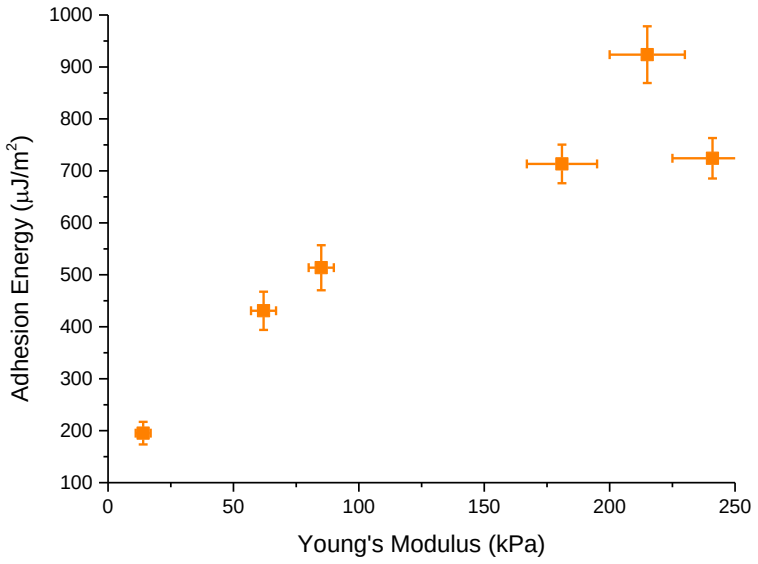

Figure 37: Adhesion energy of PEG-Biotin SCPs with various Young's modulus on avidin coated surface in PBS7.4.

To further evaluate this phenomenon, the adhesion energy was normalized with the ligand density in the swollen state of the SCPs, as previously explained for the mannose functionalized SCPs. (See Table 19) The resulting relative adhesion energies should thus represent the adhesive strength of the ligands in the softer or harder SCPs.

Table 19: Degree of biotin ligand functionalization in different unit of PEG-Biotin SCPs with various Young's modulus

Sample	Young's Modulus [kPa]	Swelling Degree [vol. %]	Biotin Functionalization Degree	
			µmol/g	µmol/mL
PEG(0)-Man	241	530	114	26
PEG(10)-Man	215	550	110	24
PEG(20)-Man	181	594	101	20
PEG(30)-Man	85	801	68	10
PEG(40)-Man	62	907	97	13
PEG(60)-Man	14	1630	67	5

Figure 38 shows that the normalized adhesion energy per ligand stays in the range of 60 % to 100 %. There is no significant difference between the adhesion energy per ligand, when the biotin ligands were connected to the SCPs with various Young's modulus and hydrogel network flexibility. This result is quite different from the result of mannose Con A interactions, where a strong increase in adhesion was observed with increasing the Young's modulus.

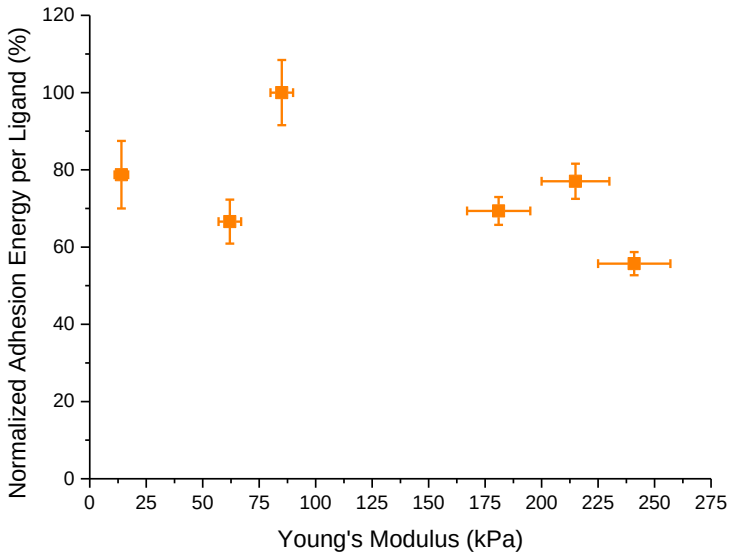

Figure 38: Normalized adhesion energy of PEG-Biotin SCPs with various Young's modulus on avidin coated surface in PBS7.4.

This result could be rationalized by a cooperative binding compensating the entropy cost when binding softer biotin SCPs to the avidin surface. It is known that the adhesion between biotin avidin ligand receptor pair is almost 7 times stronger than the mannose Con A ligand receptor pair, which also means the ‘‘Hand-shake’’ (bound to unbound) frequency of biotin avidin is several orders of magnitude times lower than for mannose Con A. The unbinding rate constant of biotin avidin is 9E-8 s^{-1} [101] whereas mannose Con A unbinds with a K_{off} of 1E-3 s^{-1} to 5 E-3 s^{-1}. [102] The difference of unbinding rate constant between biotin avidin pair and mannose Con A pair leads to a different half-life. The biotin avidin pair has an extremely long half-life ($t_{1/2}$ > 35 h) [103] and mannose Con A has a comparatively short half-life ($t_{1/2}$ ~ 4 s) [104]. This should make it possible for biotin to bind cooperatively to the avidin surface. It could thus be expected that the degree of cooperativity is increased and the binding is getting easier, when the soft scaffold becomes more flexible due to an increased spatial sampling range of the ligands. Thus, the entropy loss of a more flexible scaffold is potentially overcompensated by cooperative ligand binding. Following this hypothesis, ligand receptor interactions should lead to a similar adhesion energy for biotin on both more flexible and rigid scaffolds as was observed from this study.

3.3.2.4 Effects of SCPs Elasticity on Electrostatic Interactions

In order to further investigate the influence of the Young’s modulus on SCPs binding to surfaces, the electrostatic interactions between negatively charged carboxylic acid functionalized PEG hydrogel based SCPs and positively charged amine groups on the glass slides were investigated. As carboxylic acid functionalized PEG SCPs, the previously described PEG-CA SCPs with various Young’s modulus were used (see chapter 3.2.1) Glass slides were cleaned and coated with poly(ethylenimine) (PEI) as commercially available polycation. The charged group of PEG-CA SCPs in pure water can interact in a longer range comparing to the PEG-CA SCPs in 150 mM NaCl. PEG-CA SCPs were added to the PEI glass slides either in pure water or in 150 mM NaCl solution to test how the electrostatic interaction is influenced by the SCP Young’s modulus when short range interaction or long range interaction is applied.

Figure 39 shows the adhesion energy of PEG-CA SCPs with various Young’s modulus on PEI surface without and in the presence of high salt concentration. It was found that the overall

adhesion energy in both cases increases with the increasing of the Young's modulus. Similar to the binding of the PEG-Man SCPs on the Con A surfaces, this could be an effect of the entropic cost that has to be paid by more flexible networks making the ligand receptor binding events less likely.

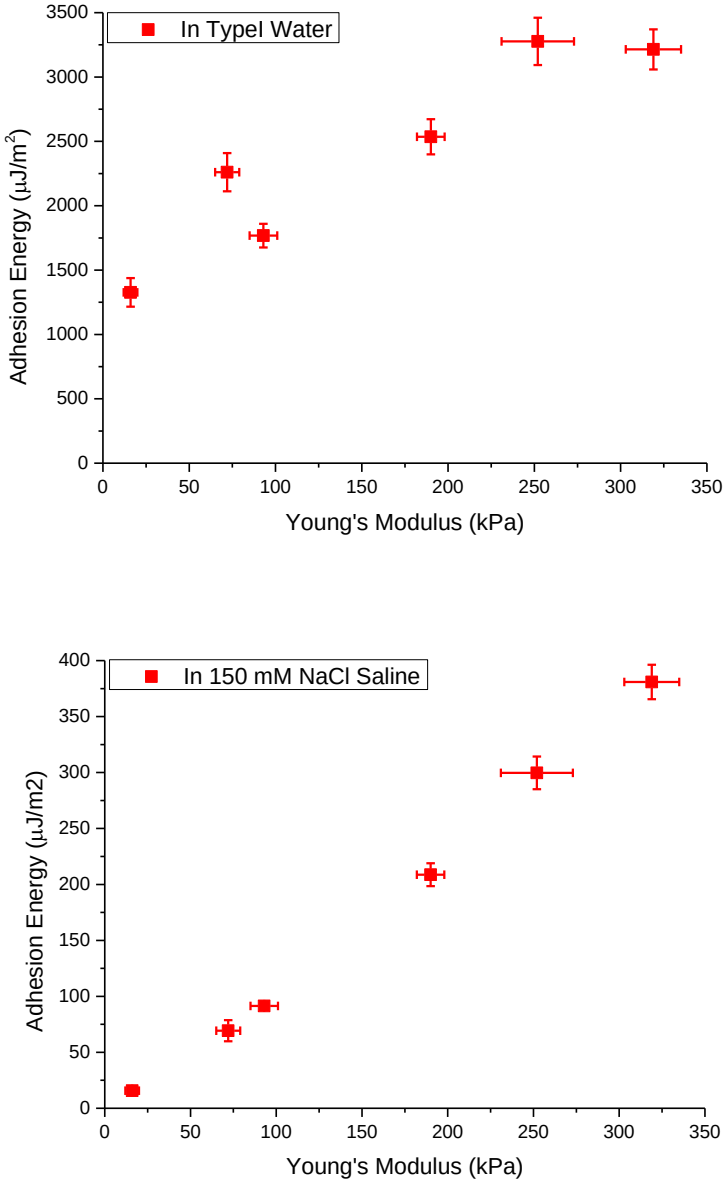

Figure 39: Adhesion energy of PEG- CA SCPs with various Young's modulus on PEI surface in type I water and in 150 mM NaCl solution.

However, here again also the volume carboxylic group concentration has to be taken into account as the low Young's modulus SCPs have a lower volume concentration. Therefore, the adhesion data was again normalized as before.

Table 20: Degree of carboxylic group (-COOH) functionalization in different unit of PEG-CA SCPs with various Young's modulus

Sample	Young's Modulus [kPa]	Swelling Degree [vol. %]	-COOH Functionalization Degree	
			µmol/g	µmol/mL
In Type I Water				
PEG(0)-CA	319	470	117	30
PEG(10)-CA	252	522	113	26
PEG(20)-CA	190	581	102	21
PEG(30)-CA	93	773	79	12
PEG(40)-CA	72	857	104	15
PEG(60)-CA	16	156	81	6
In 150 mM NaCl Solution				
PEG(0)-CA	211	559	117	25
PEG(10)-CA	180	595	113	23
PEG(20)-CA	145	648	102	19
PEG(30)-CA	72	855	79	11
PEG(40)-CA	55	951	104	13
PEG(60)-CA	13	1680	81	5

Figure 40 shows that when there is no salt present, the normalized adhesion energy per carboxylic group stays in a range between 60 % to 100 % and decreases slightly with increasing Young's modulus. When there is salt present, this trend reverses and the normalized adhesion energy per carboxylic group significantly increases when increasing the Young's modulus of SCPs and hydrogel network flexibility as was also seen for the non-normalized data.

In order to explain the above phenomenon, the conception of Debye length should be considered. Briefly, the Debye length describes the electro interaction distance. Beyond this length, the charged group can be considered as electrical neutral and does not have electrostatic interaction

with the counter charged groups any more. The presence of salt (increasing the electrolyte concentration) leads to a reduction of the Debye length due to the screening of the charged groups to about 1 nm. For the SPCs it can thus be expected that the entropic penalty that has to be payed from a more flexible network leads to a reduced adhesion energy in the presence of salt.

When there is no salt present, the interaction distance is much longer, the Debye length is several tens of nanometres large. This means, the charged carboxylic group is not electrically neutral in a longer distance. Thus, a larger number of negatively charged carboxylic groups from the network can interact with the positively charged amine groups on the PEI surface. This does not only generally increase the adhesion, but also the dependence of elastic modulus is strongly affected. Considering the SCPs mechanical deformation upon adhesion and large interaction length, softer SCPs are able to bring more interacting negative charges close to the PEG surface, therefore the overall interaction energy per charge increases (see Figure 40). When a lot of salt was added to the system, the Debye length should be significantly reduced. The electrostatic interaction becomes a short distance interaction. Thus, only some of the charged carboxylic groups can weakly interact with the surface.

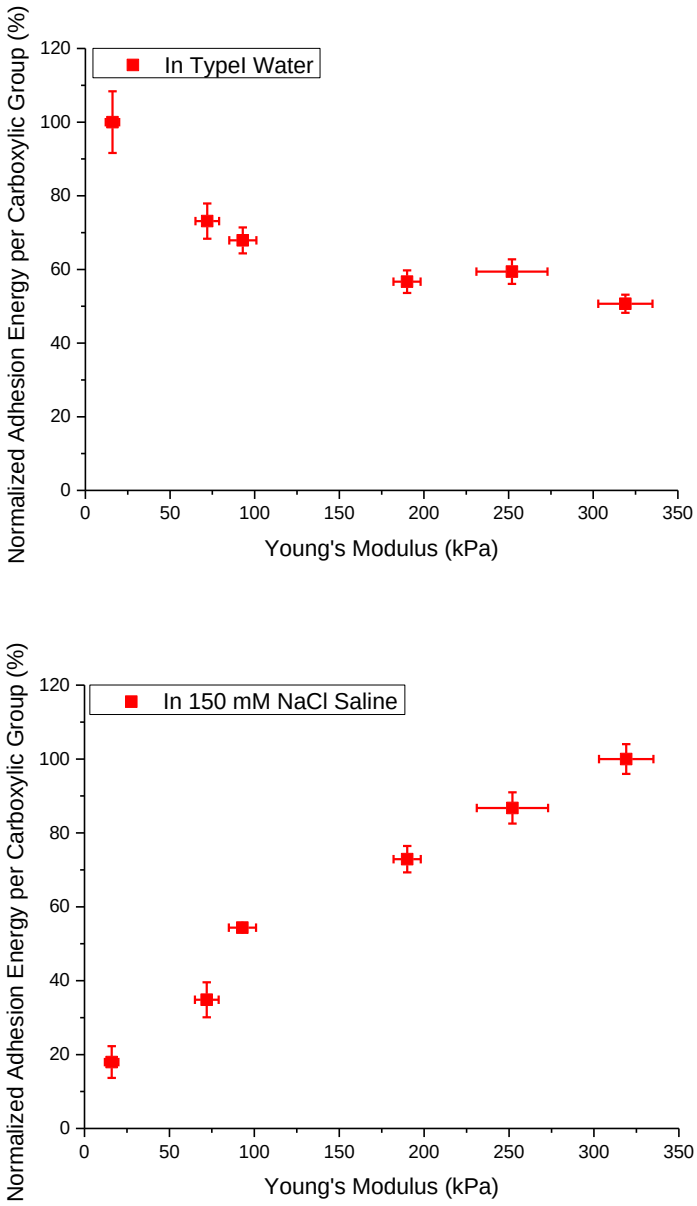

Figure 40: Normalized adhesion energy of PEG-c-CA-CA SCPs with various Young's modulus on PEI surface in type I water and in 150 mM NaCl solution.

4. Conclusion and Outlook

In this work, an optimized SCP-RICM experimental platform was developed to study the influence of Young's modulus, ligand concentration and ligand type on ligand receptor interactions at soft biomimetic interfaces.

In the first part, two different types of SCPs with various Young's modulus were synthesized. The Young's modulus of PEG hydrogel based SCPs was tuned through adding non-homopolymerizable crotonic acid to create inert chain ends on PEG-dAAm macromonomers and decrease the overall crosslinking density. In addition to the classical PEG hydrogel based SCPs, PAA hydrogel based SCPs were introduced. This type of hydrogel based SCPs were synthesized via inversed suspension polymerization and the Young's modulus of PAA SCPs was tuned by varying the cross-linker to monomer ratio.

In the second part, tunable functionalization of hydrogel based SCPs with different ligands was established. PEG SCPs needed to be functionalized firstly with carboxylic acids through benzophenone photochemistry, and then functionalized with required ligands through amide coupling reaction. In case of the PAA SCPs, the functionalization was achieved via two strategies. In one method, the ligand concentration on PAA SCPs was tuned through co-coupling ligands with non-ligands in a certain ratio. In the other method, the ligand concentration on PAA SCPs was tuned through tuning the reaction equivalents of ligands during functionalization step. Through reducing the reaction equivalent, the reaction yield and thus the ligand concentration was reduced.

In the third part, influence of Young's modulus, ligand concentration, and type were investigated through SCP-RICM experiments using the previously synthesized SCPs. For the influence of ligand concentration, highly functionalized PAA-Man SCPs were applied and it was found that higher ligand concentration leads to a higher overall adhesion energy. However, once one of the binding partners is saturated, no further increase in adhesion would be expected and a stalling of adhesion energies for highly functionalized SCPs was observed. Looking then at different ligand types and the influence of the Young's modulus, PEG-Biotin and PEG-Man SCPs were applied in adhesion experiments. It was found that higher Young's moduli of SCPs lead to higher adhesion for PEG-Man SCPs. This effect is attributed to a higher entropic loss when softer SCPs bind to the surface. For PEG-biotin SCPs a different trend was observed, where the Young's modulus does not seem to alter the adhesion. Here, this observation is attributed to an

overcompensation of entropic loss by an increased cooperative binding of biotin for softer SCPs. Cooperative binding of biotin-SCPs to avidin surfaces is likely due to the enormous half-life of a biotin - avidin complex (several days), whereas Man-Lectin complexes only last for a few seconds. This phenomenon was further investigated using negatively charged PEG-CA SCPs and it was found that higher Young's moduli of SCPs leads to higher adhesion on cationic surfaces only in the presence of salt. In the absence of salt, there is a longer interaction range of charged groups and the softer SCPs allow more charged groups to interact at the interface leading to higher adhesion energies.

Overall, this work provides deeper insights into the role of a soft scaffold presenting ligands or receptors and the resulting adhesion properties. It was found that depending on the type of ligand, the flexibility of the scaffold can strongly influence ligand receptor interactions at the interface. Further it was found that saturation of one of the binding partners leads to a stalling in adhesion. Such phenomena could now also be related to adhesion in biological systems e.g. adhesion of cells on soft surfaces or cell-cell contacts e.g. in bacterial adhesion. To further extend on this work and even more closely relate the SCP model system to biological systems, in the future, the ligand receptor interactions between two soft surfaces could be investigated, e.g. through functionalizing glass surfaces with a layer of lipids or polymers. Furthermore, living cells could be included in the SCP-RICM set-up to measure the ligand receptor interactions on a biological interface.

5. Appendix

5.1 List of Abbreviations

AA	Acrylic acid
AAm	Acrylamide
AFM	Atom Force Microscopy
Biotin	5-(2-oxohexahydro-1H-thieno[3,4-d]imidazol-4-yl)pentanoic acid
Biotin-OMe	methyl 5-(2-oxohexahydro-1H-thieno[3,4-d]imidazol-4-yl)pentanoate
Biotin-NH_2	N-(2-aminoethyl)-5-(2-oxohexahydro-1H-thieno[3,4-d]imidazol-4-yl)pentanamide
CA	Crotonic acid
Con A	Concanavalin A
DIPEA	N,N-Diisopropylethylamine
DMF	dimethylformamide
EDA	Ethylene diamine
GLYMO	(3-Glycidyloxypropyl)trimethoxysilane
h	Hour
HEPES	2-[4-(2-hydroxyethyl)piperazin-1-yl]ethanesulfonic acid
HOBt	Hydroxybenzotriazole
IC50	Half Maximal Inhibitory Concentration
LCST	Lower Critical Solution Temperature
M	Molar per litre
mol.	molar
Mannose-NH_2	(2R,3R,4S,5S,6S)-2-(acetoxymethyl)-6-(2-aminoethoxy)tetrahydro-2H-pyran-3,4,5-triyl triacetate
MBAm	N,N'-Methylenebisacrylamide
MEA	2-Aminoethanol

NaOMe	Sodium Methoxide
NMR	Nuclear Magnetic Resonance Spectroscopy
PAA	Poly(acrylic acid)
PBS	Phosphate buffered Saline
PEG	Poly(ethylene glycol)
PEG-Biotin	Poly(ethylene glycol) functionalized with biotin
PEG-CA	Poly(ethylene glycol) functionalized with crotonic acid
PEG-c-CA	Poly(ethylene glycol)-compl-(crotonic acid)
PEG-dAAm	Poly(ethylene glycol)-diacrylamide
PEG-Man	Poly(ethylene glycol) functionalized with mannose
PEI	Poly(ethylenimine)
PGPR	Polyglycerol polyricinoleate
PyBOP	(Benzotriazol-1-yloxy)tripyrrolidinophosphonium hexafluorophosphate
RICM	Reflection Interference Contrast Microscopy.
RT	Room temperature
s	second
SCP	Soft colloidal probe
UV-VIS	Ultraviolet-visible Spectroscopy
vol.	volume
wt.	weight

5.2 Experimental Section

5.2.1 Chemicals and Materials

Benzophenone and DMF are from ACROS. Calcium chloride and sodium azide are from AppliChem. PyBOP is from Carbolution. DIPEA, ethylene diamine, MEA, TEA, paraffin oil high

viscosity are from Carl Roth. GRINDSTED®PGPR is from DU PONT. ABIL® EM 90 is from Evonik. HEPES, isopropanol, methanol, sodium chloride, and toluene are from Fisher Scientific. MBAm is from Merck. Acrylic acid, amberlite® IR120 hydrogen form, Con A, crotonic acid, DMSO, ethanol, GLYMO, HOBt, manganese dichloride, methacrylic acid, PBS, and rhodamine are from Sigma-Aldrich. Hydrogenperoxide is from TH.GEYER. Ammonia solution and sodium sulfate are from VWR Chemicals.

Avidin is from ThermoFisher, Merck and AppliChem. Con A is from Cayman, LKT, and Sigma-Aldrich.

Type I Water is from Barnstead™ MicroPure™ ThermoFisher SCIENTIFIC ultrapure water system.

All the other chemicals were obtained from Sigma-Aldrich. All the other solvents were obtained from Fisher Scientific. If not noted otherwise, all the chemicals were used without further purification.

PEG-dAAm and aminoethyl linked mannose were synthesized by Fawad Jacobi.

5.2.2 Methods

Atom Force Microscopy (AFM). All experiments were performed on a NanoWizard II AFM system (JPK Instruments AG, Germany). The thermal noise method was sued to measure the spring constant of the cantilever (Nanoworld AG, Switzerland). The corresponding optical images are obtained through an Olympus IX70 inverted optical microscope (Olympus Corporation, Japan) with a HCX PL FLUOTAR 20x/0.50 PH2 objective (Leica Microsystems GmbH, Germany) and a USB 3 uEye CP CMOS camera (IDS Imaging Development Systems GmbH, Germany).

Nuclear Magnetic Resonance Spectroscopy. 1D ^{1}H-NMR (300 MHz) spectra was recorded on an AVANCE III – 300 (Bruker, USA). The proton signal of residual, non-deuterated solvent (δ 7.26 ppm for CHCl3, 3.34 ppm for MeOH) was used as an internal reference for corresponding ^{1}H spectra. Coupling constants (J) are reported in Hertz. The following abbreviations are used to indicate the multiplicities: s, singlet; d, doublet; t, triplet; m multiplet.

Reflection Interference Contract Microscopy (RICM). All experiments were performed on an Olympus IX73 inverted optical microscope (Olympus Corporation, Japan). An LED lamp with

a green monochromatic light (546 nm) was used for illumination. An Olympus UPlanFL N 60x/0.90 objective (Olympus Corporation, Japan) and a USB 3 uEye CP CMOS camera (IDS Imaging Development Systems GmbH, Germany) were used to record the RICM pattern. To analyse the RICM pattern for the adhesion energies, the obtained optical images are processed with program Hydrogel-3 and programming software Igor Pro 7 (WaveMetrics Inc., USA).

Ultraviolet-visible Spectroscopy (UV-VIS). All experiments were performed on G1103A 8453 UV spectrometer (Agilent Technologies, USA) with scanning wavelength in a range of 300-800 nm. The absorption peak was identified at 633nm. QS quartz cuvettes with 200-2500 nm spectral range, 10 mm light path, 3500 µL chamber volume (Hellma, Germany) were used to contain the samples.

5.2.3 Experimental Procedures

5.2.3.1 Synthesis of methyl 5-(2-oxohexahydro-1H-thieno[3,4-d]imidazol-4-yl)pentanoate (Biotin-OMe)

Amberlite® IR120 hydrogen form resin was washed with methanol until the eluent was transparent. 150 mg (614.53 µmol) 5-(2-oxohexahydro-1H-thieno[3,4-d]imidazol-4-yl) pentanoic acid (Biotin) was dispersed in 15 mL methanol and 100 mg Amberlite® IR120 hydrogen form resin was added into the Biotin/methanol dispersion. The dispersion was stirred at room temperature with a magnetic stir bar for 2 days until a transparent solution was formed. The solution was filtered with a syringe filter to remove the resin. Methanol was removed from the filtrate through evaporating with a rotary evaporator at 50 °C under reduced pressure. A white solid, Biotin-OMe, was obtained and further dried at RT under high vacuum (0.2 mbar) for 5 h.

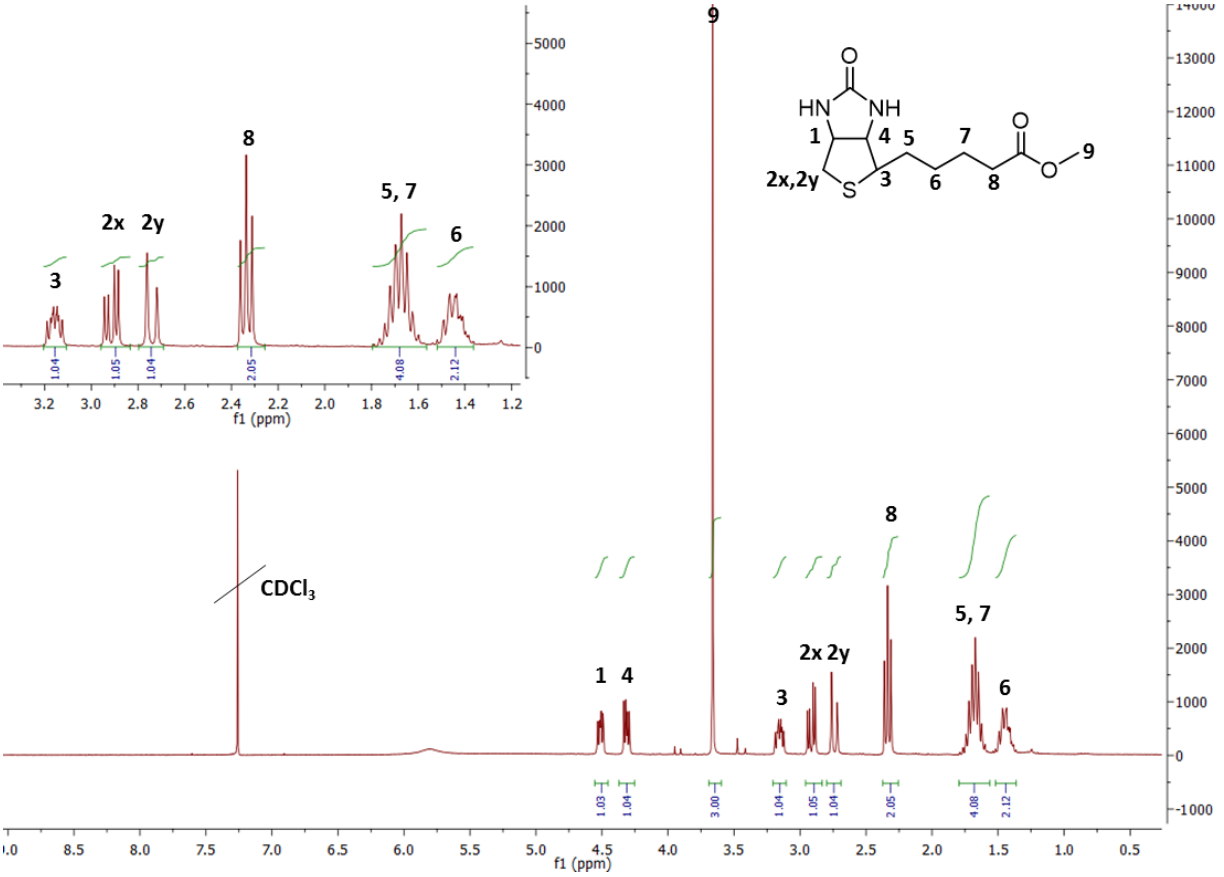

Figure 41: 1H-NMR spectrum of Biotin-OMe.

^{1}H-NMR(300 MHz; CDCl3): δ(ppm) = 4.52 (dd, *J* = 7.71, 7.83 Hz, 1H), 4.32 (dd, *J* = 7.78, 4.58, 1H), 3.67 (s, 3H), 3.17 (m, 1H), 2.92 (dd, *J* = 12.84, 4.98, 1H), 2.75 (d, *J* = 12.78, 1H), 2.35 (t, *J* = 7.44, 2H), 1.73 – 1.63 (m, 4H), 1.50 – 1.42 (m, 2H).

5.2.3.2 Synthesis of N-(2-aminoethyl)-5-(2-oxohexahydro-1H-thieno[3,4-d]imidazol-4-yl)pentanamide (Biotin-NH_2)

128.43 mg (479.13 µmol) Biotin-OMe was dissolved in 4.281 mL methanol. 1.7124 mL (25.64 mmol) ethylene diamine (EDA) was added into the Biotin-OMe/methanol solution, which is stirred at 60 °C with a magnetic sitr bar for 2 days. After the reaction was complete, methanol was removed through evaporating with a rotary evaporator at 50 °C under reduced pressure and a light yellow oil was obtained. EDA was removed through evaporating with an oven at 90 °C under high vacuum (0.2 mbar) for 5 h. A yellow flake, Biotin-NH_2, was obtained.

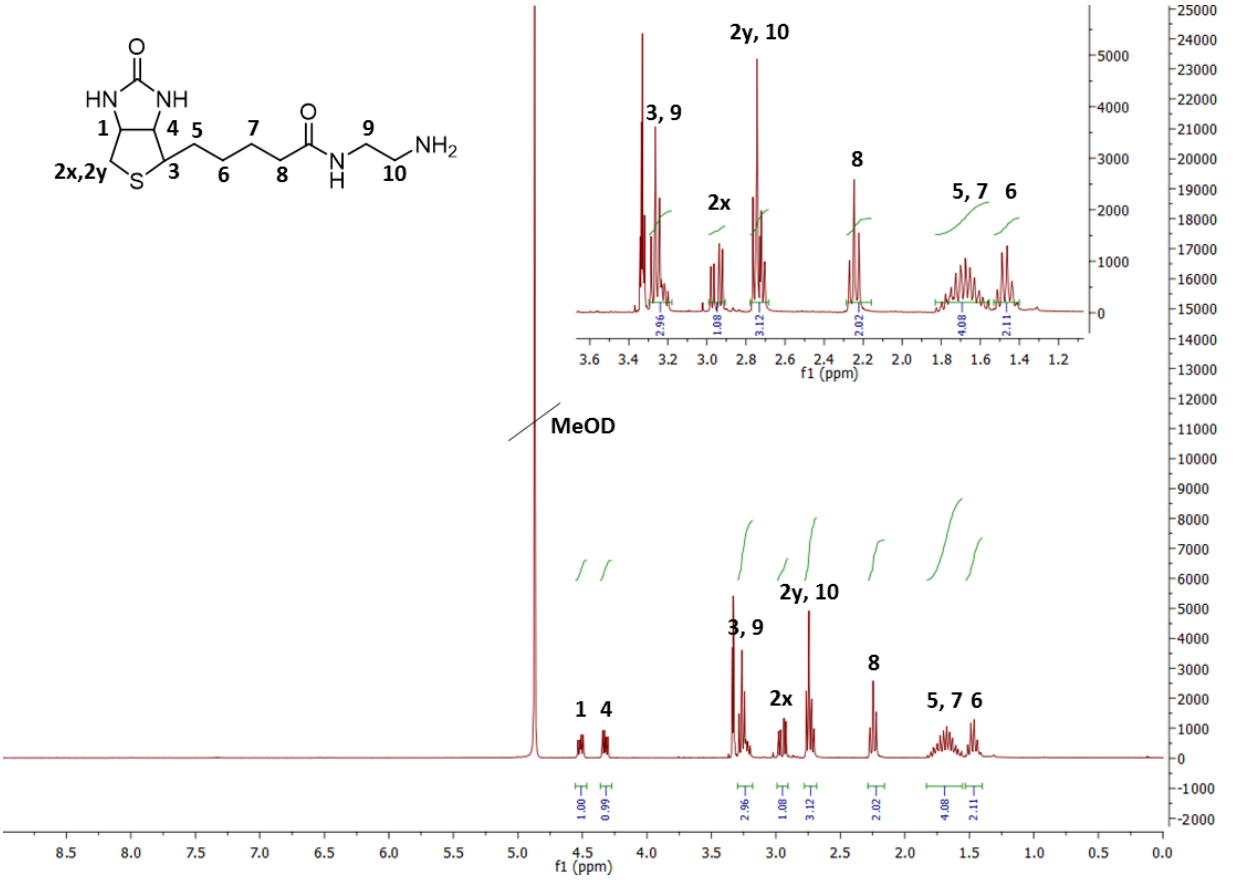

Figure 42: 1H-NMR spectrum of Biotin-NH_2.

^{1}H-NMR(300 MHz; MeOD): δ(ppm) = 4.39 (2×dd, *J* = 7.80, 7.90 Hz, 1H), 4.20 (dd, *J* = 7.87, 4.46, 1H), 3.12 (m, 3H), 2.83 (dd, *J* = 12.77, 4.97, 1H), 2.62 (m, 3H), 2.13 (t, *J* = 7.36, 2H), 1.56 (m, 4H), 1.33 (m, 2H).

5.2.3.3 Synthesis of SCPs

PEG SCPs

PEG-dAAm used in this work was synthesized by Fawad Jacobi through the protocol described by Hartmann *et. al* [105] which was adapted from Elbert and Hubbell. [106] According to previously reported methods, [51] 142.04 g sodium sulfate was dissolved in 1 L Type I water for a 1 M sodium sulfate aqueous solution. 1.2 mg photo initiator Irgacure 2959 (5.4 µmol) was dissolved in 10 mL 1 M sodium sulfate aqueous solution. 50 mg macro monomer poly(ethylene

glycol)-diacrylamide (PEG-dAAm) was added in the above solution and vigorously shaken at RT for a dispersion. The dispersion was transferred to a glass vial and photo polymerized with UV light (390-540 nm) (HiLite power - high-performance light curing unit, Heraeus Kulzer, Germany) for 90 s. The cross-linked PEG SCPs were dispersed in 40 mL Type I water and centrifuged at 4400 rpm for 15 min for maxima yield, which is called washing step. The washing step was repeated for 2 times to remove the extra salt and other impurities from the synthesis step. The cleaned SCPs were stored in Type I water for further steps.

PEG-c-CA SCPs

1 phosphate buffered saline (PBS) tablet was dissolved in 200 mL Type I water at 25 °C for a 10 mM phosphate buffer with 2.7 mM potassium chloride and 137 mM sodium chloride at pH 7.4. Without further declaration, the phosphate buffered saline was prepared directly with the tablets from Sigma Aldrich. 28.4 g sodium sulfate was dissolved in 200 mL PBS for a 1 M sodium sulfate PBS solution. Different amounts of crotonic acid was dissolved in 10 mL 1 M sodium sulfate PBS solution. The effect of crotonic acid concentration on the elasticity of PEG-c-CA SCPs was studied by varying the crotonic acid from 0 mg, 10.9 mg, 21.7 mg, 32.5 mg, 43.4 mg, and 65.1 mg. 1.2 mg photo initiator was added to the crotonic acid/1 M sodium sulfate PBS solution, and 50 mg macro monomer PEG-dAAm was added in the above solution and vigorously shaken at RT to form a dispersion. The dispersion was transferred to a glass vial and photo polymerized with UV light (390-540 nm) (HiLite power - high-performance light curing unit, Heraeus Kulzer, Germany) for 90 s. The cross-linked PEG-c-CA SCPs were dispersed in 40 mL Type I water and centrifuged at 4400 rpm for 15 min for maxima yield. The washing step was repeated for 2 times to remove the extra salt and other impurities from the synthesis step. The clean SCPs were stored in Type I water for further steps.

PAA SCPs

0.9 g (1 wt. %) ABIL EM 90 and 1.8 g (2 wt. %) PGPR were mixed with 87.3 g high viscosity paraffin oil as oil phase. 2.25 g monomer acrylic acid (31.22 mmol), 67.50 mg thermal initiator ammonium persulfate (APS) (295.82 µmol) and varying amount of cross-linker N,N'-

Methylenebisacrylamide (MBAm) were dissolved in 15 mL Type I water as water phase. The effect of MBAm concentration on the elasticity of PAA SCPs was studied by varing the MBAm from 45 mg, 180 mg, 360 mg, to 720 mg. 90 mL oil phase was injected into a round bottom flask and kept under vacuum (20 mbar) over night. While magnetic stirring, 15 mL water phase was dropped into 90 mL oil phase in a speed of 1 drop per second for an inversed suspension. The acquired suspension was kept under vacuum (20 mbar) for 30 min. Then, the suspension was heated up to 80 °C with an oil bath and stirred with a mechanical stir for 150 min. Per 10 mL cross-linked PAA SCPs were dispersed in a mixture of 50 vol. % Toluene and 50 vol. % Type I water. The dispersion was vigorously shaken for 1 min and centrifuged at 4400 rpm for 15 min for maxima yield. The PAA SCPs were again washed by a mixture of 50 vol. % Toluene and 50 vol. % Type I water for 2 times. Then, the PAA SCPs were washed with isopropanol for 3 times, and shaken in isopropanol on a shaker for 1 week. Finally, the PAA SCPs were washed with isopropanol for 3 times. The above steps remove the dispersants and impurities from the sample. The clean SCPs were stored in isopropanol for further steps.

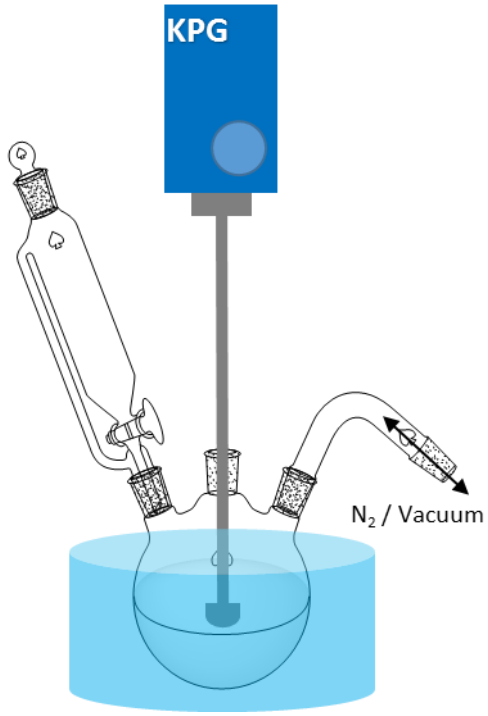

Figure 43: Reaction apparatus of PAA SCPs synthesis via inverse suspension polymerization.

5.2.3.4 Functionalization of PEG SCPs and PEG-c-CA SCPs

1.5 mg (17.7 mmol) monomer crotonic acid or 1.2 mL (17.7 mmol) monomer acrylic acid, and 250 mg (1.4 mmol) photo initiator benzophenone (BP) were pre-dissolved in 7 mL ethanol. 10 mL (ca. 30 mg) PEG based SCPs dispersion were centrifuged at 4400 rpm for 10 min, the supernatant was decanted, and 10 mL ethanol was added to the SCPs. The procedure was repeated for 2 times to exchange water with ethanol in SCP dispersion. The SCPs dispersion was centrifuged again under the same setting, 7 mL crotonic acid benzophenone / ethanol solution was added to the SCPs and the volume of the SCPs dispersion was adjusted to 10 mL with ethanol. The reaction mixture was flushed with nitrogen and irradiated with UV light (390-540 nm) (HiLite power - high-performance light curing unit, Heraeus Kulzer, Germany) for 10 × 90 s. Before the 1st irradiation, the reaction mixture was flushed with nitrogen for 60 s; before the 6th irradiation, the reaction mixture was flushed with nitrogen for 30 s; before the other irradiation steps, the reaction mixture was flushed with nitrogen for 10 s. The functionalized PEG hydrogel based SCPs were washed with ethanol for 3 times, with a mixture of 50 vol. % ethanol and 50 vol. % Type I water for 3 times, and with Type I water for 3 times. The clean SCPs were stored in Type I water for further steps.

5.2.3.5 Ligand-functionalization of SCPs

All reactants are added with fixed mole equivalents. Here, a master protocol of carboxylic SCPs dispersion with 100 µmol/g carboxylic group functionalization degree and 2 mg/mL SCPs concentration will be described as an example.

Table 21: Reactants equivalent information for coupling reaction in ligand functionalization of the carboxylic SCPs.

Reactants	Equivalent
-COOH groups of SCPs	1 eq.
PyBOP	10 eq.
HOBt	5 eq.
DIPEA or TEA	10 eq.
Man/Biotin-NH_2	10 eq.

Functionalization with ethylene amine (MEA)

3 mL (6 mg) carboxylic SCPs dispersion was centrifuged at 4400 rpm for 10 min, the supernatant was decanted, and 3 mL DMF was added to the SCPs. The procedure was repeated for 2 times to exchange water with DMF in SCPs dispersion. 3.12 mg (6 µmol) PyBOP, 0.45 mg (3 µmol) HOBt was added to the SCPs dispersion and shaken vigorously till dissolved. 1.05 µL (6 µmol) DIPEA was added to the dispersion and shaken for 5 min. 0.36 µL (6 µmol) MEA was added to the dispersion and shaken for 180 min. Then, the SCPs were washed with DMF 3 times, and with Type I water 3 times. At the end, the SCPs were stored in Type I water with 0.01 % sodium azide.

Functionalization with Mannose-NH_2

3 mL (6 mg) carboxylic SCPs dispersion was centrifuged at 4400 rpm for 10 min, the supernatant was decanted, and 3 mL DMF was added to the SCPs. The procedure was repeated for 2 times to exchange water with DMF in SCPs dispersion. 3.12 mg (6 µmol) PyBOP, 0.45 mg (3 µmol) HOBt was added to the SCPs dispersion and shaken vigorously till dissolved. 1.05 µL (6 µmol) DIPEA was added to the dispersion and shaken for 5 min. 5.57 mg (6 µmol) Mannose-NH_2 was added to the dispersion and shaken for 180 min. Then, the SCPs were washed with DFM for 3 times, and with methanol for 3 times. 0.65 mg (12 µmol) sodium methoxide were added to the SCP methanol dispersion. The reaction mixture was shaken for 30 min. Then, the SCPs were washed with methanol 3 times, and with Type I water 3 times. At the end, the SCPs were stored in Type I water with 0.01 % sodium azide.

Functionalization with Biotin-NH_2

3 mL (6 mg) carboxylic SCPs dispersion was centrifuged at 4400 rpm for 10 min, the supernatant was decanted, and 3 mL DMF was added to the SCPs. The procedure was repeated for 2 times to exchange water with DMF in SCPs dispersion. 3.12 mg (6 µmol) PyBOP, 0.45 mg (3 µmol) HOBt was added to the SCPs dispersion and shaken vigorously till dissolved. 1.05 µL (6 µmol) DIPEA was added to the dispersion and shaken for 5 min. 1.72 mg (6 µmol) Biotin-NH_2

was added to the dispersion and shaken for 180 min. Then, the SCPs were washed with DMF 3 times, and with Type I water 3 times. At the end, the SCPs were stored in Type I water with 0.01 % sodium azide.

5.2.3.6 Characterization of SCPs

Size and size distribution of SCPs via optical microscopy

The size of the SCPs was measured with an optical microscope. One drop of the acquired SCPs was placed on a glass slide. At least 3 images for one group of SCPs were recorded. The recorded images were analysed with image processing software ImageJ. For each group of SCPs, the average diameter of around 100 SCPs were used as the size of this group of SCPs.

Swelling Degree

The swelling degree of the SCPs were measured through the combination of an optical microscope and an AFM. Firstly, a drop of SCPs was placed on a glass slide under an optical microscope. The image of one random SCP were recorded. The radius of this swollen SCP was calculated with image processing software ImageJ. As the swollen SCP is sphere, the volume of the swollen SCP can be calculated with the following equation:

$$V_S = \frac{4}{3}\pi R^3 \qquad \textbf{Equation 22}$$

, where V_s is the swollen volume of the SCP, R is the radius of the SCP.

Then, under the tracking of an optical microscope, the previous SCP was dried with a heat gun. The image of this dry SCP was recorded. The radius of this dry SCP was calculated with ImageJ. However, not all SCPs will shrink into a sphere. The shape of the SCP will be scanned with an AFM. From the cross-section height curve of a SCP, the shape of this SCP can be confirmed. There are normally 3 types of dry SCP shape: sphere, half-sphere, or pan-cake.

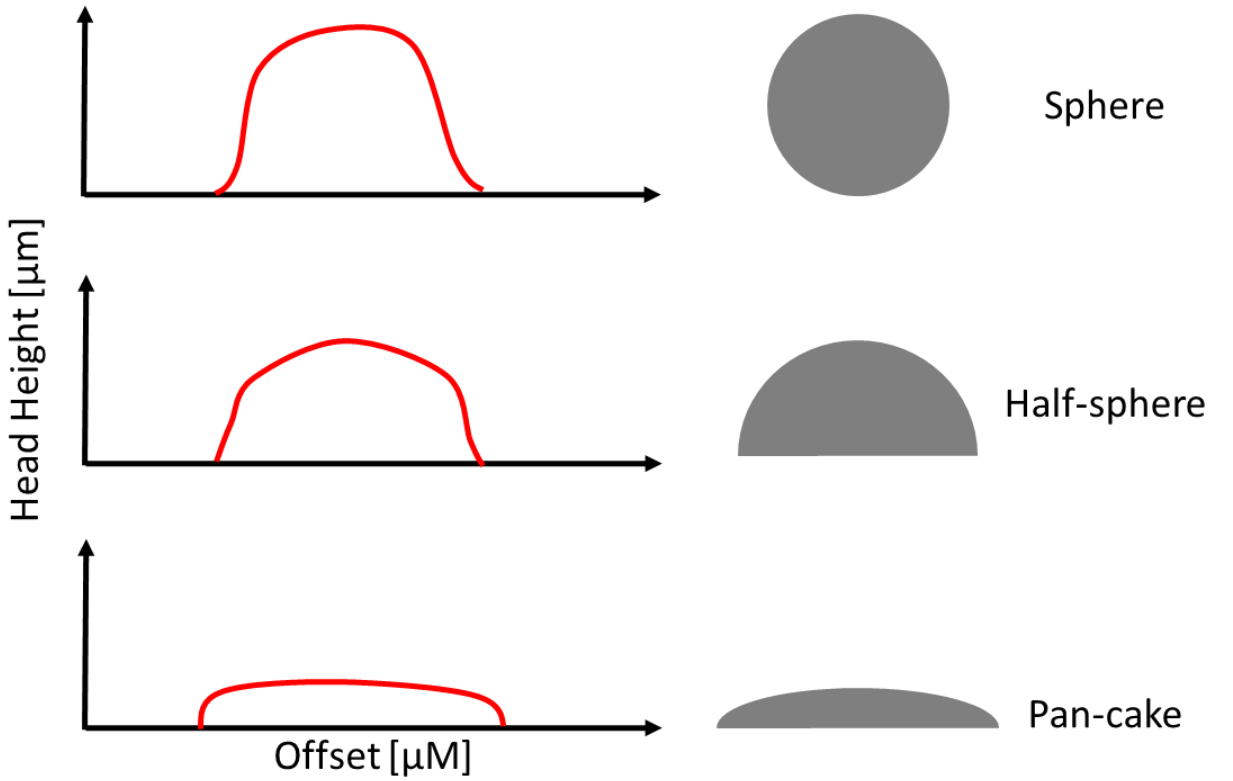

Figure 44: The possible shape of dry SCP and its corresponding cross-section curve from AFM.

For different cases, the dry volume of the SCP was calculated with different equations. When the shape of dry SCP is a sphere, the volume of this dry SCP was calculated with the following equation:

$$V_{DS} = \frac{4}{3}\pi R^3 \qquad \textbf{Equation 23}$$

When the shape of dry SCP is a half-sphere, the volume of this dry SCP was calculated with the following equation:

$$V_{DH} = \frac{2}{3}\pi R^3 \qquad \textbf{Equation 24}$$

When the shape of dry SCP is a pan-cake, the volume of this dry SCP was calculated with the following equation:

$$V_{DP} = \pi R^2 H \qquad \textbf{Equation 25}$$

, where V_{DS} is the dry volume of sphere shape SCP, V_{DH} is the dry volume of half-sphere shape SCP, V_{DP} is the dry volume of pan-cake shape SCP, R is the contact radius of the SCP and glass slide, H is the height of the pan-cake shape SCP.

The swelling degree of the SCPs were calculated with the following equation:

$$D_{Swelling\ Degree} = \frac{V_S}{V_D} \times 100\% \qquad \textbf{Equation 26}$$

, where $D_{Swelling\ Degree}$ is the swelling degree of SCPs, V_S is the swollen volume of the SCP, V_D is the dry volume of the SCP.

Young's Modulus

The Young's modulus was measured with an AFM and an optical microscope. Before the AFM measurement, the cantilever for this experiment was prepared. A tipless cantilever with resonance frequency in a range of 10 - 20 kHz and spring constant in a range of 0.03 - 0.09 N/m (Nanoworld AG, Switzerland) was used. The cantilever was clamped on a quartz glass holder and cleaned in UV Ozone cleaner UVC-1014 (NanoBioAnalytics, Germany) for 30 min. Then, the spring constant of the shortest tip were measured with AFM. A glass bead with a diameter of 4.64 µm (microParticles GmbH, Germany) was glued on the same tip with UHU plus schnellfest 2-K-Epoxidharzkleber super glue (UHU GmbH, Germany).

10 µL of SCP dispersion was diluted in 10 mL measurement solution in a petri dish. The measurement solution should be the same as the corresponding RICM experiment for this group of SCPs. For example, PEG-Man SCPs were immersed in LBB7.4 in RICM experiment. Here, the Young's modulus measurement for PEG-Man SCPs also required the SCP to be immersed in LBB7.4. The petri dish was studied by an inverted optical microscope. The image of one SCP was recorded with a CMOS camera. The diameter of this SCP was detected with image processing software ImageJ. The effective tip radius was calculated with the following equation:

$$\frac{1}{R_E} = \frac{1}{D_P/2} + \frac{1}{D_G/2} \qquad \textbf{Equation 27}$$

, where R_e is the effective tip radius, D_P is the diameter of this SCP, D_G is the diameter of the glass bead on the tip.

The sensitivity of the AFM tip was calibrated every time when the tip entered aqueous phase from air phase. The force vs. height curve of this SCP was recorded with AFM. With sensitivity of tip, spring constant of tip, and effective radius, the curve was fitted with Hertz model. The Young's modulus of this SCP can be acquired.

For each group of SCPs, at least eight SCPs were measured. The average of their Young's modulus was calculated as the Young's modulus of this group of SCPs.

Functional Group Concentration

TBO Titration Method for carboxylic group functionalized SCPs

0.5 mL carboxylic group functionalized SCPs dispersion was washed with ethanol for one time and dried under vacuum at 50 °C for 5 h till the weight of the dry SCPs was stable. 1 mL 312.5 μM toluidine blue O (TBO) aqueous solution at pH 10 - 11 was added to the dry SCPs and shaken in dark overnight to stain the SCPs. The stained SCPs dispersion was centrifuged for 30 min at 4400 rpm. 0.3 mL of the supernatant was diluted to 2 mL with Type I water. The absorbance at 633 nm of this solution was measured with UV-VIS spectroscopy. Meanwhile, the absorbance at 633 nm of a mixture of 1 mL 312.5 μM toluidine blue O (TBO) aqueous solution at pH 10 - 11 and 1.7 mL Type I water was measured as reference. The carboxylic group functionalization degree of this group of SCPs was calculated with the following equation:

$$D_{CGF} = \frac{(1-\frac{A_S}{A_R})\times 0.3125}{W_{Dry}} \qquad \textbf{Equation 28}$$

, where D_{CGF} is the carboxylic group functionalization degree, A_S is the UV-VIS absorbance of sample, A_R is the UV-VIS absorbance of reference, W_{Dry} is the dry weight of 0.5 mL SCPs, 0.3125 is the amount of TBO in reference solution with a unit of μmol.

For each group of SCPs, the TBO titration experiment should be repeat three times and the average carboxylic group functionalization degree of the three experiments was used as the carboxylic group functionalization degree of this group of SCPs.

Via Optical TBO Method for ligand functionalized SCPs

0.1 mL ligand functionalized SCPs dispersion was washed with sodium hydroxide aqueous solution at pH 10 - 11 for three times. 1 mL 312.5 μM toluidine blue O (TBO) aqueous solution at pH 10 - 11 was added to the dry SCPs and shaken in dark overnight to stain the SCPs. The stained SCPs were washed with sodium hydroxide aqueous solution at pH 10 - 11 for three times.

Meanwhile, 0.1 mL of the same SCPs before ligand functionalization was also processed with the above steps as a reference. The stained ligand functionalized SCPs, stained carboxylic group functionalized SCPs, and not stained carboxylic group functionalized SCPs were placed on glass slide and immersed in sodium hydroxide aqueous solution at pH 10 - 11. The SCPs were studied by an optical microscope under same light condition. The image of these SCPs was recorded with a CMOS camera with the same settings. The grey value of these SCPs was detected with image processing software ImageJ. The ligand functionalization degree of ligand functionalized SCPs was calculated with the following equation:

$$D_{LF} = \frac{G_1 - G_2}{G_3 - G_2} \times D_{CGF} \qquad \textbf{Equation 29}$$

, where D_{LF} is the ligand functionalization degree, G_1 is the grey value of stained ligand functionalized SCPs, G_2 is the grey value of stained carboxylic group functionalized SCPs, G_3 is the grey value of not stained carboxylic group functionalized SCPs.

5.2.3.7 Cleaning of Glass Surface

Coverslips (Ø 24 mm)

Coverslips (Thickness 0.13-0.16 mm, Ø 24 mm, Paul Marienfeld, Germany) are immersed in a 2 vol. % Mucasol (BRAND, Germany) aqueous solution and ultra-sonicated for 15 min. Then, the coverslips are flushed with Type I water till all the detergent is removed. 150 mL Type I water, 30 mL ammonia aqueous solution (25 wt. %) , and 30 mL hydrogen peroxide aqueous solution (30 wt. %) in a volume ration of 5:1:1 are mixed as RCA cleaning solution. [107] The coverslips are immersed in 210 mL RCA solution at 70 °C for 60 min. Then, the coverslips are flushed with Type I water till all the reactants are removed and directly used for further steps.

Glass Slides (15 µ-Slide 8 well)

Glass Slides (15 µ-Slide 8 well 80827, ibidi, Germany) are cleaned in a UV ozone cleaner (UVC-1014, NanoBioAnalytics, Germany) for 30 min and used directly for further steps.

5.2.3.8 Functionalization of Glass Surface

With Poly(ethylenimine) (PEI)

5 mg branched PEI (M_n 10000) was dissolved in 5 mL Type I water for a 1 mg/mL PEI aqueous solution. To each well of the cleaned glass slide, 400 µL PEI aqueous solution was added. The glass slide was shaken on a shaker for 120 min and flushed with Type I water to remove the excess PEI aqueous solution. 400 µL Type I water was added to each well of the PEI coated glass slide, which stored for further steps in reflection interference contrast microscope (RICM) experiment.

With Proteins

Via (3-Glycidyloxypropyl)trimethoxysilane (GLYMO)

182.4 mL ethanol, 9.6 mL Type I water, 192 µL acetic acid, 1920 µL GLYMO was mixed as the reaction solution. Glass surfaces are immersed in the above reaction solution and shaken on a shaker for 120 min. After the reaction, the glass surfaces were rinsed with ethanol and annealed at required temperature for 120 min.

1 mg protein was dissolved in 5 mL PBS for a 0.2 mg/mL protein / PBS solution. Required amount of protein / PBS solution was added on the GLYMO coated glass surface and shaken on a shaker for 60 min. The protein coated surface was flushed with PBS to remove excess protein.

Via Physical Absorption

1 mg protein was dissolved in 5 mL PBS for a 0.2 mg/mL protein / PBS solution. Required amount of protein / PBS solution was added on the cleaned glass surface and shaken on a shaker for 60 min. The protein coated surface was flushed with PBS to remove excess protein.

5.2.3.9 Reflection Interference Contrast Microscopy (RICM) Measurements

The functionalized cover slip or glass slide surface was covered with measurement buffer. 10 µL SCPs dispersion were add on the surface. The SCPs were studied by an inverted reflection interference contrast microscope. The monochromatic green light with 546 nm wave length was used as working light for RICM measurements. [108] The images of 20 SCPs interference pattern

were recorded with a CMOS camera. These images were analysed with RICM image processing software Hydrogel-3 to detect the contact radius (Figure 45 A) and the particle radius were calculated automatically with mathematic software Igor (Figure 45 B).

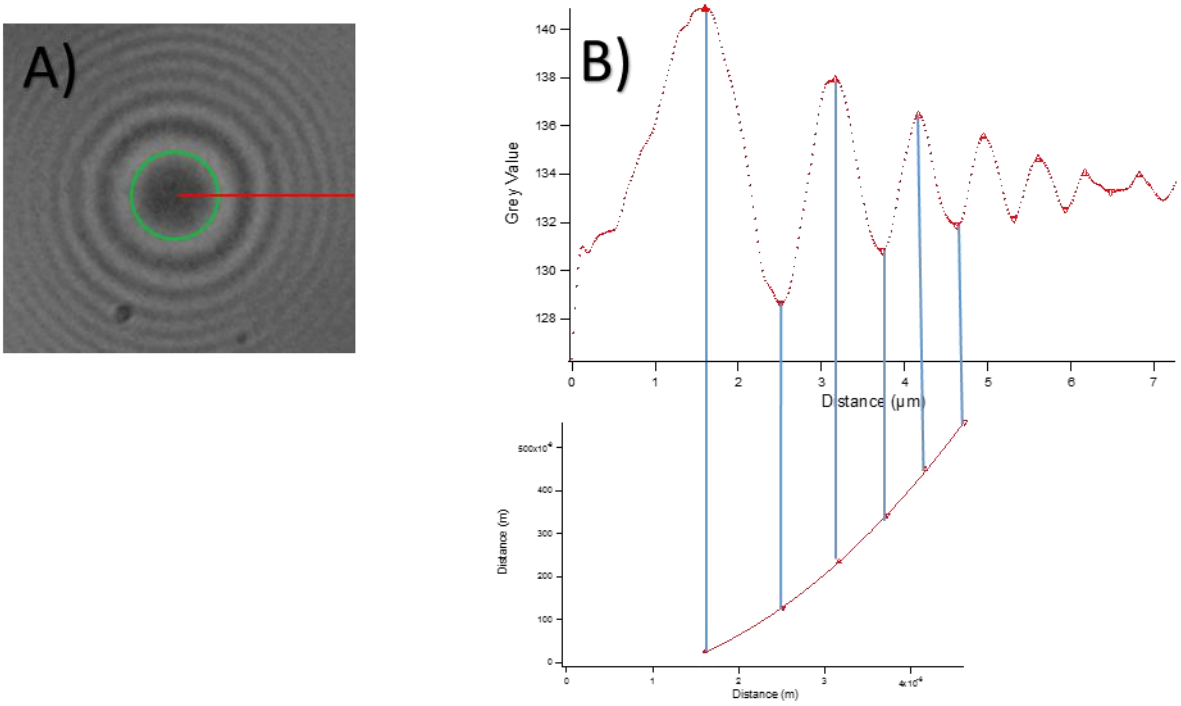

Figure 45: Detection of contact radius (A) and reconstruction of the SCP profile for radius calculation with software (B).

The SCP-RICM curve can be fitted and the adhesion energy was calculated automatically at the same time by Igor. (Figure 46- Figure 53)

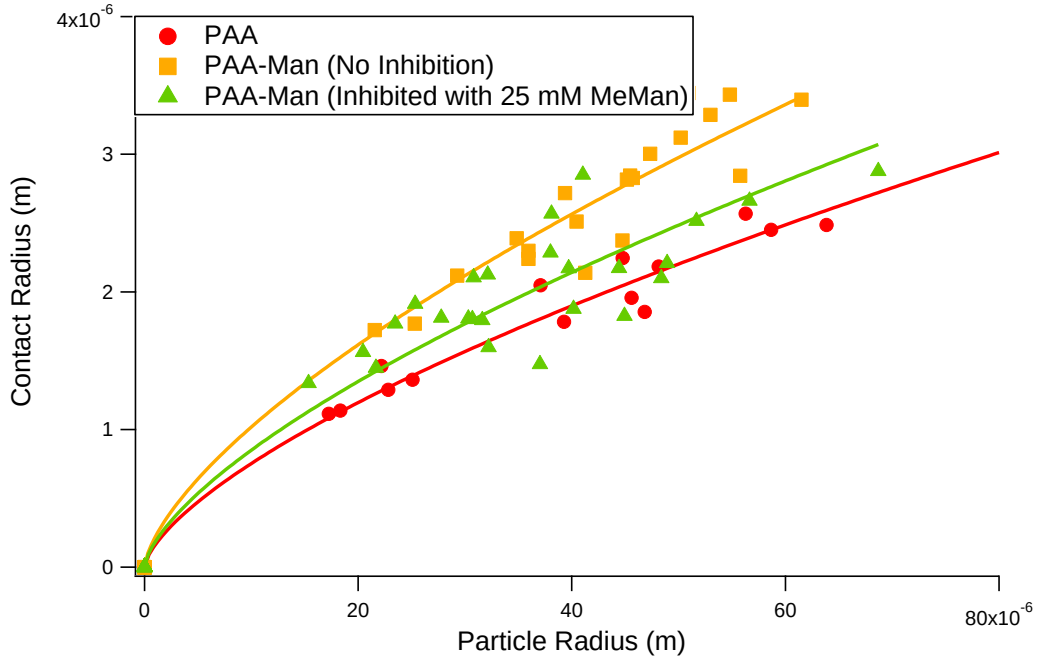

Figure 46: SCP-RICM curve from Igor software for PAA SCPs and PAA-Man under inhibition.

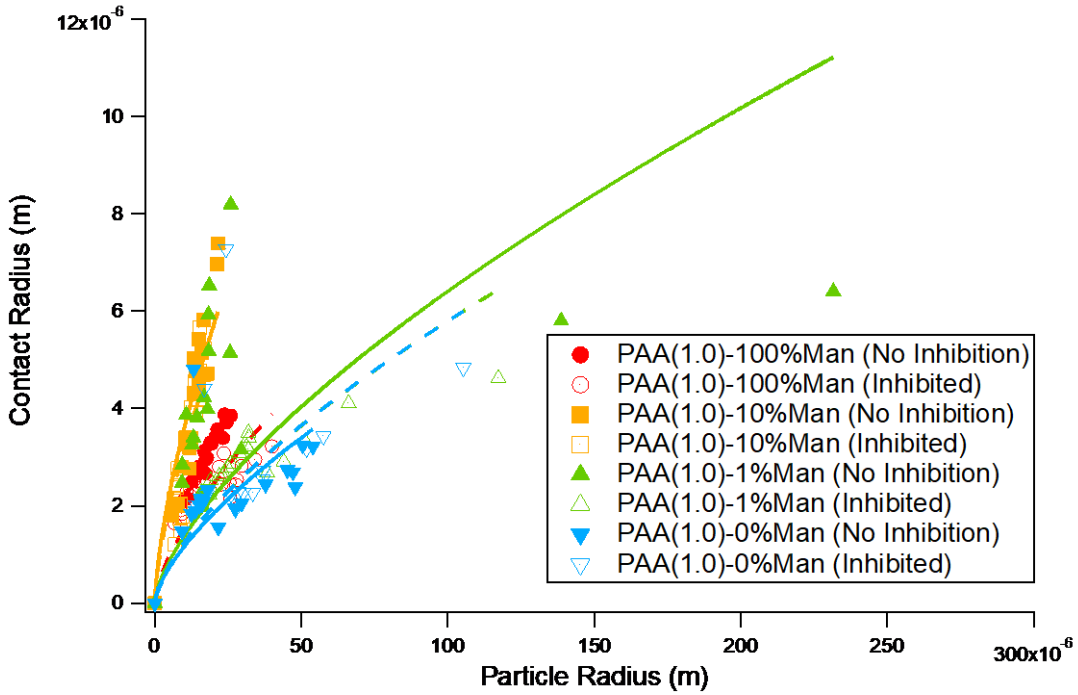

Figure 47: SCP-RICM curve from Igor software for PAA-Man SCPs with various degree of mannose functionalization.

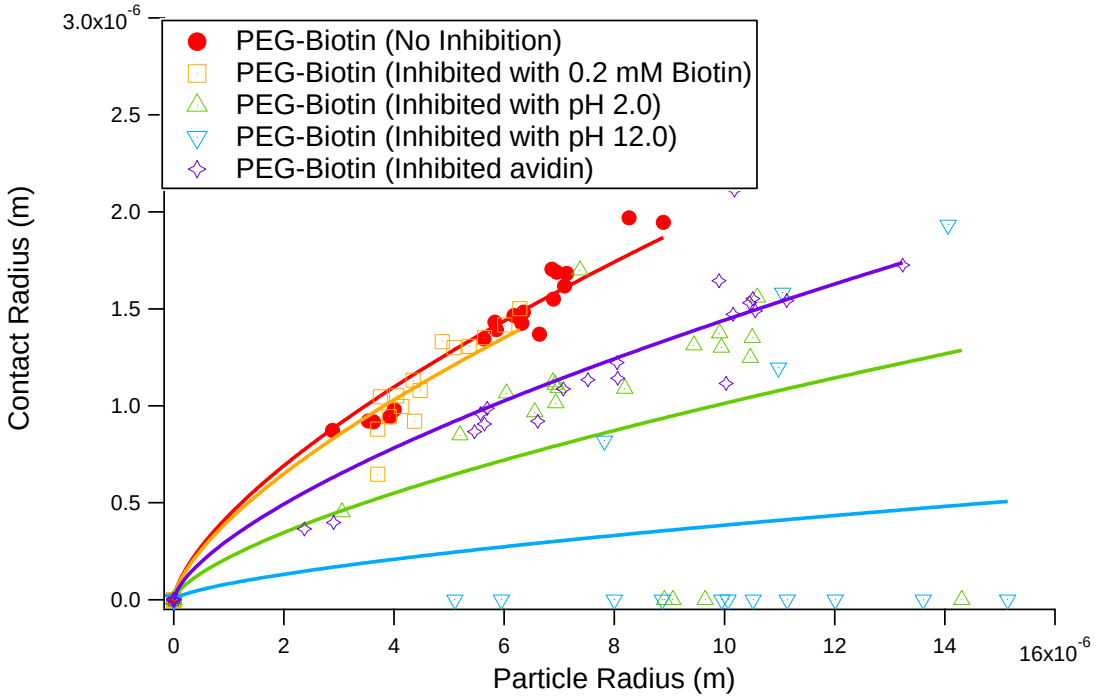

Figure 48: SCP-RICM curve from Igor software for PEG-Biotin SCPs under various inhibition condition.

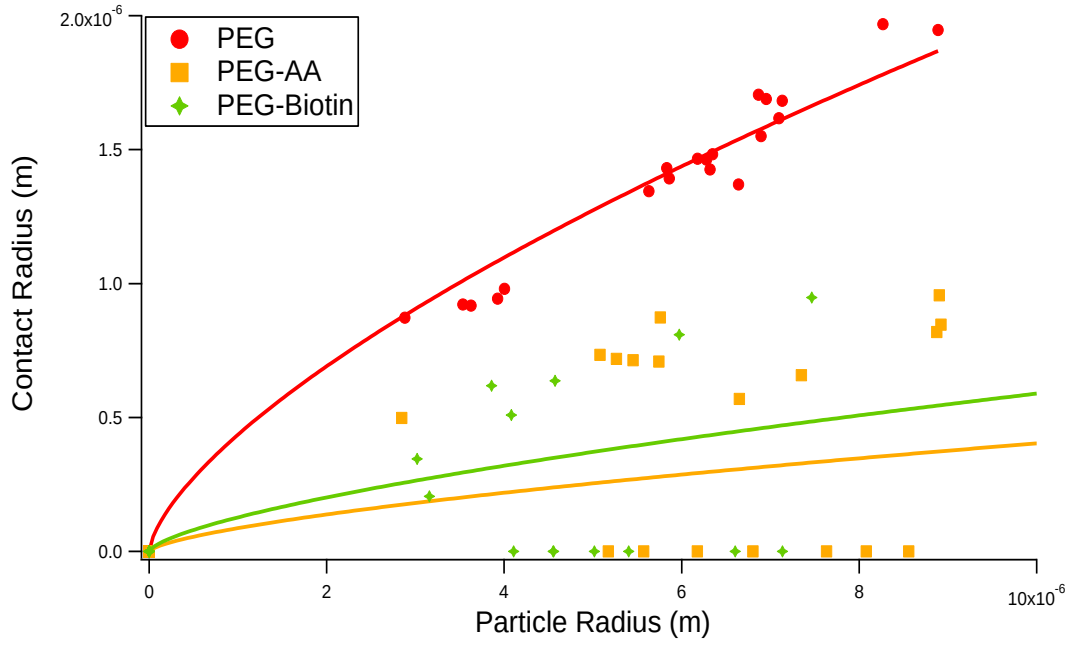

Figure 49: SCP-RICM curve from Igor software for PEG, PEG-AA, and PEG-Biotin SCPs on avidin.

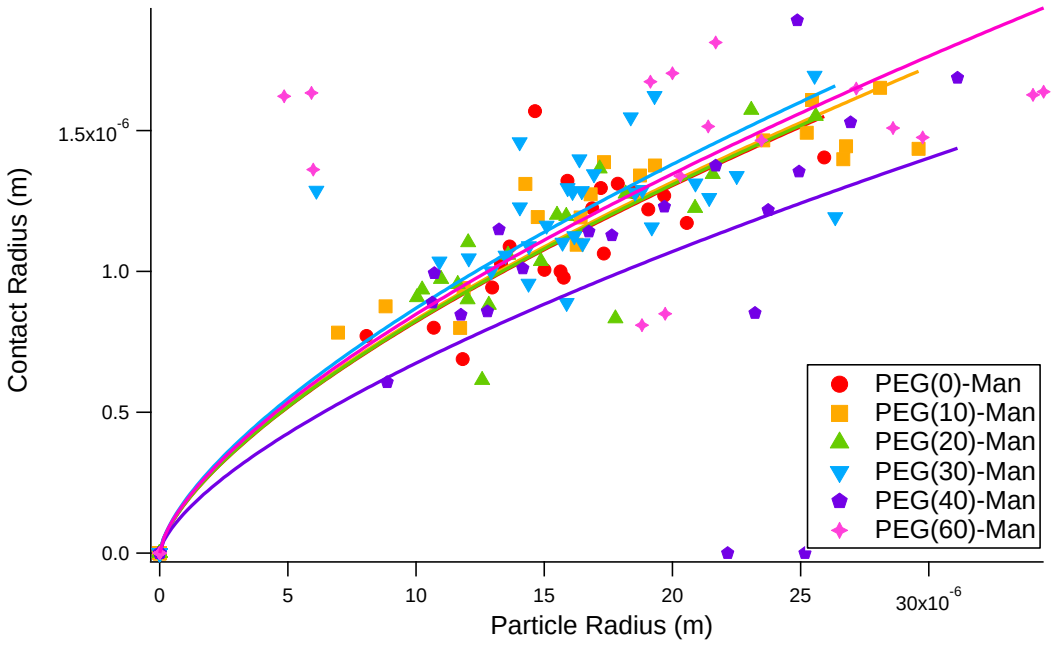

Figure 50: SCP-RICM curve from Igor software for PEG-Man SCPs with various Young's modulus.

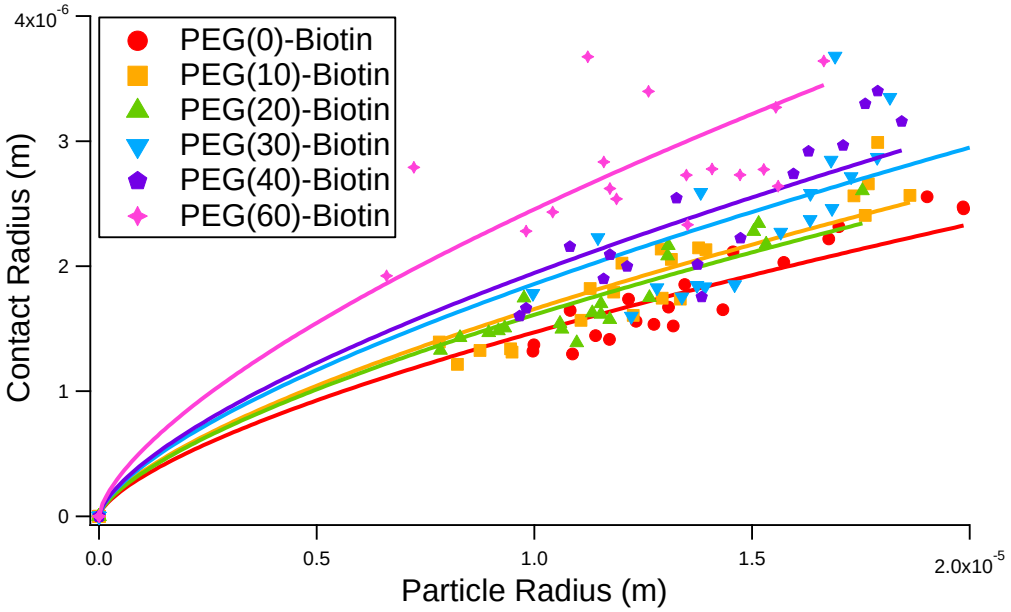

Figure 51: SCP-RICM curve from Igor software for PEG-Biotin SCPs with various Young's modulus.

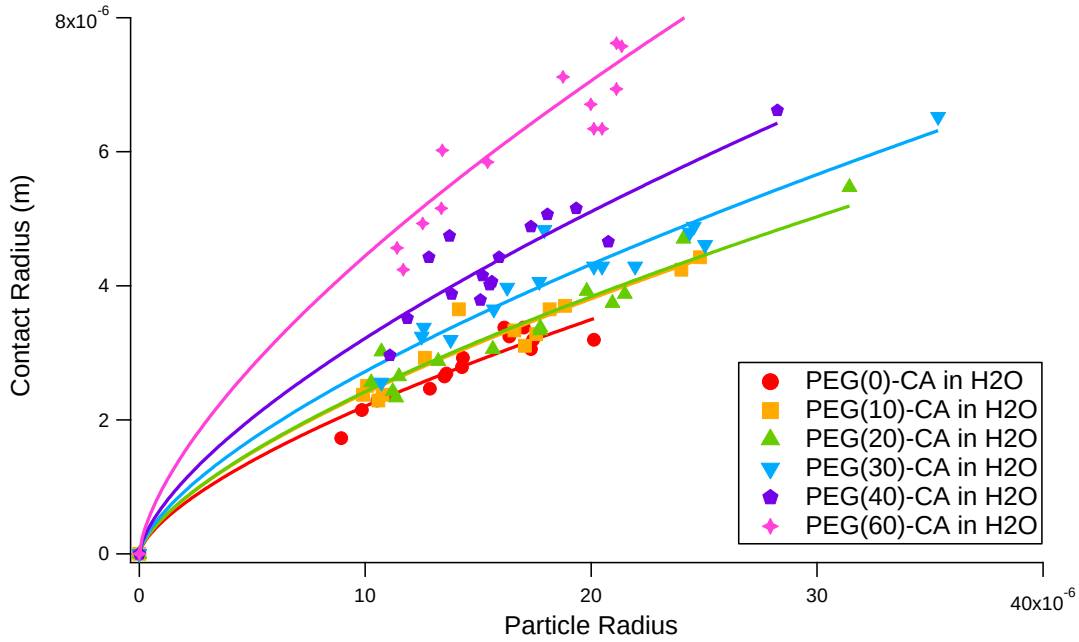

Figure 52: SCP-RICM curve from Igor software for PEG-CA SCPs with various Young's modulus in H_2O.

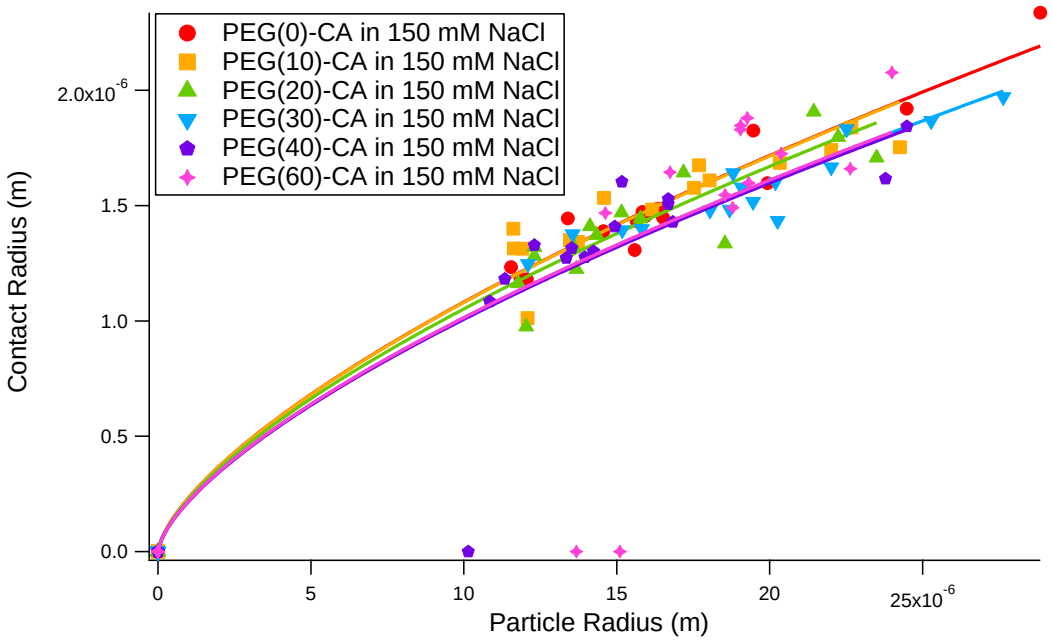

Figure 53: SCP-RICM curve from Igor software for PEG-CA SCPs with various Young's modulus in 150 mM NaCl.

5.2.3.10 Inhibition / Competition Experiment via RICM

The inhibition / competition experiment was performed via the RICM method. The adhesion energy of the SCPs on a corresponding surface was measured via RICM. Then, the surface was inhibited with a required concentration of free ligand, or a buffer solution at required pH value. The adhesion energy of the same SCPs on the inhibited surface was measured again via RICM. The adhesion energy difference before and after surface inhibition is the specific adhesion energy of this ligand.

5.2.3.11 Half Maximal Inhibitory Concentration (IC_{50}) for mannose Con A via RICM

The IC50 experiment was performed via RICM method. Two ibidi glass slides was cleaned and functionalized with Con A. The cells of the glass slides were filled with methyl mannose / LBB7.4 solution according to Table 22.

Table 22: Methyl mannose concentration in LBB7.4 for IC50 experiment.

Slide	Methyl Mannose Concentration in LBB7.4 [µM]							
A	0	1	10	50	200	500	2000	10000
B	0	100	300	600	1000	3000	6000	10000

Each cell was added with 5 µL SCPs and the RICM experiment was performed. The adhesion energy of each cell was calculated and normalized according to the lowest adhesion energy and the highest adhesion energy on the same slides. The normalized adhesion energy of slides A and B were plotted in a logarithmic graph and fitted with Hill1 function in mathematical software Origin. The methyl mannose concentration at 50 % adhesion energy on Hill1 fitting curve is the final IC50 value for this group of PEG-Man SCPs on Con A functionalized surface. Table 23 shows the IC_{50} results. Figure 54 shows the data point and fitted curves of IC_{50} result.

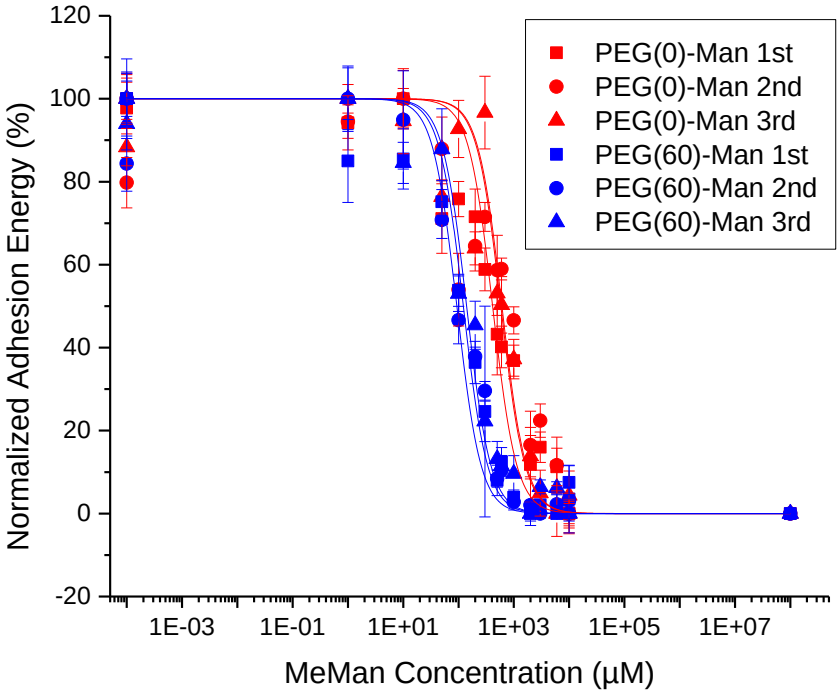

Figure 54: IC50 measurement curve of PEG-Man SCPs with various Young's modulus.

Table 23: IC_{50} value of PEG-Man SCPs with various Young's modulus.

Sample	Young's Modulus [kPa]	IC50 [µM]			
		1st Measurement	2nd Measurement	3rd Measurement	Average
PEG(0)-Man	211 ± 12	413	583	610	535 ± 122
PEG(60)-Man	13 ± 2	122	93	140	118 ± 25

6. References

[1] G. U. Lee, D. A. Kidwell and R. J. Colton, “Sensing Discrete Streptavidin-Biotin Interactions with Atomic Force Microscopy,” *Langmuir,* vol. 10, pp. 354-357, 1994.

[2] Ajay and M. A. Murcko, “Computational Methods to Predict Binding Free Energy in Ligand-Receptor Complexes,” *J. Med. Chem.,* vol. 38, pp. 4953-4967, 1995.

[3] E.-L. Florin, V. T. Moy and H. E. Gaub, “Adhesion forces between individual ligand-receptor pairs,” *Science,* vol. 264, pp. 415-417, 1994.

[4] Y. Zhang, H. Gu, Z. Yang and B. Xu, “Supramolecular Hydrogels Respond to Ligand−Receptor Interaction,” *J. Am. Chem. Soc.,* vol. 125, pp. 13680-13681, 2003.

[5] H. Lodish, A. Berk, C. A. Kaiser, M. Krieger and A. Bretscher, Molecular Cell Biology, 4th edition, New York: Freeman & Company, W. H., 2007.

[6] I. A. Wilson and R. L. Stanfield, “Antibody-antigen interactions,” *Curr. Opin. Struct. Biol.,* vol. 3, pp. 113-118, 1993.

[7] C. F. Hawkins, A. Borges and R. N. Perham, “A common structural motif in thiamin pyrophosphate-binding enzymes,” *FEBS Lett.,* vol. 255, pp. 77-82, 1989.

[8] N. C. Andrews and D. V. Faller, “A rapid micropreparation technique for extraction of DNA-binding proteins from limiting numbers of mammalian cells,” *Nucleic Acids Res.,* vol. 19, p. 2499, 1991.

[9] M. Mammen, S.-K. Choi and G. M. Whitesides, “Polyvalent Interactions in Biological Systems: Implications for Design and Use of Multivalent Ligands and Inhibitors,” *Angew. Chem. Int. Ed.,* vol. 37, pp. 2754-2794, 1998.

[10] E. Fischer, “Einfluss der Configuration auf die Wirkung der Enzyme,” *Ber. Dtsch. Chem. Ges.,* vol. 27, pp. 2985-2993, 1894.

[11] D. L. Garland, “Kinetics and mechanism of colchicine binding to tubulin: evidence for ligand-induced conformational changes,” *Biochemistry,* vol. 17, pp. 4266-4272, 1978.

[12] M. Totrov and R. Abagyan, “Flexible ligand docking to multiple receptor conformations: a practical alternative,” *Curr. Opin. Struct. Biol.,* vol. 18, pp. 178-184, 2008.

[13] D. Sprinzak, A. Lakhanpal, L. LeBon, J. Gracia-Ojalvo and M. B. Elowitz, “Mutual Inactivation of Notch Receptors and Ligands Facilitates Developmental Patterning,” *PLoS Comput. Biol.,* vol. 7, pp. 1-11 (e1002069), 2011.

[14] H. Gohlke, Protein-Ligand Interactions, Weinheim: John Wiley & Sons, 2012.

[15] B. Goldstein and M. Dembo, “Approximating the effects of diffusion on reversible reactions at the cell surface: ligand-receptor kinetics,” *Biophys J.,* vol. 68, pp. 1222-1230, 1995.

[16] H. Gohlke and G. Klebe, “Approaches to the Description and Prediction of the Binding Affinity of Small-Molecule Ligands to Macromolecular Receptors,” *Angew. Chem. Int. Ed.,* vol. 41, pp. 2644-2676, 2002.

[17] N. M. Green, “Avidin,” *Adv. Protein. Chem.,* vol. 29, pp. 85-133, 1975.

[18] L.-H. Lee, Fundamentals of Adhesion, New York: Springer, 1991.

[19] G. Weber, “Energetics of Ligand Binding to Proteins,” *Adv. Protein. Chem.,* vol. 29, pp. 1-83, 1975.

[20] D. Boal, Mechanics of the Cell, Cambridge: Cambridge University Press, 2012.

[21] K. D. Puri, R. G. Bhat and A. Surolia, “Thermodynamics of Monosaccharide Binding to Concanavalin A, Pea (Pisum sativum) Lectin, and Lentil (Lens culinaris) Lectin,” *J. Biol. Chem.,* vol. 268, pp. 7668-7677, 1993.

[22] B. K. Brandley, S. Swiedler and P. W. Robbins, “Carbohydrate ligands of the LEC cell adhesion molecules,” *Cell,* vol. 63, pp. 861-863, 1990.

[23] G. A. Rabinovich, L. G. Baum, N. Tinari, R. Paganelli, C. Natoli, F.-T. Liu and S. Lacobelli, "Galectins and their ligands: amplifiers, silencers or tuners of the inflammatory response?," *Trends. Immunol.,* vol. 23, pp. 313-320, 2002.

[24] T. Andre, A. Reichel, K.-H. Wiesmüller, R. Tampe, J. Piehler and R. Brock, "Selectivity of Competitive Multivalent Interactions at Interfaces," *ChemBioChem,* vol. 10, pp. 1878-1887, 2009.

[25] R. T. Lee and Y. C. Lee, "Affinity enhancement by multivalent lectin–carbohydrate interaction," *Glycoconjugate J.,* vol. 17, pp. 543-551, 2000.

[26] J. Rao, J. Lahiri, L. Isaace, R. M. Weis and G. M. Whitesides, "A Trivalent System from Vancomycin·d-Ala-d-Ala with Higher Affinity Than Avidin·Biotin," *Science,* vol. 280, pp. 708-711, 1998.

[27] P. Kitov, J. M. Sadowska, G. Mulvey, G. D. Armstrong, H. Ling, N. Pannu, R. J. Read and D. R. Bundle, "Shiga-like toxins are neutralized by tailored multivalent carbohydrate ligands," *Nature,* vol. 403, pp. 669-672, 2000.

[28] J. N. Israelachvili, Intermolecular and Surface Forces, Waltham: Academic Press, 2011.

[29] J. W. Gibbs, "On the Equilibrium of Heterogeneous Substances," *Trans. Conn. Acad. Arts Sci.,* vol. 2, pp. 300-320, 1879.

[30] H. Jung, A. D. Robison and P. S. Cremer, "Multivalent ligand–receptor binding on supported lipid bilayers," *J. Struct. Biol.,* vol. 168, pp. 90-94, 2009.

[31] J. S. Lee, T. Kuroha, M. Hnilova, D. Khatayevich, M. M. Kanaoka, J. M. McAbee, M. Sarikaya, C. Tamerler and K. U. Torri, "Direct interaction of ligand–receptor pairs specifying stomatal patterning," *Genes Dev,* vol. 26, pp. 126-136, 2016.

[32] P. Czodrowski, C. A. Sotriffer and G. Klebe, "Protonation Changes upon Ligand Binding to Trypsin and Thrombin: Structural Interpretation Based on pKa Calculations and ITC Experiments," *J. Mol. Biol.,* vol. 367, pp. 1347-1356, 2007.

[33] S. Rinker, Y. Ke, Y. Liu, R. Chhabra and H. Yan, “Self-assembled DNA nanostructures for distance-dependent multivalent ligand–protein binding,” *Nat. Nanotechnol.,* vol. 3, pp. 418-422, 2008.

[34] P. Pattnaik, “Surface plasmon resonance,” *Biotechnol. Appl. Biochem.,* vol. 126, pp. 79-92, 2005.

[35] Y. Tang, X. Zeng and J. Liang, “Surface Plasmon Resonance: An Introduction to a Surface Spectroscopy Technique,” *J Chem Educ.,* vol. 87, pp. 742-746, 2010.

[36] R. J. Green, J. Davies, M. C. Davies, C. J. Roberts and S. J. B. Tendler, “Surface plasmon resonance for real time in situ analysis of protein adsorption to polymer surfaces,” *Biomaterials,* vol. 18, pp. 405-413, 1997.

[37] K. V. Gobi, H. Iwasaka and N. Miura, “Self-assembled PEG monolayer based SPR immunosensor for label-free detection of insulin,” *Biosens. Bioelectron.,* vol. 22, pp. 1382-1389, 2007.

[38] S. Covaceuszach, S. Capsoni, G. Ugolini, F. Spirito, D. Vignone and A. Cattaneo, “Development of a Non Invasive NGF-Based Therapy for Alzheimer's Disease,” *Curr. Alzheimer. Res.,* vol. 6, pp. 159-170, 2009.

[39] C. Fasting, C. A. Schalley, M. Weber, O. Seitz, S. Hecht, B. Koksch, J. Dernedde, C. Graf, E.-W. Knapp and R. Haag, “Multivalency as a Chemical Organization and Action Principle,” *Angew. Chem. Int. Ed.,* vol. 51, pp. 10472-10498, 2012.

[40] O. Nahshol, V. Bronner, A. Notcovich, L. Rubrecht, D. Laune and T. Bravman, “Parallel kinetic analysis and affinity determination of hundreds of monoclonal antibodies using the ProteOn XPR36,” *Anal. Biochem.,* vol. 383, pp. 52-60, 2008.

[41] J. Dernedde, A. Rausch, M. Weinhart, S. Enders, R. Tauber, K. Licha, M. Schirner, U. Zügel, A. von Bonin and R. Haag, “Dendritic polyglycerol sulfates as multivalent inhibitors of inflammation,” *Proc. Natl. Acad. Sci.,* vol. 107, pp. 19679-19684, 2010.

[42] G. Binnig, C. F. Quate and C. Gerber, "Atomic Force Microscope," *Phys. Rev. Lett,* vol. 56, pp. 930-934, 1986.

[43] L. Meagher, "Direct measurement of forces between silica surfaces in aqueous CaCl2 solutions using an atomic force microscope," *J. Colloid Interface Sci.,* vol. 152, pp. 293-295, 1992.

[44] M. Rief, F. Oesterhelt, B. Heymann and H. E. Gaub, "Single Molecule Force Spectroscopy on Polysaccharides by Atomic Force Microscopy," *Science,* vol. 275, pp. 1295-1297, 1997.

[45] G. Meyer and N. M. Amer, "Erratum: Novel optical approach to atomic force microscopy," *Appl. Phys. Lett.,* vol. 53, pp. 2400-2402, 1988.

[46] D. Pussak, D. Ponader, S. Mosca, T. Pompe, L. Hartmann and S. Schmidt, "Specific Adhesion of Carbohydrate Hydrogel Particles in Competition with Multivalent Inhibitors Evaluated by AFM," *Langmuir,* vol. 30, pp. 6142-6150, 2014.

[47] H. Handa, S. Gurczynski, M. P. Jackson and G. Mao, "Immobilization and Molecular Interactions between Bacteriophage and Lipopolysaccharide Bilayers," *Langmuir,* vol. 26, pp. 12095-12103, 2010.

[48] R. Hovius, P. Vallotton, T. Wohland and H. Vogel, "Fluorescence techniques: shedding light on ligand–receptor interactions," *Trends Pharmacol. Sci.,* vol. 25, pp. 69-74, 2008.

[49] R. Karamanska, J. Clarke, O. Blixt, J. I. MacRae, J. Q. Zhang, P. R. Crocker, N. Laurent, A. Wright, S. L. Flitsch, D. A. Russel and R. A. Field, "Surface plasmon resonance imaging for real-time, label-free analysis of protein interactions with carbohydrate microarrays," *Glycoconj. J.,* vol. 25, pp. 69-74, 2008.

[50] M. Horton, G. Charras and P. Lehenkari, "ANALYSIS OF LIGAND–RECEPTOR INTERACTIONS IN CELLS BY ATOMIC FORCE MICROSCOPY," *J. Recept. Sig. Transd.,* vol. 22, pp. 169-190, 2002.

[51] D. Pussak, M. Behra, S. Schmidt and L. Hartmann, “Synthesis and functionalization of poly(ethylene glycol) microparticles as soft colloidal probes for adhesion energy measurements,” *Soft Matter,* vol. 8, pp. 1664-1672, 2012.

[52] L. Limozin and K. Sengupta, “Quantitative Reflection Interference Contrast Microscopy (RICM) in Soft Matter and Cell Adhesion,” *ChemPhysChem,* vol. 10, pp. 2752-2768, 2009.

[53] D. Pussak, Synthesis and Functionalization of Soft Colloidal Probes based on Poly(ethylene glycol) as Carbohydrate Biosensors, Berlin: Freie Universität Berlin (Doctoral Thesis), 2014.

[54] G. B. Airy, M. A., F. R. A. S. and F. G. S., “On the phænomena of Newton's rings when formed between two transparent substances of different refractive powers,” *Philos. Mag. Ser. 3,* vol. 2, pp. 20-30, 1833.

[55] K. L. Johnson, K. Kendall and A. D. Roberts, “Surface Energy and the Contact of Elastic Solids,” *Proc. R. Soc. A,* vol. 324, pp. 301-313, 1971.

[56] A. Makishima and J. D. Mackenzie, “Direct calculation of Young's moidulus of glass,” *J. Non-Cryst. Solids,* vol. 12, pp. 35-45, 1973.

[57] M. Ahearne, Y. Yang, A. J. E. Haj, K. Y. Then and K.-K. Liu, “Characterizing the viscoelastic properties of thin hydrogel-based constructs for tissue engineering applications,” *J. R. Soc. Interface,* vol. 5, pp. 455-463, 2005.

[58] E. Vivaldo-Lima, P. E. Wood and A. E. Hamielec, “An Updated Review on Suspension Polymerization,” *Ind. Eng. Chem. Res.,* vol. 36, pp. 936-965, 1997.

[59] M. V. Dimonie, C. M. Boghina, N. N. Marinescu, M. M. Marinescu, C. I. Cincu and C. G. Oprescu, “Inverse suspension polymerization of acrylamide,” *Eur. Polym. J.,* vol. 18, pp. 639-645, 1982.

[60] R. Archady, “Suspension, emulsion, and dispersion polymerization: A methodological survey,” *Colloid Polym. Sci.,* vol. 270, pp. 717-732, 1992.

[61] S. M. Ahmed, “EFFECTS OF AGITATION, AND THE NATURE OF PROTECTIVE COLLOID ON PARTICLE SIZE DURING SUSPENSION POLYMERIZATION,” *J Disper. Sci. Technol.,* vol. 5, pp. 421-432, 1984.

[62] K. Li and D. H. Stöver, “Synthesis of Monodisperse Poly (divinylbenzene) Microspheres,” *Polym. Chem.,* vol. 31, pp. 3257-3263, 1993.

[63] J. S. Downey, R. S. Frank, W.-H. Li and D. H. Stöver, “Growth Mechanism of Poly(divinylbenzene) Microspheres in Precipitation Polymerization,” *Macromolecules,* vol. 32, pp. 2838-2844, 1999.

[64] S. Shen, E. D. Sudol and M. S. El-Aasser, “Dispersion polymerization of methyl methacrylate: Mechanism of particle formation,” *Polym. Chem.,* vol. 32, pp. 1087-1100, 1994.

[65] G. S. Whitby and M. Katz, “Synthetic Rubber,” *Rubber Chem. Technol.,* vol. 7, pp. 40-88, 1934.

[66] W. D. Harkins, “A General Theory of the Mechanism of Emulsion Polymerization,” *J. Am. Chem. Soc.,* vol. 69, pp. 1428-1444, 1947.

[67] W. V. Smith and R. H. Ewart, “Kinetics of Emulsion Polymerization,” *J. Chem. Phys.,* vol. 16, pp. 592-599, 1948.

[68] “Product information sheet P 4463 polyethylene glycol,” Sigma-Aldrich, [Online]. Available: https://www.sigmaaldrich.com/content/dam/sigma-aldrich/docs/Sigma/Product_Information_Sheet/1/p4463pis.pdf. [Accessed 17 November 2016].

[69] M. J. Hey, D. P. Jackson and H. Yan, “The salting-out effect and phase separation in aqueous solutions of electrolytes and poly(ethylene glycol),” *Polymer,* vol. 46, pp. 2567-2572, 2005.

[70] D. R. Paul and C. B. Bucknall, Polymer Blends: Formulation and Performance, Two-Volume Set, Wiley, 2000.

[71] Y. C. Bae, S. M. Lambert, D. S. Soane and J. M. Prausnitz, "Cloud-point curves of polymer solutions from thermooptical measurements," *Macromolecules,* vol. 24, pp. 4403-4407, 1991.

[72] J. G. Jung and Y. C. Bae, "Liquid–Liquid Equilibria of Polymer Solutions: Flory-Huggins with Specific Interaction," *J. Polym. Sci. Part B Polym. Phys.,* vol. 48, pp. 162-167, 2009.

[73] F. Hofmeister, "Zur Lehre von der Wirkung der Salze," *Archiv f. experiment. Pathol. u. Pharmakol,* vol. 24, pp. 247-260, 1888.

[74] R. L. Baldwin, "How Hofmeister ion interactions affect protein stability," *Biophys. J.,* vol. 71, pp. 2056-2063, 1996.

[75] S. Moelbert, B. Normand and P. De Los Rios, "Kosmotropes and chaotropes: modelling preferential exclusion, binding and aggregate stability," *Biophys. Chem.,* vol. 112, pp. 45-57, 2004.

[76] S. Schmidt, H. Wang, D. Pussake, S. Mosca and L. Hartmann, "Probing multivalency in ligand-receptor-mediated adhesion of soft, biomimetic interfaces," *Beilstein J. Org. Chem.,* vol. 11, pp. 720-729, 2015.

[77] W. Hanqing, Functionalization of soft colloidal probes for biosensing, Potsdam: Freie Universität Berlin (Master Thesis), 2013.

[78] M. L. Miller and J. Skogman, "Polymerization of tert-Butyl Crotonate," *J. Polym. Sci., Part A: Gen. Pap.,* vol. 2, pp. 4551-4558, 1964.

[79] D. Pussak, D. Ponader, S. Mosca, S. Vargas Ruiz, L. Hartmann and S. Schmidt, "Mechanical Carbohydrate Sensors Based on Soft Hydrogel Particles," *Angew. Chem. Int. Ed.,* vol. 52, pp. 6084-6087, 2013.

[80] J. A. Gilmore, L. E. McGann, J. Liu, D. Y. Gao, A. T. Peter, F. W. Kleinhans and J. K. Critser, "Effect of Cryoprotectant Solutes on Water Permeability of Human Spermatozoa," *Biol. Reprod.,* vol. 55, pp. 985-995, 1995.

[81] V. J. Goyanes, A. Ron-Corzo, E. Costas and E. Maneiro, "Morphometric categorization of the human oocyte and early conceptus," *Hum. Reprod.,* vol. 5, pp. 613-618, 1990.

[82] "ICSC 0423 - Crotonic Acid," International Programme on Chemical Safety (IPCS), 27 03 1996. [Online]. Available: http://www.inchem.org/documents/icsc/icsc/eics0423.htm. [Accessed 18 11 2016].

[83] S. Mukhopadhyay, B. C. Mitra and S. R. Palit, "Determination of Carboxyl Groups in Water-Soluble Copolymers by a Reverse Dye Partition Method and Calculation of r1," *J. Polym. Sci. A Polym. Chem.,* vol. 2444, p. 2442, 1969.

[84] H. Hertz, "Über die Berührung fester elasticher Körper," *J. für die reine und Agew. Math.,* vol. 92, pp. 156-171, 1881.

[85] H.-J. Butt, B. Cappella and M. Kappl, "Force measurements with the atomic force microscope: Technique, interpretation and applications," *Surf. Sci. Rep,* vol. 59, pp. 1-152, 2005.

[86] M. Lekka, D. Sainz-Serp, A. J. Kulik and C. Wandrey, "Hydrogel Microspheres: Influence of Chemical Composition on Surface Morphology, Local Elastic Properties, and Bulk Mechanical Characteristics," *Langmuir,* vol. 20, pp. 9968-9977, 2004.

[87] N. P. Desai and J. A. Hubbell, "Biological responses to polyethylene oxide modified polyethylene terephthalate surfaces," *J. Biomed. Mater. Res.,* vol. 25, pp. 829-843, 1991.

[88] M. Mikolajczyk and P. Kielbasinski, "Recent developments in the carbodiimide chemistry," *Tetrahedron,* vol. 37, pp. 233-284, 1981.

[89] J. Coste, D. Le-Nguyen and B. Castro, "PyBOP®: A new peptide coupling reagent devoid of toxic by-product," *Tetrahedron Lett.,* vol. 31, pp. 205-208, 1990.

[90] E. T. Kang, K. L. Tan, K. Kato, Y. Uyama and Y. Ikada, "Surface Modification and Functionalization of Polytetrafluoroethylene Films," *Macromolecules,* vol. 29, pp. 6872-6879, 1996.

[91] R. J. McMahon, Avidin-Biotin Interactions: Methods and Applications, Evansville: Humana Press, 2008.

[92] D. Ponader, F. Wojcik, F. Beceren-Braun, J. Dernedde and L. Hartmann, "Sequence-Defined Glycopolymer Segments Presenting Mannose: Synthesis and Lectin Binding Affinity," *Biomacromolecules,* vol. 13, pp. 1845-1852, 2012.

[93] J. Geng, G. Mantovani, L. Tao, J. Nicolas, G. Chen, R. Wallis, D. A. Mitchell, B. R. G. Johnson, S. D. Evans and D. M. Haddleton, "Site-Directed Conjugation of "Clicked" Glycopolymers To Form Glycoprotein Mimics: Binding to Mammalian Lectin and Induction of Immunological Function," *J. Am. Chem. Soc.,* vol. 129, pp. 15156-15163, 2007.

[94] T. Lei, G. Jin, C. Gaojian, X. Yingjian, L. Vincent, M. Giuseppe and H. David M., "Bioconjugation of biotinylated PAMAM dendrons to avidin," *Chem. Commun.,* no. 33, pp. 3441-3443, 2007.

[95] T. K. Dam and C. F. Brewer, "Thermodynamic Studies of Lectin−Carbohydrate Interactions by Isothermal Titration Calorimetry," *Chem. Rev.,* vol. 102, pp. 387-429, 2002.

[96] C. Boss, E. Meurville, J.-M. Sallese and P. Ryser, "Size-selective diffusion in nanoporous alumina membranes for a glucose affinity sensor," *J. Membrane Sci.,* vol. 401, pp. 217-221, 2012.

[97] V. T. Moy, Y. Jiao, T. Hillmann, H. Lehmann and T. Sano, "Adhesion Energy of Receptor-Mediated Interaction Measured by Elastic Deformation," *Biophys. J.,* vol. 76, pp. 1632-1638, 1999.

[98] G. Hild, R. Okasha, M. Macret and Y. Gnanou, "Relationship between elastic modulus and volume swelling degree of polymer networks swollen to equilibrium in good diluents, 4.

Interpretation of experimental results on the basis of scaling concepts," *Macromol. Chem. Phys.*, vol. 187, pp. 2271-2288, 1986.

[99] D. Ponader, P. Maffre, J. Aretz, D. Pussak, N. M. Ninnemann, S. Schmidt, P. H. Seeberger, C. Rademacher, G. U. Nienhaus and L. Hartmann, "Carbohydrate-Lectin Recognition of Sequence-Defined Heteromultivalent Glycooligomers," *J. Am. Chem. Soc.*, vol. 136, pp. 2008-2016, 2014.

[100] R. T. Lee, Y. Shinohara, Y. Hasegawa and Y. C. Lee, "Lectin-Carbohydrate Interactions: Fine Specificity Difference Between Two Mannose-Binding Proteins," *Biosci. Rep.*, vol. 19, pp. 283-292, 1999.

[101] N. M. Green, "Avidin 1. The use of 14C Biotin for Kinetic Studies and for Assay," *Biochem. J.*, Vols. 585-591, p. 89, 1963.

[102] S. Goto and H. Terada, "Analysis of binding affinity of sugars to concanavalin A by surface plasmon resonance sensor BIACORE," *Spectroscopy*, vol. 16, pp. 285-288, 2002.

[103] A. Chilkoti and P. S. Stayton, "Molecular origins of the slow streptavidin-biotin dissociation kinetics," *J. Am. Chem. Soc.*, vol. 117, pp. 10622-10628, 1995.

[104] A. Chen and V. T. Moy, "Cross-Linking of Cell Surface Receptors Enhances Cooperativity of Molecular Adhesion," *Biophys. J.*, vol. 78, pp. 2814-2820, 2000.

[105] L. Hartmann, K. Watanabe, L. L. Zheng, C.-Y. Kim, S. E. Beck, P. Huie, J. Noolandi, J. R. Cochran, C. N. Ta and C. W. Frank, "Toward the development of an artificial cornea: Improved stability ofinterpenetrating polymer networks," *J. Biomed. Mater. Res. B. Appl. Biomater.*, vol. 98, pp. 8-17, 2011.

[106] D. L. Elbert and J. A. Hubbell, "Conjugate Addition Reactions Combined with Free-Radical Cross-Linking for the Design of Materials for Tissue Engineering," *Biomacromolecules*, Vols. 430-441, p. 2, 2001.

[107] W. Kern, “The Evolution of Silicon Wafer Cleaning Technology,” *J. Electrochem. Soc.*, vol. 137, pp. 1887-1892, 1990.

[108] S. Zhou, C. Burger, B. Chu, M. Sawamura, N. Nagahama, M. Toganoh, U. E. Hackler, H. Isobe and E. Nakamura, “Spherical Bilayer Vesicles of Fullerene-Based Surfactants in Water: A Laser Light Scattering Study,” *Science,* vol. 291, pp. 1944-1947, 2001.

[109] J. A. Bonham, M. A. Faers and J. S. v. Duijneveldt, “Non-aqueous microgel particles: synthesis, properties and applications,” *Soft Matter,* vol. 10, pp. 9384-9398, 2014.

[110] K. D. Hardman and C. F. Ainsworth, “Structure of concanavalin A at 2.4-Ang resolution,” *Biochemistry,* vol. 11, pp. 4910-4919, 1972.

[111] S. G. Korenman, “Comparative binding affinity of estrogens and its relation to estrogenic potency,” *Steroids,* vol. 13, pp. 163-177, 1969.

[112] R. P. Haugland and W. W. You, “Coupling of antibodies with biotin,” *Methods Mol. Biol.*, vol. 418, pp. 13-24, 2008.

[113] Z. Markovic-Housley, J. Balbach, B. Stolz and J.-C. Genovesio-Taverne, “Predicted topology of the N-terminal domain of the hydrophilic subunit of the mannose transporter of Escherichia coli.,” *FEBS Lett.,* vol. 340, pp. 202-206, 1994.

[114] E. J. Cocinero, J. P. Simons, E. C. Stanca-Kaposta, B. G. Davis and D. P. Gamblin, “Hydrophilic and hydrophobic carbohydate interactions,” Central Laser Facility, Oxford, 2008.

[115] M. E. Davis, Z. (. Chen and D. M. Shin, “Nanoparticle therapeutics: an emerging treatment modality for cancer,” *Nat. Rev. Drug Discov.,* vol. 7, pp. 771-782, 2008.

[116] I. Papp, C. Sieben, K. Ludwig, M. Roskamp, C. Böttcher, S. Schlecht, A. Herrmann and R. Haag, “Inhibition of Influenza Virus Infection by Multivalent Sialic-Acid-Functionalized Gold Nanoparticles,” *Small,* vol. 6, pp. 2900-2906, 2010.

[117] L. L. Kiessling, J. E. Gestwicki and L. E. Strong, “Synthetic multivalent ligands in the exploration of cell-surface interactions,” *Curr. Opin. Chem. Biol.,* vol. 4, pp. 696-703, 2000.

[118] I. Jelesarov and H. R. Bosshard, “Isothermal titration calorimetry and differential scanning calorimetry as complementary tools to investigate the energetics of biomolecular recognition,” *J. Mol. Recognit.,* vol. 12, pp. 3-18, 1999.

[119] B. N. Murthy, S. Sinha, A. Surolia, S. S. Indi and N. Jayaraman, “SPR and ITC determination of the kinetics and the thermodynamics of bivalent versus monovalent sugar ligand–lectin interactions,” *Glycolconj. J.,* vol. 25, pp. 313-321, 2008.

[120] R. C. Hillig, S. Urlinger, J. Fanghänel, B. Brocks, H. Cornella, Y. Stark, D. Sülzle, D. I. Svergun, S. Baesler, G. Malawski, D. Moosmayer, A. Menrad, M. Schirner and K. Licha, “Fab MOR03268 Triggers Absorption Shift of a Diagnostic Dye via Packaging in a Solvent-shielded Fab Dimer Interface,” *J. Mol. Biol.,* vol. 1, pp. 206-219, 2008.

[121] N. H. Yennawar, J. A. Fecko, S. A. Schowalter and P. C. Bevilacqua, “Chapter Seventeen – A High-Throughput Biological Calorimetry Core: Steps to Startup, Run, and Maintain a Multiuser Facility,” *Methods Enzymol.,* vol. 567, pp. 435-460, 2016.

[122] J. Voskuhl, M. C. A. Stuart and B. J. Ravoo, “Sugar-Decorated Sugar Vesicles: Lectin–Carbohydrate Recognition at the Surface of Cyclodextrin Vesicles,” *Chem. Eur. J.,* vol. 16, pp. 2790-2796, 2010.

[123] W. Jiang, K. Nowosinski, N. L. Löw, E. V. Dzyuba, F. Klautzsch, A. Schäfer, J. Huuskonen, K. Rissanen and C. A. Schalley, “Chelate Cooperativity and Spacer Length Effects on the Assembly Thermodynamics and Kinetics of Divalent Pseudorotaxanes,” *J. Am. Chem. Soc.,* vol. 134, pp. 1860-1868, 2012.

7. Author Contributions: Thesis and Related Publications

The work in this thesis has led to three co-author publications of Hanqing Wang. In the following, the contributions of Hanqing Wang, co-authors, and supervisors on this thesis and publications are listed. For co-author publications, only the contributions of Hanqing Wang are specified.

Ph.D. thesis

- **Hanqing Wang** (Ph.D. student, Freie Universität Berlin, Max Planck Institute of Colloids and Interfaces, Heinrich-Heine-Universität Düsseldorf, group of Prof. Dr. Laura Hartmann):
  All synthesis, functionalization, and characterization of PEG based SCPs and PAA based SCPs. Synthesis and characterization of Biotin-NH_2. Functionalization of glass surfaces. SCP-RICM measurements and data analysis, including direct binding studies, inhibition/competition studies, IC_{50} studies.

- **Fawad Jacobi** (Ph.D. student, Heinrich-Heine-Universität Düsseldorf, group of Prof. Dr. Laura Hartmann):
  Synthesis and characterization of PEG-dAAm macromonomers, and mannose-NH_2. Support with writing the German translation of summary chapter.

- **Laura Hartmann** (Supervisor, Professor, Heinrich-Heine-Universität Düsseldorf):
  Design of research and research coordination, collaborative data analysis.

- **Stephan Schmidt** (Co-supervisor, Professor, Heinrich-Heine-Universität Düsseldorf):

Design of research and research coordination, collaborative data analysis. Writing scripts of Igor. These scripts allowed the automatic calculation of the adhesion energy from SCP-RICM experiments.

- **Maria Beuer** (Technical assistant, Heinrich-Heine-Universität Düsseldorf):
  NMR measurements.

- **Johannes Waschke** (Master student, Universität Leipzig, Biophysical Chemistry Group):
  Development of automated contact area finder software ("Hydrogel").

Publications

S. Schmidt, H. Wang, D. Pussak, S. Mosca and L. Hartmann, "Probing multivalency in ligand–receptor-mediated adhesion of soft, biomimetic interfaces," *Beilstein J. Org. Chem.*, vol. 11, pp. 720-729, 2015.

Contributions from Hanqing Wang:

Synthesis and characterization of PEG based SCPs. Proof-reading of the manuscript.

S. Martin, H. Wang, L. Hartmann L, T. Pompe and S. Schmidt, "Quantification of protein–materials interaction by soft colloidal probe spectroscopy," *Phys. Chem. Chem. Phys.*, vol. 17, pp. 3014-3018, 2015.

Contributions from Hanqing Wang:

Synthesis and characterization of PAA based SCPs. Proof-reading of the manuscript.

S. Martin, H. Wang, T. Rathke, U. Anderegg, S. Möller, M. Schnabelrauch, T. Pompe and S. Schmidt, "Polymer hydrogel particles as biocompatible AFM probes to study CD44/hyaluronic acid interactions on cells," *Polymer*, pp. 342-346, 2016.

Contributions from Hanqing Wang:

Synthesis and characterization of PEG based SCPs. Proof-reading of the manuscript.

8. Acknowledgements

I would like to thank my supervisor and mentor Prof. Dr. Laura Hartmann for this interesting and challenging topic, her countless ideas and steady motivation, the scientific and personal support to move my thesis forward. I would like to thank my co-supervisor Prof. Dr. Stephan Schmidt for his fruitful collaboration, support, and review of my thesis. The discussion with him gave me a lot of new ideas, and his humour brought a lot of fun to my work. I am also thankful to Prof. Dr. Peter H. Seeberger for the opportunity to work in a challenging and cooperative department for the start of my Ph.D. thesis and my master thesis.

Besides my first supervisors, I would like to thank my second supervisor Prof. Rainer Haag for agreeing to review my thesis.

I would like to thank senior scientist Dr. Monir Tabatabai, for her scientific and personal support, her review of my NMR analysis. I would also like to thank lab technician Ms. Stefanie Scheelen and secretary Ms. Michaela Kitza for their support in the lab and the office, always providing me enough material to work with, and their encouragement to improve my German from A1 to B1.

I would like to thank my collaborators, Dr. Steve Martin, Maria Meißler, and Antje Reinecke for the challenging project we had.

Further, I would like to thank lab mates and friends, Dr. Daniel Pussak, Alberto Camaleño de la Calle, Fawad Jacobi, Christoph Gerke, Tanja Freichel, Mischa Baier, Kira Neuhaus, and Katarina Bücher for their support in work and in life, for the lunch talks we had, and most importantly for our friendship outside the lab. Especially, I want to thank my buddies Alberto and Fawad, for the countless discussions about science, history, language, and culture during coffee breaks, which broadens my horizons and awareness of the world.

Last but not least, I would like to thank my parents Liping and Jian, my grandparents Meijuan and Rongshun, for their love and support, the weekly facetime chatting, and their encouragement. I would like to thank my uncle Miao, and Hao, for their support and tutoring of my life in Germany.